Optimisation of the squeeze forming process.

Ahmad, Rosli

School of Engineering

University of Wales, Swansea

OPTIMISATION OF THE SQUEEZE FORMING PROCESS

ROSLI AHMAD

BEng.

Thesis submitted to the University of Wales in candidature for the degree of

Doctor of Philosophy

September 2006

Summary

This thesis presents the optimisation of the squeeze forming process, considering both the thermal and mechanical aspects. The Finite Element Method has been used to simulate the process and a Genetic Algorithm was used as an optimisation tool.

The thermal optimisation has been applied to the squeeze forming process to achieve near simultaneous solidification in the cast part. The positions of the coolant channels were considered as design variables in order to achieve such an objective. The formulation of the objective functions involved two points and also considered the whole domain. The validation aspects of the optimisation of the casting processes for 2D and axi-symmetric problems were presented. The influence of the interfacial heat transfer coefficient related to optimisation of the process was explored.

For the multi-objective optimisation problem, the objective was to achieve near simultaneous solidification in the cast part and also near uniform von Mises stress distribution in the die for the first and also tenth cycles. This is because it has been found that the process starts to reach cyclic stabilisation after the tenth cycle. The comparison

between the design obtained from the practical solution derived from the optimisation process and also the design which has been applied in industry was also discussed.

The Design Sensitivity Analysis and Design Element Concept have been applied to the squeeze forming process. For parameter sensitivity analysis, the Youngs Modulus was considered as a design variable. A few design element subdivisions have been employed to explore its application to the process. For shape sensitivities involving the coolant channels, the parameterisation was required in order to consider the coolant channel as an entity. The extent to which the tendency to move the coolant channel either in the X or Y-direction with respect to the particular von Mises stress constraint in the die was also discussed.

Declaration

This work has not previously been accepted in substance for any degree and is not being concurrently submitted in candidature for any degree.

Signed ..... (Candidate)

Date ..... 20 Sept 2006

Statement 1

This thesis is the result of my own work/investigation except where otherwise stated. Other sources have been acknowledged by footnotes giving explicit references. Bibliographies are appended.

Signed ..... (Candidate)

Date ..... 20 Sept 2006

Statement 2

I hereby give consent for my thesis, if accepted, to be available for photocopying and for inter-library loan, and for the title and summary to be made available to outside organisations.

Signed ..... (Candidate)

Date ..... 20 Sept 2006

To my parents.

Contents

List of Figures

List of Tables

Acknowledgements

I would like to express my deepest gratitude to Professor D.T. Gethin for his optimism, expert advice and guidance throughout this work. I would like to thank to Professor R.W. Lewis for giving me permission to be one of the members of the Squeeze Forming Group from which invaluable practical experience has been gathered from the professional group. Thanks are also given to Dr. E.W. Postek for the invaluable discussions about the Design Sensitivity Analysis and Design Element Concept. Special thanks also go to Professor R. Bialecki from Silesian University of Technology, Poland for the fruitful discussions about Genetic Algorithms, during his short visit to Swansea University. My gratitude is extended to Dr. W. Kus, also from Silesian University of Technology, Poland, where the communication through emails has given insight to the Genetic Algorithms based Optimisation. I am indebted to my parents who have always provided me with their support and encouragement. My gratitude is also extended to Government of Malaysia, for sponsoring me during the duration of this work. Finally, I wish to thank my friends for making my stay in Swansea enjoyable.

Notation

t	Time
s	Second
π	Pi
min	Minimum
max	Maximum
ave	Average

Chapter 1

Introduction

1.1 Background

Design-simulate-evaluate-redesign is the standard procedure that is implemented in traditional optimisation that is carried out with the assistance of computational tools. It is executed until an acceptable design is achieved within the time scale that is available. This process is not only time consuming, it is also unlikely that a true optimum has been achieved. If this sequence can be fully automated, significant benefit will be derived. Numerical optimisation techniques were first explored in structural design in the early 80's [1]. During this period, a framework to undertake the process evolved and became established. It was, however, in the mid 90's when researchers started exploiting this framework in casting process simulation [2] and recently it is being explored for other applications, such as injection moulding and extrusion [3,4,5].

Optimisation studies have explored the application of a number of strategies. These include principally gradient methods and genetic algorithms. The former require the calculation of gradients that link design parameters with system response and combined with optimisation routines, they are used to find the best design according to a specified objective function and design variable constraints. Although they require gradient calculation, they are less computationally demanding, but are restricted in their search field. Genetic algorithms, also recognised as free-derivative methods, find the actual optimum based on a stochastic approach. They require more computational effort due to the use of a broader search field to find this solution.

The application of optimisation techniques to thermo-mechanical forming processes is particularly challenging due to the coupled and highly non-linear mechanisms that are present. However, optimisation of such processes is very desirable to facilitate high quality part manufacture and efficient process operation. For a prescribed part geometry, such optimisation will need to account for process setting changes as well as tooling design, i.e. shape. The current project will focus on the squeeze forming process, the characteristics of which will be summarised in a later section.

As mentioned previously, optimisation depends on establishing design sensitivity expressed in terms of derivatives. In previous studies on process simulation, these have been estimated via difference equations and analytical equations have been developed in structural analysis. These have been shown to be advantageous and give accurate values of design sensitivity. Their application in process simulation has received little attention to date.

Some work in structural analysis has led to the concept of a Design Element. The design element represents a region of the structure and design sensitivity may be based on the design element, rather than the discretised element values that may be associated with the solution of the governing equations. Potentially this has advantages through reduction of computational effort in sensitivity calculation. It also offers the potential to undertake shape sensitivity analysis, for example a coolant channel may be treated as a design element and this may be positioned to achieve control over cooling behaviour. Again the application of this technique to simulation in highly nonlinear processes has received limited attention.

1.2 Automatic Shape Optimisation

One of the difficulties involved in shape optimisation is to robustly automate the remeshing procedures that are required as a consequence of any shape change. For many researchers working in the computational optimisation field this is one of the biggest challenges to be tackled due to the need for absolute reliability to generate high quality elements. This becomes particularly arduous for complex geometries that are typical of many cast parts. This is particularly relevant in the squeeze forming process, due to the process design need to move the coolant channels in the die to achieve the desired cooling behaviour. The optimisation procedure also relies on the successful integration of the remeshing procedure with the optimisation software and the Finite Element method that is used to solve the governing thermodynamic equations.

1.3 Application of Multi-Objective Optimisation in Process Simulation

Multi-objective optimisation techniques in process simulation have achieved a growing interest in engineering, due to the prospect of obtaining an optimum process design concerning different conflicting requirements. In order to provide sound-engineering designs, often, conflicting objectives must be considered. This research will deal with the multi-objective optimisation of the squeeze forming process involving such conflicting requirements. For instance, in this work, the multi-objective optimal design problem can be formulated to determine the optimal solutions in order to obtain simultaneously the near simultaneous solidification in the cast component and near uniform von Mises stress in the die.

1.4 Casting and Squeeze Forming

The work in this thesis is concerned with simulating and optimising the thermomechanical process that take place in squeeze forming, so it is appropriate to summarise the process and contrast it with other casting processes. The casting process is one of the oldest manufacturing processes. It is believed that the process was used by the Egyptians to make gold jewelry some 5000 years ago. Even though the process has a long history, its application is still relevant and it is being used today in many industries such as aerospace and automotive sectors to produce complex shape components.

There are a number of casting processes available and among them are investment casting, gravity die casting, pressure die casting, sand casting and squeeze forming [6]. There are two main variants of squeeze forming as shown in Figure 1.1. In direct squeeze forming, liquid metal is poured into a lower die, the upper die is then closed over it and high pressure is applied until the part is completely solidified. In indirect squeeze forming, molten metal is poured into the shot sleeve of a squeeze forming machine. Then, it is injected into the die at relatively slow velocity. Molten metal in the die cavity is then solidified under the applied pressure.

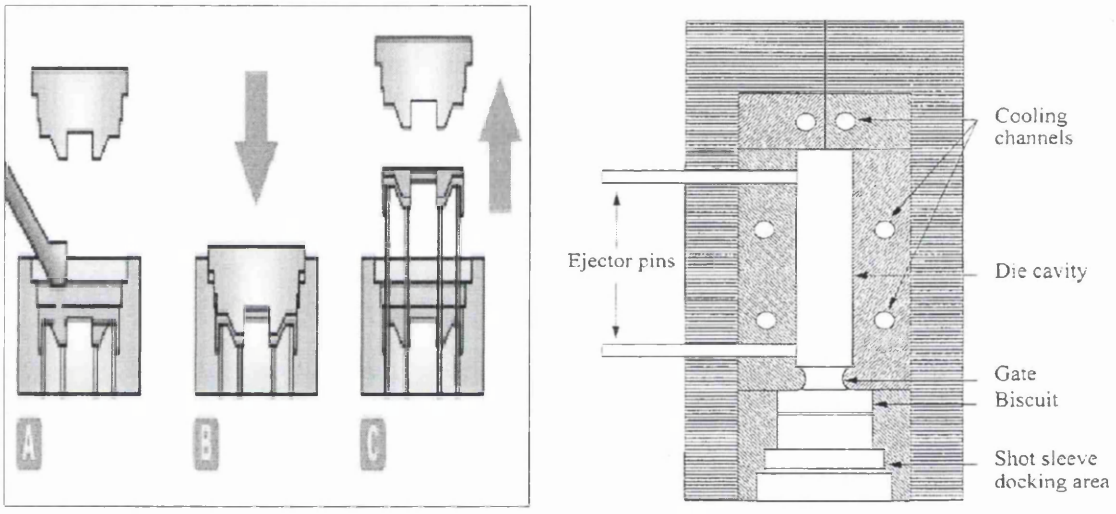

Figure 1.1 Direct and Indirect Squeeze Forming (The pictures were obtained from Azom.com website and reference [7])

Direct squeeze forming is a combination of casting and forging processes. It is currently being employed to produce safety-critical and high performance components such as steering, brake and suspension parts. This is due to the fact that the components produced from the squeeze forming process have several superior properties such as refined grain structure, improved mechanical strength and almost complete elimination of all shrinkage and gaseous porosity. These features are the outcome of the prolonged high

contact pressure and intimate contact between the molten alloy and the metal die surfaces [8]. Figure 1.2 shows example components formed by the squeeze forming process.

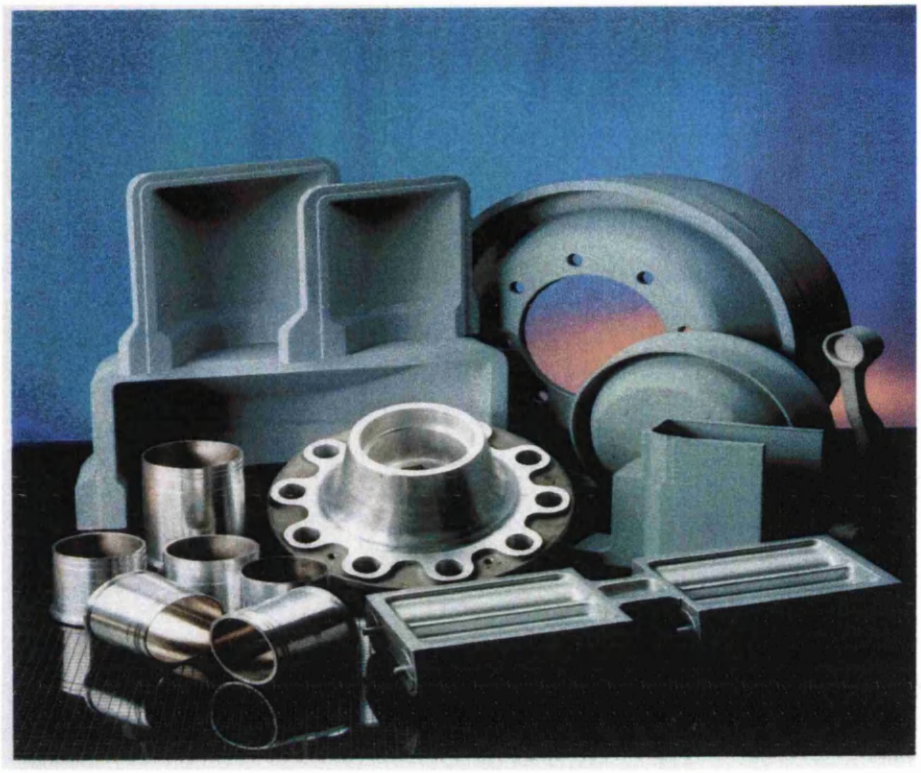

Figure 1.2 Example components obtained by the Squeeze Forming (from GKN)

The major advantages claimed for the squeeze forming process over casting and forging can be listed as follows [9,10,11]:

(1) The ability to produce parts with complex profile and thin sections beyond the capability of conventional casting and forging techniques.

(2) Substantial improvement in material yield because of the elimination of gating and feeding systems.

(3) Significant reduction in pressure requirements, in comparison with conventional forging, while at the same time increasing the degree of complexity that can be obtained in the parts.

(4) The ability to use both cast and wrought compositions.

(5) Improvements in product quality with regard to surface finish, dimensional accuracy and mechanical properties.

(6) Almost complete elimination of shrinkage and/or gas porosity leading to the ability to heat treat the casting

(7) Potential for using cheaper, recycled material without the loss of properties that would occur with other processes.

(8) The potential for increased productivity in comparison with gravity die casting or low pressure die casting.

(9) It is suitable for the production of cast composite materials and reinforcement through the inclusion of fibres.

Despite its advantages, the squeeze forming process also has a few disadvantages. These disadvantages are as follows [9,10,11]:

(1) High capital costs, comparable with pressure die casting but lower than forging.

(2)Relatively low die life, in comparison with the die casting processes.

(3) Shape complexity limitation, in comparison with the die casting processes.

(4) The need for a very accurate metal metering system.

(5) Longer cycle time in comparison with forging.

In the squeeze forming process, there are a number of process control parameters and these can be grouped under pressure cycle and cooling rate controls. For the latter, the die and coolant system design play a key role in achieving a defect free product. However, further complexity is introduced since these control groups interact. For example, it is evident from [12], that the pressure applied in the squeeze forming process has a direct effect on heat flux by influencing the heat transfer coefficient at the die-cast interface. This is due to the fact that any air gap evolution at the die-casting interface is controlled through pressure application. Similarly the position of cooling channels and the heat removal rates will have a significant impact on the temperature field within the die and hence the solidification of the squeeze formed part.

1.5 Thesis Scope and Layout

From the preceding it is evident that there is scope for exploring a number of issues concerning optimisation in thermomechanical forming processes that are complex due to their highly nonlinear nature. Strategically, the work will be concerned with developing and exploring the use of genetic algorithm based optimisation techniques. Analytical gradient expressions in sensitivity studies will also be demonstrated to express sensitivity with respect to material parameters. The project will also look at the use of a design element concept in process optimisation since it offers potential computational savings in parameter optimisation and is attractive since the dies used in thermomechanical forming processes are usually constructed from discrete building blocks and each block may be

treated as a design element. Demonstration will be achieved through its application to the squeeze forming process.

The research contributions are summarised as follows:

- An automatic shape optimisation procedure has been proposed with respect to cooling system design by using a Genetic Algorithm approach in order to achieve desired thermodynamic control. The defined objective is to achieve near simultaneous solidification of the casting section and this implies identical cooling rates with consequent consistency of mechanical properties for uniform section castings. The influence of process parameters and operation on their positioning has also been explored.
- Through application of the Genetic Algorithm approach, multi-objective optimisation has been explored with the prospect of obtaining good thermodynamic control and acceptable stress levels within the tool set. Again, the influence of process parameters and operation on their positioning has also been explored.
- Design sensitivity analysis and the application of a design element concept have been explored. The Design Element Concept has been applied to the die domain since the design elements can be considered as a direct mapping of the blocks that make up a die. Exploration has focused on expressing sensitivity with respect to material property and coolant system design.

The work reported in this thesis is laid out in the following way. Chapter two will be focused on a literature review which generally covers the previous works on the squeeze

forming process and also the recent works on modeling the squeeze forming process, design sensitivity analysis and design element concept, the key issues in shape optimisation problem and the latest works on the multi-objective optimisation. Chapter three will mainly cover thermal optimisation of the squeeze forming process using Genetic Algorithms. Chapter four will deal with the multi-objective optimisation of the squeeze forming process considering thermal and mechanical aspects. Finally, Chapter five will be concerned with design sensitivity analysis and the Design Element Concept for sequentially coupled thermo-mechanical problems. The application of Design Element Concept for parameter and shape sensitivities will be explored.

References:

[1] O.C. Zienkiewicz and J.S. Campbell,'Shape optimization and sequential linear Programming', in R.H. Gallagher and O.C. Zienkiewicz (eds.), Optimum structural Design, Wiley, New York, 1973.

[2] D.A. Tortorelli, J.A. Tomasko, T.E. Morthland and J.A. Dantzig, 'Optimal design of nonlinear parabolic systems, Part II: Variable spatial domain with applications to casting optimization', Computer Methods in Applied Mechanics and Engineering, **113**:157-172 (1994).

[3] W. Sosnowski, I. Marczewska, and A. Marczewski, Sensitivity based optimization of sheet metal forming tools, Journal of Material Processing Technology, 2002:124,319-328.

[4] C.H. Wu and Y.L. Su, 'Optimization of wedge-shaped parts for injection molding and injection compression molding', Int. Comm. Heat Mass Transfer, **30**:215-224 (2003).

[5] A. Bikas, N. Pantelelis and A. Kanarachos, 'Computational tools for the optimal design of the injection moulding process', Journal of Material Processing Technology, **122**:112-126, 2002.

[6] G.J. Davis, 'Solidification and Casting ', Applied Science Publishers Ltd,1973.

[7] T. Rolland, R. Schmidt, L. Arnberg and W. Thorpe, 'Macrosegregation in indirectly squeeze cast Al-0.9wt%Si', Material Science and Engineering, **A212**:235-241, 1996.

[8] I.S. Cho and C.P. Hong, ' Modeling of microstructural evaluation in squeeze casting of an Al-4.5mass%Cu Alloy', ISIJ International, 37:1098-1106 (1997).

[9] A.J. Clegg, ' Precision Casting Processes', Pergamon Press, 1991.

[10] S. Rajagopal, 'Squeeze Casting: a review and update', J. Applied Metalworking,**1**:3-14 (1981).

[11] J.R. Franklin and A.A. Das, 'Squeeze Casting – a review of the status', The British Foundryman,**77**:150-158 (1984)

[12] I.S. Cho and C.P. Hong, 'Evaluation of heat transfer coefficients at the casting/die interface in squeeze casting', Int. J. Cast Metals Res, **9**:227-232 (1996).

Chapter 2

Literature Review

2.1 Introduction

A literature survey shows that although there have been many works carried out in the application of numerical optimisation techniques to manufacturing processes, limited applications have been explored for casting process optimisation and there are no reported works for the squeeze forming process. As mentioned in Chapter 1, numerous studies have highlighted the importance of exploring alternative techniques to solve the automatic shape optimisation problem. Usually, these require remeshing procedures and also there is a need to satisfy a number of objectives that often pose conflicting requirements. Finally, little attention has been given to the use of a Design Element

Concept that may prove to be attractive in reducing the effort that is required in computing sensitivity information.

To illustrate, structural optimisation was the first area in which the application of the optimisation technique was implemented. Typically, in structural problem, the purpose of optimisation is to minimise for example, the weight of a structure or to maximise its stiffness. For example, Sienz and Hinton [1] described a reliable and robust tool for structural shape optimisation problem where the objective was minimisation of the volume of the connecting rod. This tool formed part of the integrated system ISO-P (2D) which stands for integrated structural optimisation package.

In order to review previous works related to this research, this chapter is divided into six sections. The first section is concerned with the previous works on the squeeze forming process, primarily focusing on the new findings related to the process. The second section is involved with the application of sensitivity analysis and Design Element Concept to the optimisation of manufacturing processes. It is observed that little attention has been given to the use of the Design Element Concept in this class of optimisation problem. The third section is devoted to reviewing works on the application of genetic algorithms in the optimisation of manufacturing processes. In the fourth section, attention is given to the previous research works involving application of numerical optimisation method for the casting processes and also thermodynamic control through coolant system design which has a direct impact on controlling the solidification behaviour in the component. Section five focuses on consideration of the associated remeshing requirements for shape optimisation. Lastly, the final section is related to reviewing the

current works in multi-objective optimisation in engineering problems. In completing this review, it became clear that a large body of work could be included in each section. However, the author has attempted to restrict this to what are the most pertinent or typical studies.

2.2 Squeeze Forming Process Review

The Squeeze Forming Process is an attractive route to manufacture shaped high performance parts and it is receiving research attention as well as exploitation. This is evident from a number of research papers that have covered work on the process. These include processing aspects as well as metallographic issues. For the processing aspects, it is convenient to divide the section into three parts; the effect of pressure on the process, the initial conditions for molten metal and die temperatures, and, cooling rate control. The current work is concerned with processing rather than focusing on metallographic issues. Thus, the metallographic literature will not be surveyed in depth, it is merely cited to underpin the component structural performance improvements associated with this manufacturing route.

2.2.1 Pressure Influence

Pressure application is important since it is well established that it has a direct impact on the heat transfer that occurs between the cast part and the die. Thus pressure application level and the profile that is employed during the squeeze forming cycle provide a method for process control. There have been a number of works on pressure effects, principally in high pressure die casting studies and the works in [2,3] include some typical examples.

Specific to squeeze casting, pressure application influences the material mechanical properties and these will be discussed initially.

Hong [4] examined a range of applied pressure from which sound castings can be obtained. In his study, the sound castings were defined as free from macrosegregation and shrinkage cavities. For the aluminium alloy Al-4.5wt Cu, having a freezing range from 502°C to 648°C he found that sound castings cannot be obtained when the pouring temperature is relatively high, typically 112°C to 162°C above the liquidus temperature. However, sound castings can be obtained with a relatively low temperature that is typically 32°C above the liquidus temperature. Also he found that success depended on pressure level for which he defined two levels, P_{SC} and P_{MS} where P_{SC} and P_{MS} indicate the critical applied pressure under which shrinkage cavities form and the applied pressure above which macrosegregation forms in the castings respectively. Acceptable castings were produced when the applied pressure was higher than P_{SC} and lower than P_{MS}. Based on this new finding, it is crucial that a relatively low pouring temperature is applied, about 5% above the liquidus temperature in order to obtain cast components which possess several good properties such as free from macrosegregation and shrinkage cavities.

Skolianos [5] investigated and found that by increasing the applied pressure, the ultimate tensile strength of the heat treatable alloy that was cast could also be increased. For the alloy concerned, above a certain pressure, it was observed that the increase appeared to be independent of the magnitude of the applied pressure as illustrated in the graph of Ultimate Tensile Strength vs Applied Pressure that levelled out as the applied pressure was increased. He also observed that the increase in pressure decreased both the

volume fraction of porosity and the micropore size, as well as the size of the dendrites and the interdendritic areas.

Yue [6] discovered contrastingly that increasing the squeeze pressure increased the grain size of the casting when the pressure was applied when the temperature within the sample was above the liquidus temperature. Also a squeeze pressure of 50 MPa was found to be sufficient to produce pore-free AA7010 composition castings for a simple cylindrical shape. Again, it should be noted that he found that there is a certain applied pressure above which it has little effect on the improvement of the properties of the component. In a similar manner, Yong [7] found that the applied pressure in squeeze forming promoted rapid solidification and a refined cell structure. From metallographic examination, he found that the cell size reduced from 127 to 21 μm when the applied pressure was increased from 0.1 to 60 MPa. In common with [5], it was observed that increasing the applied pressure beyond 60 MPa provided little improvement in the tensile properties of the squeeze cast alloy. Other studies, Maeng [8] found that the mechanical properties such as hardness was also greatly improved as the applied pressures were increased. This was attributed to the increase in solubility of solute atoms (such as Si, Cu, Mg and Zn) and a decrease of inter-dendritic pores. However, it is likely that the increase in solubility of solute atoms is due to undercooling physics, the applied pressure has an effect only when the pressure is very high.

With regard to impact properties, Chen[9] discovered that increasing the squeeze pressure over the range from 30 to 100 MPa did not significantly affect the impact energy of the central and lower parts of the casting.. Also, he found that the presence of

macrosegregation appeared to give rise to a decrease in impact energy in the as-cast condition. Finally, Cay [10] observed that the fatigue resistance of the squeeze cast alloys was superior to that of the gravity-cast alloys. He discovered from the microstructure examination that small and very tight morphologies had been obtained in squeeze forming with respect to gravity-casting technique.

The benefits highlighted in the preceding publications illustrate the reasons why pressure application in the squeeze forming process is important. It leads to superior part performance when compared with parts manufactured using other casting processes. In addition, pressure has a significant impact on interfacial heat transfer coefficient, but this will be discussed more fully in Chapter 3 when model build is presented.

2.2.2 Melt Temperature Influence

Increasing the melt temperature has two important effects. It influences the molten metal viscosity [11].This has a consequent effect on metal flow during the filling and displacement stages of the cycle, for example, a low temperature will lead to premature solidification and it will prevent the metal from being displaced within the die. Secondly, a high temperature will lead to an increase in heat content within the melt and hence imposes a higher cooling load and an increased cycle time. Thus melt temperature will have a direct influence on the final parts produced as studied in [12,13]. In [12], Lee examined the effects of melt flow and temperature on the macro and microstructure of a compressor scroll manufactured by direct squeeze forming. He found that the melt temperature greatly affected the flow and the final shape of the compressor scroll. The best melt filling patterns were obtained at 70°C below the liquidus temperature, 670°C.

The reason that the part could continue filling was because the mushy condition of the B390 alloy persists over a wide temperature range and the temperature of the metal was maintained over the filling stage. Yang [13] explored the effect of casting temperature on the properties of gravity and squeeze cast aluminium and zinc alloys. It was found from his study that the casting temperature had an effect on the mechanical properties derived from both casting methods. For the squeeze forming of the aluminium alloy Al-13.5wt Si, the best temperature to use was either 86°C or 116°C above the liquidus temperature (574°C). Common to the observation in [9], the former gave better properties at the top section of the casting while the latter, gave better properties within the bottom section. However, for the squeeze forming of the zinc alloy, the best temperature was 77°C above the liquidus (383°C).

2.2.3 Cooling Rate Influence

The combined influence of pressure and fill temperature also has a direct impact on the cooling rate within the squeeze cast part. In fact, cooling rate control plays a dominant role in achieving good mechanical property in the cast components. In connection with squeeze forming, Hwu [14] discovered that high cooling rates improved the mechanical performance of the parts. In common with all rapid solidification technologies, it was found that the fast cooling rates reduced the grain size of the matrix which in turn raised the strength of the part. Kim [15] found that the micro-structures of billets cast at pressures of 25, 50 and 75 MPa, respectively were more refined and dense than those of non-pressurised casts, because of a greater cooling rate. Maleki [16] discovered that hardness of the samples (alloy LM13) steadily increases from 97 HB for the sample

solidified under atmospheric pressure to about 110 HB at an external pressure of 171 MPa and becomes constant at higher applied pressures. Ideally, the cooling rate within the cast component should be identical throughout since this will be reflected in uniformity of mechanical properties.

Recently, a few works have explored the modeling of the complex physical phenomena associated with the squeeze forming process [17,18] to examine the contact behaviour between the die and cast part. These works primarily focused on a three dimensional thermo-mechanical analysis of the tool set and component. The starting point for this analysis was a full die, there was no consideration of fluid flow or displacement of the molten metal. In the former, Postek et al. [17] predicted the air gap in the squeeze forming processes from which the air gap had a direct influence on the interfacial heat transfer coefficient at the die-cast interface. In this work, the mechanical problem was treated as elasto-viscoplastic with the assumption of small displacement. It was found that squeeze formed parts solidify faster when compared with the typical die cast part. This was concluded to be due to the small or closed gap between the die and part which directly affected the interfacial heat transfer coefficient. In [18], Postek et al. extended their work to include the thermo-mechanical analysis with the addition of large displacement theory in the mechanical model. They found that solidification including these non-linear effects reduced the solidification rate. They concluded that the geometrically non-linear effects should be included due to the fact that it has a significant effect on the solidification rate within the part.

A general observation from these types of studies is that a higher applied pressure has a larger the impact on the component produced from the microscopic and macroscopic point of view and this is due to the fact that the applied pressure promotes rapid solidification, thus achieving a refined cell structure because of the combined effect from both aspects. However, typically, there is a ceiling pressure above which little effect can be observed on the properties of the component obtained. This review also highlights the direct effect that the melt temperature will have on the properties within different sections of simple shaped cast components. This effect will be more difficult to predict on real parts due to their geometric complexity, which is typical in industries such as aerospace and automotive sectors. From the above discussions, it is evident that the process parameters such as applied pressure and cooling rate controls and also melt temperature of cast parts play a dominant role in obtaining sound cast components in squeeze forming process. Again, it has also been shown that over the past 10 years, squeeze forming is one of the manufacturing processes which is being researched due to its potential to manufacture parts having superior mechanical properties.

2.3 Design Sensitivity Analysis and Design Element Concept Review

The coupling of optimisation techniques with process simulation is desirable and timely since computing power to undertake such analysis is becoming available and there is a growing industrial interest in this type of simulation. This is evident from the amount of research that has been carried out involving application of numerical optimisation in manufacturing processes such as extrusion, forging and metal forming processes.

A sensitivity analysis is central to any optimisation process. During the last decade, there have been many works on the application of design sensitivity analysis in connection with structural and manufacturing processes including metal forming processes. The latter present significant challenge due to the fact that metal forming processes require complex analysis since the nonlinearities that are present have to be taken into account. This includes for example friction, contact evolution at the tool-part interface and also material deformation behaviour. Such complexity is amplified when considering the calculation of sensitivity analysis itself which plays a vital role in gradient-based optimisation especially to ensure the accuracy of the sensitivity gradients. It is evident from the literature review that gradients may be derived in two basic ways, either, and most commonly as finite difference type expressions or as analytical expressions where the latter represent a reduced computing demand. These will be discussed within this section.

The analytical sensitivity analysis of a linear structural system has been explored in [19,20]. In [19], the parameter and shape sensitivities of linear structural analysis were covered in detail with a few numerical examples provided as benchmarks based on a cantilever truss, beam, plate and fillet. For the latter, procedures for structural analytical design sensitivity analysis of deformable solids with the finite element program POLSAP were described. The effectiveness of an Adjoint Variable Method (AVM) and a Direct Differentiation Method (DDM) depending on the number of design variables and constraints was discussed.

In connection with forming processes, Antunez and Kleiber [21] studied the sensitivity analysis of metal forming involving frictional contact under steady state

conditions. The interest in such a model arose from the analysis of rolling processes and a two dimensional approach to cutting problems, where the contact zone was determined. Although these are dynamic applications, the stable conditions that were assumed allowed analysis based on a stationary state to be carried out to describe the operation. In their work, the friction coefficient based on a Coulomb friction law was considered as a design variable. They explored the effect of changing the friction coefficient on the velocity at the boundary. They calculated sensitivities using the DDM. In this method, the derivative of the functional with respect to the design variables could be found by performing additional calculations, differentiating the equilibrium equation with respect to the design variables and solving for gradients for nodal velocity and pressure. In comparison it was found that this gave a close result with the one performed using a Central Finite Difference Method (CFDM). The CFDM calculates the sensitivities numerically, where the equation is solved twice before and after perturbation. Thus, it suffers from two drawbacks, involving the accuracy of the calculated sensitivities due to the choice of the magnitude of perturbation and also it takes longer time to calculate sensitivities because the Finite Element analysis has to be run twice at each iteration of the optimisation process. These will have a significant effect in the optimisation process especially when dealing with a highly nonlinear problem. In contrast, DDM has absolute accuracy because of the analytical differentiation. Besides, the calculated sensitivities using DDM are faster than Finite Difference Method (FDM) because the sensitivities derived from DDM are obtained by solving the finite element equation only once at each iteration of the optimisation process. Antunez [22] has also extended his sensitivity analysis work to metal forming process that include thermo-mechanical coupled analysis.

Again, he used the DDM to perform the sensitivity gradients calculation. He considered the static yield stress and the heat transfer coefficient at the interface as the design variables and studied the sensitivity of temperature with respect to these design variables. In his work, all the results obtained by DDM were checked and compared with the FDM in which he found that the results showed close agreement.

Kim and Huh [23] applied design sensitivity analysis to the sheet metal forming processes. A design sensitivity analysis scheme was proposed for an elasto-plastic finite element analysis with explicit time integration using the DDM to perform the sensitivity calculation. The DDM was used to deal with the large deformation. The elasto-plastic constitutive relation included planar anisotropy, shell elements with reduced integration and an advanced scheme to model the contact between the sheet and the dies. The result obtained using the DDM was compared with the result obtained from FDM in the drawing of a cylindrical cup and a 'U-shaped' bend. The results showed closed agreement, thus demonstrating the accuracy of the calculated analytical DDM.

Smith et al. demonstrated the application of sensitivity analysis to the optimal design of polymer extrusion [24,25]. For the former, the work focused on sensitivity analysis for nonlinear steady-state systems. In this work, the sensitivities were derived using both the DDM and the AVM. The AVM method calculates the design sensitivities by finding the adjoint vector first and then substitutes the vector into the equation of the functional sensitivity with respect to the design variable. On the other hand, the DDM solves directly the response derivative with respect to the design variable and substitutes the derivative into the equation of the functional sensitivity with respect to the design variable. A detailed description on the effectiveness of the AVM and the DDM for

specific problems was discussed in [20], depending on the number of design variables and applied constraints. It can briefly be summarised as follows; if the number of design variables are less than number of constraints, the DDM is preferred. On the other hand, if a number of applied constraints are less than number of design variables, the AVM is preferred. Again, the AVM and the DDM are the two variants of the analytical method, they have distinctive advantages compared to the FDM as described previously. In this work it was found that the two sensitivity analysis methods yielded identical expressions. The design variables were die thickness and prescribed inlet pressure. These were optimised to minimise pressure drop and to generate an uniform velocity across the die exit. It was summarised that sensitivities derived from the FDM for this nonlinear problem were both inaccurate and inefficient.

The Design Element is a concept where the sensitivities are calculated based on predefined zones, possibly identified by a die designer. These sensitivities are used by supplying them to the optimisation routines to achieve the optimal solution. It is potentially useful in a way that since a die is constructed from a number of steel blocks, this allows some pre-selection of the zones of steel blocks based on the zones defined for the Design Elements in a die. The Design Element Concept was clearly defined in 1989 where the key nodes of the design elements can be treated as design variables for shape optimisation problems. Arora [26] defined two levels of discretisation, the first level corresponded to the finite element model for analysis, and the second level corresponded to the design element model for optimisation. He applied the Design Element Concept to the fillet shape design problem, where his objective was to minimise the volume of the piece and he successfully achieved a reduction of 8.5% from the initial volume.

However, little attention has been given to the use of the Design Element Concept in optimisation. The Design Element was first applied to the optimisation of plate and shell structures [27]. Botkin [27] used this scheme to define the domain of a plate with two holes under tensile load. In his work, he introduced the concept of a plate or shell shape design element. He used the Design Elements to change the plate shape by adjusting the boundaries of the element. This work featured the use of four design elements to capture the fillet plate, there have been fewer studies that use a number of design elements to map a part geometry.

Based on the previous works using the Design Element Concept, no attention has been given to the parameter Design Element Concept, especially on the decision of how the Design Elements may be mapped on to the domain under consideration. Further, the shape design element concept has not been applied in casting process simulations and thus this new application will be discussed in a subsequent chapter.

2.4 Genetic Algorithms and Optimisation

There are a number of optimisation techniques which can be used to assist with the design of complex engineering products, but based on the previous work that has been carried out, it can be concluded that there are two optimisation techniques which have been dominant when coupled with numerical simulation. The previous work also suggested that excellent results have been derived from the two techniques, namely analytical gradient-based optimisation and genetic algorithms.

This section is devoted to reviewing the application of genetic algorithms and evolutionary algorithms to optimisation in manufacturing processes. Genetic algorithms

are completely different from gradient based techniques. They have the potential to perform a wider search and are more likely to identify a global optimum as opposed to a local optimum that may be a characteristic of gradient based schemes. Details concerning genetic algorithms (GAs) are set out in [28], from which the key points are:

A) It can be said that most GA methods have at least the following elements in common: populations of chromosomes, selection according to fitness, crossover to produce new offspring and random mutation of new offspring.

B) The chromosomes (or set of design variables) in a GA population typically take the form of bit strings.

For instance, Castro et al. [29] explored the shape and process parameters optimisation in the metal forging process. They used Genetic Algorithms as an optimisation tool to search for the optimal solution. The chosen design variables were work-piece preform shape and work-piece temperature. The objective function was to reduce the difference between the realised and the prescribed final forged shape. The above works used Finite Element Simulation in the modeling of the forging process. Antonio et. al [30] used genetic algorithms and applied the technique to the optimal design of non-isothermal metal forming processes. Again, the goal was to determine the shape of the first-stage forming tool and the initial work-piece temperature which minimised the gap between the final forged shape and the desired one. Schenk and Hillmann [31] studied the optimisation of the automotive sheet metal forming processes using an evolutionary automatic design (EAD) tool. The EAD is an integrated computer-based systematic approach where the main components of the system are:

A) An automatic parametric tool design generated from the CAD surface data of the sheet metal part.

B) The evolutionary strategy as the optimisation algorithm.

C) The integrated objective function evaluation by applying the implicit finite-element sheet metal forming simulation software package AutoForm-Incremental [32], where a single simulation may take anywhere from a few minutes to several hours of computation on a single processor.

It was pointed out in this work that the automatic parametric die surface generation using the integrated evolutionary algorithm and a specialised objective function were a major contribution to the automatic optimisation of the sheet metal forming processes. It was concluded that from the results obtained, the Evolutionary Automated Design was more efficient than the conventional CAD die surface generation structural design approach.

This has led to the following key findings:

1) GAs suffer from a long computational time to find the optimal solution. However, this can be compensated for by the implementation of parallel computing to speed up the evaluation of the fitness function.

2) GAs are more straight forward to implement where only the definitions of the objective functions and constraints are required in the optimisation process, as opposed to gradient-based optimisation, where the sensitivities of the objective function and constraints must be calculated and supplied to the optimisation routines.

3) GAs have a broader search field due to the mechanisms that are used to drive to optimal solution such as mutation and crossover operators. On the other hand, the

search area of gradient based optimisation is more restricted due to its dependency on the gradients or derivatives to search for the optimal solution.

2.5 Numerical Optimisation Method for Casting Processes

Thermodynamic control of permanent mould phase change processes may be achieved by the placement of cooling channels within the manufacturing die set. This is applicable for example, in injection moulding tools. Only a few researchers have explored the application of optimisation to locate the position of coolant channels within a die as discussed in [33,34,35]. For instance, Tang et al. [33] presented a methodology for optimal design of cooling systems for a multi-cavity injection mold tooling. In this work, the design variables were cooling channel size, locations and coolant flow rate. Powell's conjugate direction with the penalty function optimal method was used to solve the constraint optimal design problem. The objective function was defined to achieve the uniformity in temperature distribution in the parts produced where it is interesting to note that they optimised for the cyclically stable temperature solution. It was found that the optimised diameter of the cooling channels was less than their initial guess, thus the coolant flow rate became larger and as a result the cooling rate was increased. This is because the heat transfer coefficient is proportional to the coolant flow rate and inversely proportional to the diameter of the cooling channel. It was also pointed out that the choice of coolant channel placement has been primarily dependent on the designer's past experience, thus as part geometry becomes more complicated, an experience-based approach becomes less feasible. This work restricted the movement of coolant channels along predefined paths.

Lin (34) investigated the optimum cooling system design of a free-form injection mold using an abductive network which was used to create the equation of the parting-line and the cooling line. He then applied a Simulated Annealing (SA) optimisation algorithm to the abductive network for obtaining the cooling system parameters based on an objective function to secure the minimum warpage in the component parts. Since there were three design variables involved in this work, two of the design variables were fixed in order to find the optimum solution for the remaining design variables. The other design variables were then treated in a similar manner. Subsequently, he applied the same optimisation technique with the same design variables to a die-casting die with a free-form surface [35]. In this work, he successfully optimised the process by achieving minimum deformation in a casting-die. It is also interesting to note again that the coolant channels were moved with respect to a defined path, the so-called cooling line.

Many works have focused on the application of gradient-based optimisation methods to metal forming processes, to the author's knowledge, little attention has been given to the application of analytical gradient-based optimisation to the casting process [36,37]. Work has been done by Tortorelli et. al [36] who coupled the sensitivity analysis with nonlinear programming to optimise the design of a sand casting. In this work, they showed how to eliminate porosity in the casting, by controlling a positive vertical temperature gradient from the centre of the casting to the centre of the riser. This was achieved by changing the shape of the riser neck. They also compared the calculated analytical sensitivities using the DDM with the FDM and the results showed excellent correlation between the sensitivities, thus, proving that the sensitivities computed using the efficient the DDM were correct. In another study, Ebrahimi et al. [37] applied

sensitivity analysis to the optimisation of the investment casting design. In this study, a significant reduction of material was achieved by decreasing the riser volume by approximately 40% and at the same time maintaining directional solidification. They used the DDM to perform the calculation of design sensitivity gradients in their optimisation procedure.

Lewis et al. [38] explored the thermal optimisation of the gravity die-casting processes. In their studies, the optimisation based on thermal control and shape was presented where they successfully eliminated the mushy zones from inside the cast parts. Furthermore, the accuracy of modeling was compared with the examination from experiment where it could be seen that the porous regions were present in the cast part for both cases, thus highlighting the accuracy of the results obtained from simulation. Later, Lewis et al. [39] extended their work on thermal optimisation of the sand casting processes. In this work, they successfully optimised the process through a few numerical examples for 2-D and axi-symmetric sand casting processes where the mushy zones were located in the feeders. In this work, the positions of chills were optimised to remove the mushy zone from inside the cast part. In another work, Lewis and Ransing [40] implemented the optimal design of casting process through interfacial heat transfer coefficients control. A thermal stress model from which the thermo-mechanical analysis of the solidification process was computed to predict an air gap width was used. This allowed an estimate of the interfacial heat transfer coefficients. The result showed that the desired freezing time contours were achieved where the hot spot was successfully eliminated from inside the cast part. However, under some circumstances this can lead to

interface heat transfer coefficients that can not be achieved practically and so this approach has limitations.

Tai and Lin [41] presented a runner-optimisation design study of a die-casting die. In this work, again they used an abductive network to model a die casting process (Temperature and residual stresses). The results obtained from the network modeling were compared with the results from experiment and the results were in close agreement, all within 5% . A year later, Tai and Lin [42] explored the optimal position for the injection gate of a die-casting die using the same optimisation program for casting process. They claimed that by doing so, a significant reduction in the wastage on the cost due to trials of the die could be achieved. The deformation in the cast part was modeled using the abductive network. The comparisons of percentage error between the abductive network and FEM, and abductive network and experiment were within 6% and 15% respectively.

Santos et al. [43] applied the artificial intelligence technique to the continuous casting of steel. In this work, the process parameters were shell thickness at the mould exit, surface temperature at the mould exit, maximum reheating between sprays zones, minimum surface temperature, point of final solidification and surface temperature at the straightening point. The objective of the optimisation was to achieve maximum production rate and the result showed a rise of 10% on the production scale. Syrcos [44] analysed various significant process parameters of the die casting method of $AlSi_9Cu_{13}$ aluminium alloy. However, the alloy composition appears to be inappropriate and it is more likely to be $AlSi_9Cu_3$, most likely attributable to a typographical error in reporting the work. The objective was to achieve the optimum density within the casting. The

process parameters were piston velocity, metal temperature, filling time and hydraulic pressure. The effects of the selected process parameters on the casting density and the subsequent optimal settings of the parameters were accomplished using Taguchi's method. The results indicated that the selected parameters significantly affected the density of the aluminium alloy castings with the highest impact achieved by hydraulic pressure, 48%. The predicted range of optimum casting density was in between 2.749g/cm^3 and 2.7525 g/cm^3.

Based on the above discussions, it is clear that numerical optimisation techniques have not yet been explored for the squeeze forming process. This will be addressed in the following chapters.

2.6 Shape Optimisation Problem

Shape optimisation has become an important technique in the numerical optimisation process due to its capability to change the geometry of the structure domain to obtain an optimal solution. Besides, shape optimisation is a nonlinear process due to the fact that the solution depends implicitly on the coordinates of the structure's geometry. Typically, for large distortion, remeshing is required at each stage of the optimisation iteration. Thus a fully automatic remeshing procedure is necessary to ensure the smooth search for the optimal solution in the given domain without affecting the accuracy of the numerical solution.

The work on shape optimisation using an automatic remeshing procedure was explored by Botkin [45] where he demonstrated the technique of three-dimensional shape optimisation using fully automatic mesh generation. He selected a suspension steering

knuckle. In this work, he discovered that mesh generation contributed a relatively small part of the overall cost of automated design where only 17.5% was spent in mesh generation. Tang et al. [33] implemented successfully the automatic remeshing procedure for shape optimisation in the injection molding process with respect to the positions of the coolant channels, thus, demonstrating the effectiveness of the conventional numerical grid generation to obtain good and accurate optimal solution.

Several researchers have adopted several strategies to avoid using automatic remeshing in shape optimisation. There are two numerical strategies to eliminate the need for an automatic remeshing procedure; by employing mesh-free and fixed-grid methods [46,47]. For example, for the former, Bobaru and Rachakonda [46] formulated a general framework based on a meshfree solution of the non-linear heat transfer equations coupled with a gradient-based optimisation to determine the optimal shape and configuration or spacing between fins in a cooling fin array under natural convection conditions. They employed the Element-Free Galerkin (EFG) method as the analysis method for solving the heat equations for every iteration of the shape optimisation setup. By doing so, the remeshing procedure could be avoided. In fact, they claimed that for a typical shape optimisation problem, remeshing is needed every time a large shape change is attempted. A detailed description of the EFG method can be found in [48]. In brief, a meshless method relies on solution at points within domain, where no element connectivity is needed [49]. Thus, without the mesh, it relaxes mesh generation constraints. This method has been demonstrated to be quite successful in elasticity, heat conduction and fatigue crack growth modeling [50]. However, the achievement of a solution generally requires a longer calculation duration when compared with finite element analysis. Jang et [47]

developed a new remesh-free shape optimisation method based on the adaptive wavelet-Galerkin analysis. In this work, in order to avoid the remeshing process, they embedded the original analysis design domain inside a simple fictitious domain. A detailed description of the fixed-grid finite element method is set out in [51].

For the two methods discussed above, the fixed-grid finite element method by [47] is much easier to implement for shape optimisation than the meshfree method [46]. This is compensated by the fact that when employing the fixed-grid method, the objective function or the constraints may loose differentiability in the situation as discussed in [52] and convergence of gradient-based optimisers can be compromised [46].

Shape optimisation using the Boundary Element Method (BEM) for the numerical analysis coupled with an optimisation techniques has also been addressed. This is due to the fact that mesh generation using the BEM is far easier than the Finite Element Method (FEM). For example, Parvizian and Fenner [53] studied structural shape optimisation by using the BEM. The aim of the work was to find the boundary shape of a structural component under certain loading, to have minimum weight. This work took advantage of simple mesh generation using the BEM which can be used to tackle problems involving geometrically complicated mechanical components. Kita and Tanie [54] investigated the shape optimisation of the continuum structures. Genetic Algorithms were coupled with the BEM to find the optimal solution. In this work, it was highlighted that the Genetic Algorithms can deal with the multi-objective problems easily. It was also argued that computational accuracy using the BEM is better than the FEM due to the fact that mesh distortion does not occur, since the BEM can solve the problem by boundary discretisation alone.

Based on the above discussions, there are a few alternative techniques that can be used to assist with the shape optimisation problem. However, it is worth mentioning that the BEM does not cope with problem involving material nonlinearities well and the more recent methods do not always reaching convergence state. Thus, this highlights the robustness of FE and although it requires remeshing robustness, it will still be used in this work.

2.7 Multi-Objective Optimisation

Recently, many researchers have begun embarking on multi-objective optimisation. This has been driven by the need to facilitate design subject to constraints, some of which will be conflicting. For example, Katayama et. al [55] applied multi-objective optimisation techniques to press forming, where they attempted to eliminate defects such as body wrinkle and fracture simultaneously. In this work, the Sweeping Simplex Technique was used to drive to an optimal solution. Madeira et. al [56] developed a computational model for multi-objective topology optimisation for linear elastic structures where Genetic Algorithms were used as the optimisation tool. Also, a more recent numerical technique, the so-called *'ants colony'* algorithm was applied to the multi-objective optimisation of surface grinding where production cost and production rate were considered in the conflicting requirements [57]. Spallino et.al [58] investigated the multi-objective discrete optimisation of laminated structures using evolution strategies where vertical displacement, rotation and first natural frequency of a cantilever laminated plate were considered in the formulation of the objective function. Again, genetic algorithms were used in [59], for simultaneous optimisation of composite structure considering

mechanical performance and manufacturing cost from the early stage of design of composite laminated plates.

It is apparent that the application of multi-optimisation techniques has not yet been applied widely in casting simulation in general and specifically to the squeeze forming process. It is the intention of this research to cover such analysis and to demonstrate the applicability of multi-objective optimisation in the squeeze forming process.

2.8 Closure

Based on the above literature survey, no work has been done to achieve optimal thermodynamic control of solidification behaviour in the squeeze forming process. Also, the current trend in optimisation of engineering problems highlights the importance of the multi-objective optimisation where different conflicting requirements may be considered to achieve better design. Also application of the Design Element Concept has not yet been explored widely in forming processes.

Thus, in order to obtain high performance parts, optimum thermodynamic control design in the squeeze forming process will be explored through the positions of coolant channels. This will be attempted using Genetic Algorithms optimisation. Also, the work will include multi-objective optimisation of the squeeze forming process due to the prospects that it will bring to achieve optimal solutions with respect to different conflicting requirements. Lastly, the possible reduction in computing demand by using Design Element Concept will be investigated, incorporating analytical design element sensitivity gradients. Emphasise will be given to the application of the Design Element Concept to a die, since it is constructed from a number of Steel blocks.

Due to the complex physical phenomena of the squeeze forming process in which thermal and mechanical response are coupled, the possibility of multiobjective optimisation will be explored, accounting for nonlinearities in the thermal analysis, but being restricted to linear mechanical analysis at this time. In this work, the sequentially coupled thermo-mechanical analysis is employed where the temperature distribution in the die is directly supplied to the mechanical module for the structural evaluation.

References

1. J. Sienz and E. Hinton, 'Reliable structural optimization with error estimation, adaptivity and robust sensitivity analysis', *Computers & Structures*, **64**, 31-63 (1997).
2. N.A. El-Mahallawy, M.A. Taha, E. Pokora and F. Klein, 'On the influence of process variables on the thermal conditions and properties of high pressure die-cast magnesium alloys', *Journal of Materials Processing Technology*, **73**, 125-138 (1998).
3. G. Dour, M. Dargusch, C. Davidson and A. Nef, 'Development of a non-intrusive heat transfer coefficient gauge and its application to high pressure die casting: Effect of the process parameters', *Journal of Materials Processing Technology*, **169**, 223-233 (2005).
4. C.P. Hong, H.F. Shen and I.S. Cho, 'Solidification characteristics in Squeeze Casting of Aluminium Alloys', *Proceedings of the 4th Decennial International Conference on Solidification Processing*, Sheffield, July 1997.

5. S.M. Skolianos, G. Kiourtsidis and T. Xatzifotiou, 'Effect of applied pressure on the microstructure and mechanical properties of squeeze-cast aluminium AA6061 alloy', *Materials Science and Engineering* **A231**,17-24 (1997).
6. T.M. Yue, ' Squeeze casting of high-strength aluminium wrought alloy AA7010', *Journal of Materials Processing Technology*, **66**, 179-185 (1997).
7. M.S. Yong and A.J. Clegg, ' Process optimisation for a squeeze cast magnesium alloy', *Journal of Materials Processing Technology*, **145**, 134-141 (2004).
8. D.Y. Maeng, J.H. Lee, C.W. Won, S.S. Cho and B.S. Chun, 'The effects of processing parameters on the microstructure and mechanical properties of modified B390 alloy in direct squeeze casting', *Journal of Materials Processing Technology*, **105**,196-203 (2000).
9. Z.W. Chen and W.R. Thorpe, 'The effect of squeeze casting pressure and iron content on the impact energy of Al-7Si-0.7Mg alloy', *Materials Science and Engineering*, **A221**,143-153 (1996).
10. F. Cay and S.C Kurnaz, 'Hot tensile and fatigue behaviour of zinc-aluminium alloys produced by gravity and squeeze casting', *Materials & Designs*,2004.
11. C.J. Smithells and E.A. Brandes. Metals reference book. London: Butterworths, 1976.
12. J.H. Lee, C.W. Won, S.S. Cho, B.S. Chun and S.W. Kim, ' Effects of melt flow and temperature on the macro and microstructure of scroll compressor in direct squeeze casting', *Materials Science and Engineering*, **A281**,8-16 (2000).
13. L.J. Yang, 'The effect of casting temperature on the properties of squeeze cast aluminium and zinc alloys', *Journal of Materials Processing Technology*, **140,** 391-396 (2003)

14. B.K. Hwu, S.J. Lin and M.T. Jahn, 'Effects of process parameters on the properties of squeeze-cast SiCp-6061 Al metal-matrix composite', *Material Science and Engineering*, **A207**,135-141 (1996).

15. S.W. Kim, D.Y. Kim, W.G. Kim and K.D. Woo, 'The study on characteristics of heat treatment of the direct squeeze cast 7075 wrought Al alloy', *Material Science and Engineering*, **A304-306**, 721-726 (2001).

16. A. Maleki, B. Niroumand and A. Shafyei, 'Effects of squeeze casting parameters on density, microstructure and hardness of LM13 alloy', *Material Science and Engineering*, **A 428**, 135-140 (2006).

17. E.W. Postek, R.W. Lewis, D.T. Gethin and R.S. Ransing, 'Airgap prediction in the squeeze forming processes', *Computer Methods in Mechanics*, Gliwice, Poland (2003).

18. E.W. Postek, R.W. Lewis, D.T. Gethin and R.S. Ransing, 'Influence of initial stresses on the cast behaviour during squeeze forming processes', *Journal of Material Processing Technology*, **159**, 338-346 (2005).

19. E.J. Haug, K.K. Choi and V. Komkov, ' Design sensitivity analysis of structural systems', London, UK: Academic Press;1986.

20. T.D. Hien and M. Kleiber, 'Computational aspects in structural design sensitivity analysis for statics and dynamics', *Computers & Structures*, **33(4)**, 939-950 (1989).

21. H.J. Antunez and M. Kleiber, 'Sensitivity analysis of metal forming processes involving frictional contact in steady state', *Journal of Material Processing Technology*, **60**, 485-491 (1996).

22. H.J. Antunez, 'Thermo-mechanical modeling and sensitivity analysis for metal-forming operations', *Comput. Methods Appl. Mech. Engrg*, **161**, 113-125 (1998).

23. S.H. Kim and H. Huh, 'Design sensitivity analysis of sheet metal forming processes with a direct differentiation method', *Journal of Materials Processing Technology*, **130-131**, 504-510 (2002).

24. D.E. Smith, D.A. Tortorelli and C.L. Tucker, 'Optimal design for polymer extrusion. Part I: Sensitivity analysis for nonlinear steady-state systems, *Comput. Methods Appl. Mech. Engrg*, **167**, 283-302 (1998).

25. D.E. Smith, D.A. Tortorelli and C.L. Tucker, 'Optimal design for polymer extrusion. Part II: Sensitivity analysis for weakly-coupled nonlinear steady-state systems, *Comput. Methods Appl. Mech. Engrg.*, **167**, 303-323 (1998).

26. J.S. Arora and J.E.B. Cardoso, 'A design sensitivity analysis principle and its implementation into ADINA', *Computers & Structures*, **32(3/4)**, 691-705 (1989).

27. M.E. Botkin, 'Shape optimization of plate and shell structures', *AIAA Journal*, **20(2)**,268-273 (1982).

28. M. Mitchell, 'An introduction to genetic algorithms', Cambridge, London : MIT press, 1996.

29. C.F. Castro, C.A.C. Antonio and L.C. Sousa, 'Optimisation of shape and process parameters in metal forging using genetic algorithms', *Journal of Materials Processing Technology,* **146**, 356-364 (2004).

30. C.A.C. Antonio, C.F. Castro and L.C. Sousa, ' Optimisation of metal forming processes', *Computers and Structures* (2004).

31. O. Schenk and M. Hillmann, 'Optimal design of metal forming die surfaces with evolution strategies', *Computers and Structures*, **82**, 1695-1705 (2004).

32. Autoform Engineering Inc. AutoForm-Incremental reference manual. AutoForm Engineering Inc.; 2003, Available from http://www.autoform.com (2003)

33. L.Q. Tang, C. Chassapis and S. Manoochehri, 'Optimal cooling system design for multi-cavity injection molding', *Finite Elements in Analysis and Design*, **26**, 229-251 (1997).

34. J.C. Lin, 'Optimum cooling system design of a free-form injection mold using an abductive network', *Journal of Material Processing Technology*, **120**, 226-236 (2002).

35. J.C. Lin, 'The optimal design of a cooling system for a die-casting Die with a free form surface', *Int. J. Adv. Manuf. Technol.*, **21**, 612-619 (2003).

36. D.A. Tortorelli, J.A. Tomasko, T.E. Morthland and J.A. Dantzig, 'Optimal design of nonlinear parabolic systems. Part II: Variable spatial domain with applications to casting optimization', *Comput. Methods Appl. Mech. Engrg.*, **113**, 157-172 (1994).

37. S.A. Ebrahimi, D.A. Tortorelli and J.A. Dantzig, ' Sensitivity analysis and nonlinear programming applied to investment casting design', *Appl. Math. Modelling*, **21**, 113-123 (1997).

38. R.W. Lewis, M.T. Manzari, R.S. Ransing and D.T. Gethin, 'Casting shape optimisation via process modelling', *Materials and Design*, **21**, 381-386 (2000).

39. R.W. Lewis, M.T. Manzari and D.T. Gethin, 'Thermal optimisation in the sand casting process', *Engineering Computations*, **18 (3/4)**, 392-416 (2001).

40. R.W. Lewis and R.S. Ransing, 'The optimal design of interfacial heat transfer coefficients via a thermal stress model', *Finite Elements in Analysis and Design*, **34**, 193-209 (2000).

41. C.C. Tai and J.C. Lin, 'A runner-optimization design study of a die-casting die', *Journal of Material Processing Technology*, **84**, 1-12 (1998).

42. C.C. Tai and J.C. Lin, 'The optimal position for the injection gate of a die-casting die', *Journal of Material Processing Technology*, **86**, 87-100 (1999).

43. C.A. Santos, J.A. Spim Jr., M.C.F. Ierardi and A. Garcia, 'The use of artificial intelligence technique for the optimisation of process parameters used in the continuous casting of steel', *Applied Mathematical Modelling*, **26**, 1077-1092 (2002).

44. G.P. Syrcos, 'Die casting process optimization using Taguchi methods', *Journal of Material Processing Technology*, **135**, 68-74 (2003).

45. M.E. Botkin, 'Three-dimensional shape optimization using fully automatic mesh generation', *AIAA Journal*, **30(7)**, 1932-1934 (1992).

46. F. Bobaru and S. Rachakonda, 'Optimal shape profiles for cooling fins of high and low conductivity', *International Journal of Heat and Mass Transfer*, **47**, 4953-4966 (2004).

47. G.W. Jang, Y.Y. Kim and K.K. Choi, 'Remesh-free shape optimization using the wavelet-Galerkin method', *International Journal of Solids and Structures*, **41**, 6465-6483 (2004).

48. T. Belytschko, Y.Y. Lu and L. Gu, 'Element-Free Galerkin Methods', *International Journal for Numerical Methods in Engineering*, **37**, 229-256 (1994).

49. J. Bonet and S. Kulasegaram, 'A simplified approach to enhance the performance of smooth particle hydrodynamics methods', *Applied Mathematics and Computation* **126**, 133-155 (2002).

50. Y.Y. Lu, T. Belytschko and M. Tabbara, 'Element-free Galerkin method for wave propagation and dynamic fracture', *Comput. Methods Appl. Mech. Engrg.* **126**, 131-153 (1995).

51. M.J. Garcia and G.P. Steven, 'Fixed grid finite elements in elasticity problems', Eng. Comput., 16(2), 154-164 (1998).

52. J. Haslinger, R.A.E. Makinen, 'Introduction to shape optimization, *SIAM*, Philadelphia, (2003).

53. J. Parvizian and R.T. Fenner, 'Shape optimisation by the boundary element method: a comparison between mathematical programming and normal movement aprroaches', *Engineering Analysis with Boundary Elements*, **19**, 137-145 (1997).

54. E. Kita and H. Tanie, 'Shape optimization of continuum structures by genetic algorithm and boundary element method', *Engineering Analysis with Boundary Elements*, **19**, 129-136 (1997).

55. T. Katayama, E. Nakamachi, Y. Nakamura, T. Ohata, Y. Morishita and H. Murase, 'Development of process design system for press forming – multi-objective optimization of intermediate die shape in transfer forming', *Journal of Materials Processing Technology*, **155-156**, 1564-1570 (2004).

56. J.F.A. Madeira, H. Rodrigues and H. Pina, 'Multi-objective optimization of structures topology by genetic algorithms', *Advances in Engineering Software*, **36**, 21-28 (2005).

57. J.H. Zhao, Z. Liu and M.T. Dao, 'Reliability optimization using multiobjective ant colony system approaches', *Reliability Engineering and System Safety*, 1-11 (2005).

58. R. Spallino and S. Rizzo, 'Multi-objective discrete optimization of laminated structures, *Mechanics Research Communications*, **29**, 17-25 (2002).

59. C.H. Park, W.I. Lee, W.S. Han and A. Vautrin, 'Simultaneous optimization of composite structures considering mechanical performance and manufacturing cost', *Composite Structures*, **65**, 117-127 (2004).

Chapter 3

Genetic Algorithms

3.1 Introduction

There are several kinds of optimisation algorithms that are readily available to be used by computational researchers to integrate with numerical schemes as discussed in Chapter two. Among the two popular optimisation techniques are Deterministic and Non-Deterministic approaches. The novel aspects of the Deterministic Approach or Gradient Based optimisation will be covered in Chapter five including the Design Element Concept.

In this chapter, the Non-Deterministic optimisation approach will be explored in conjunction with process simulation. Genetic Algorithms (GA) utilise a stochastic approach to find the optimum value of the objective function. Derived from the principles that are applicable to genetics, it has been developed based on a 'survival of the fittest' model whereby only the fittest or best chromosomes will survive to reach the final stage

of the optimisation process. GA works with a population of individuals that represent candidate solutions to a problem. Its general working principle is that the information from previous iterations is used to generate the next approximate best solution based on the application of genetic operators. The algorithm evaluates, selects and recombines members of the population to form succeeding populations.

3.2 Characteristics of Genetic Algorithm based Optimisation

The distinctive characteristics of GA based optimisation are as follows,

1) Genetic Algorithms employ binary coding of design variables and as such are a direct resemblance of the evolution process of living beings.

2) The continuity of the objective function and its derivatives are not required in finding the optimal solution. Only the definition of the objective function is needed. It acts as an environment to find the best solution from the possible design parameters.

3) The initial point in the search direction is generated randomly from a wide range of possible designs.

4) Due to the breadth of the search field, it is computationally most demanding, often requiring a long solution time.

Basically, Genetic Algorithm operators involve manipulation of simple binary operations. There are four main types of operators in Genetic Algorithms that act as manipulators for such binary operations [Appendix I] :

- Mutation
- Crossover

- Cloning
- Selection

A detailed description of these operators is available in many references related to Genetic Algorithms [1,2,3,4]. However, a few terminologies need to be defined before proceeding to the next section. In genetic algorithms, a design variable is known as a gene and a sequence of all design variables is called a chromosome. A set of chromosomes is termed a population and the objective function is called a fitness function.

According to [3], there are a number of Genetic Algorithm architectures, but these can be grouped as serial and parallel. In this research, serial Genetic Algorithms are implemented in the optimisation process. This has been chosen because the finite element analyses in this work are not expensive. It is also the simplest way to use a GA. However, for FE problems such as highly nonlinear structures involving parameter and geometrical nonlinearities, the parallel genetic algorithms are required in order to expedite the calculation process by speeding up the evaluation of fitness function for each population by evaluating them concurrently.

The architecture of the serial algorithm is shown in Figure 3.1. In serial genetic algorithms involving structure and shape, coupled with finite element analysis, the optimisation process is started by the random creation of the population from a wide range of possible designs. A first trial design is then meshed and a finite element analysis executed. Then, a new chromosome is obtained from the GA program to define a variation in geometry and remeshing is performed to facilitate further finite element analysis. The finite element analysis is executed to evaluate the defined fitness function

for each chromosome. After that, the genetic algorithm generates the subsequent population based on the operators and selection mechanisms.

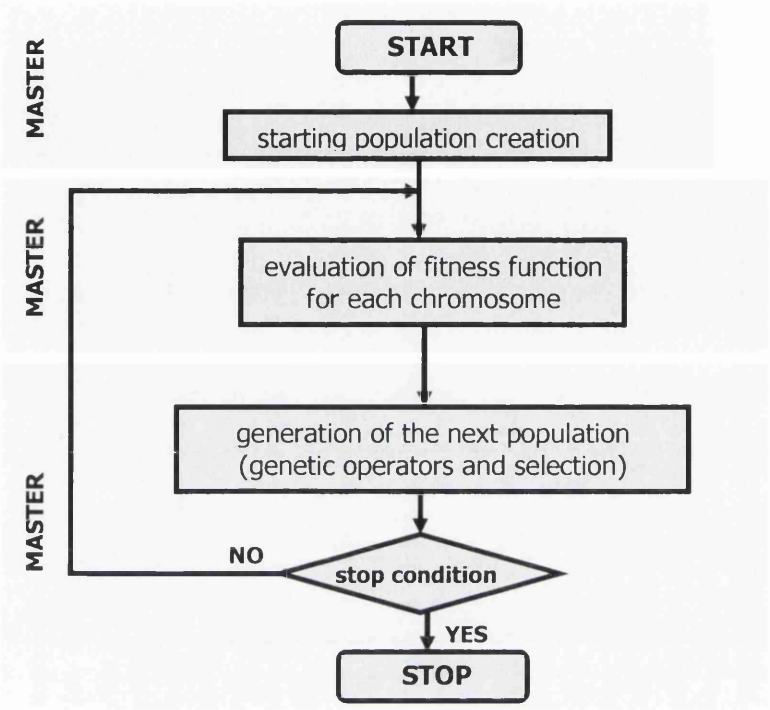

Figure 3.1

Serial Genetic Algorithms flowchart [The flowchart was obtained from [3]]

In this research, the genetic algorithms program GENOCOP has been used [1]. GENOCOP represents GEnetic algorithm for Numerical Optimisation for COnstrained Problems. It is a system that has been developed for convex search spaces (where it has a surface or boundary that curves or bulges outward) and is appropriate for this work due to the search space being large. Also it is not expected to be perfectly smooth and unimodal because of the nonlinearities of the partial differential equation and there are many

possibilities that the design variables will be on the same positions with the same contour of temperature distribution.

3.3 Modelling of Transient Nonlinear Heat Conduction.

There are a number of commercial casting codes available to simulate the casting process. These include advanced features that are directly relevant to the casting process and popular examples include MAGMAsoft and Procast [5,6]. However, these codes do not allow integration with the GA algorithm program, thus, source code having limited, but sufficient capability was developed and Finite Element Simulations were undertaken as discussed below.

It is appropriate at this point to summarise the basis of the finite element analysis that will be coupled with the GA optimisation approach. Simulation of all forming processes is particularly demanding since they are inherently complex and non linear. The cooling and solidification cycle in the casting process can be described by the transient energy equation which in the absence of convection may be written [7],

$$\nabla \cdot [k(T) \nabla T] + Q = \rho c(T) \dot{T} \qquad (3.1)$$

where k is the conductivity, T is the unknown temperature field, Q is the heat generation, ρ is the density, c is the specific heat and $\dot{T}$ is the derivative of temperature with respect to time.

In equation 3.1, the conductivity and heat capacity are temperature dependent.

Boundary conditions are required in time and space, thus initial, Dirichlet and Neumann boundary conditions for this system are described as follows [8] :

Initial boundary condition

$T(r,\theta,z,0) = T_0(r, \theta,z)$ in Ω

where r, θ and z are the coordinates axis, T_0 is the prescribed temperature distribution in Ω and Ω is the domain.

Dirichlet boundary Condition

$T = T(r,\theta,z,t)$ on Γ_T

where r, θ and z are the coordinates axis, t is the time and Γ_T is the boundary curve where the essential boundary condition is applied.

Neumann boundary condition

$$q = -k\frac{\partial T}{\partial n} \quad \text{on } \Gamma q$$

where q is the heat outflow in the direction n normal to the boundary Γq, k is the conductivity, $\frac{\partial T}{\partial n}$ is the partial derivative of temperature in normal direction and Γq is the boundary curve where natural boundary condition is applied.

In the case of phase transformation, the enthalpy method was applied,[7]. The essence of the application of the enthalpy method is the involvement of a new variable, enthalpy, denoted by H, such that, $\rho c = dH/dT$, equation 3.1 is transformed to the following form

$$\nabla \cdot [k(T)\nabla T] + Q = \frac{\partial H}{\partial T}\dot{T} \qquad (3.2)$$

The definition of the enthalpy for a metal alloy is given as follows [7]

$$H(T) = \int_{T_r}^{T_s} \rho c_s(T)dT + \rho L + \int_{T_s}^{T_l} \rho c_f(T)dT + \int_{T_l}^{T} \rho c_l(T)dT \qquad (T \geq T_l) \qquad (3.3)$$

$$H(T) = \int_{T_r}^{T} \rho c_s(T)dT + \int_{T_s}^{T} \left(\rho \left(\frac{dL}{dT} \right) + \rho c_f(T) \right) dT \qquad (T_s \leq T \geq T_l) \qquad (3.4)$$

$$H(T) = \int_{T_r}^{T} \rho c_s(T)dT \qquad (T \leq T_s) \qquad (3.5)$$

where subscripts l and s refer to liquid and solid respectively, ρ is the density (constant), L is the latent heat. C_f is the specific heat in the freezing region and T_r is a reference temperature lower that T_s, generally 25°C.

Enthalpy may be computed in a number of ways, however, due to its improved accuracy in tracking the phase change inside the metal alloy, the following averaging formula [5] was used for the estimation of the enthalpy variable.

$$\rho c \cong \left(\frac{(\frac{\partial H}{\partial x})^2 + (\frac{\partial H}{\partial y})^2}{(\frac{\partial T}{\partial x})^2 + (\frac{\partial T}{\partial y})^2} \right)^{\frac{1}{2}} \qquad (3.6)$$

By employing the weighted residual method and the standard Galerkin technique [8], Equation 3.2 is transformed to yield the following linear system of equations [7],

$$\boldsymbol{C(T)\{\dot{T}\} + K(T)\{T\} = F} \qquad (3.7)$$

where $\boldsymbol{K}$ and $\boldsymbol{C}$ are the conductivity and heat capacity matrices. $\boldsymbol{F}$ is the thermal loading vector. For an axi-symmetric framework, $\boldsymbol{C}$, $\boldsymbol{K}$ and $\boldsymbol{F}$ are defined as follows,

$$\boldsymbol{C}(T) = \sum_{e} \int_{\Omega_e} \rho c N_i^e N_j^e d\Omega \tag{3.8}$$

$$\boldsymbol{K}(T) = \sum_{e} \int_{\Omega_e} \left[k \frac{\partial N_i}{\partial r} \frac{\partial N_j}{\partial r} + k \frac{\partial N_i}{\partial z} \frac{\partial N_j}{\partial z} \right] d\Omega + \sum_{e} \int_{\Gamma_{he}} N_i h_c N_j d\Gamma \tag{3.9}$$

$$\boldsymbol{F} = \sum_{e} \int_{\Gamma_{he}} N_i^e h_c T_\infty d\Gamma - \sum_{e} \int_{\Gamma_{qe}} N_i^e q d\Gamma \tag{3.10}$$

$$d\Omega = 2\pi r dr dz \tag{3.11}$$

$$d\Gamma = 2\pi r (dr^2 + dz^2)^{1/2} \tag{3.12}$$

For the conductivity matrix, the first term is due to the diffusive part whereas the second is due to convection, either to the surroundings or to the coolant channels.

A finite difference approximation was used for the temporal discretisation [7].

$$[\frac{C_{n+\alpha}}{\Delta t} + \alpha K_{n+\alpha}](T_{n+1}) = [\frac{C_{n+\alpha}}{\Delta t} - (1-\alpha) K_{n+\alpha}](T_n) + (F_{n+\alpha}) \tag{3.13}$$

and a Crank Nicolson scheme [7] where α=0.5 was used for the time marching scheme. Crank Nicolson scheme was chosen due to its balance between accuracy and stability as opposed to other schemes such as Forward Euler and Backward Euler schemes.

3.3.1 Interfacial Heat Transfer between Two Parts in Contact

Modeling of the heat transfer phenomenon between the die and casting plays an important role in obtaining accurate simulation of the cooling behaviour in a casting component. This is particularly relevant for the squeeze forming process in which control of thermal response through application of a pressure cycle is critical to process

success. Interfacial heat transfer may be handled in a number of ways within a numerical scheme, for example in a finite element formulation thin elements may be introduced at this interface, where they act as a layer between casting and die. It is also possible to use a coincident node approach that represents an interfacial element of zero thickness. In this work, the heat transfer at the die-casting interface is modeled using a convection heat transfer type mechanism [9]. This has been done to deal with the situation where nodes in the die and casting are not constrained to be coincident, hence simplifying the finite element meshing and remeshing requirements.

It is necessary that the heat transfer mechanism at the interface is explained in depth as it is directly relevant to the works in the subsequent chapters. Its detailed implementation will be explained in the following section.

One of the attractive features in implementing this model is that there is no need to introduce additional elements. The interface surfaces interact naturally with each other. In two dimensions, any two parts in contact with each other, for example a casting and its die, are separated by an interface boundary line. This is illustrated in Figure 3.2.

The interface boundary can be divided into a number of segments and these segments can capture different interface conditions. Common to all segments is that one part of the interface represents the casting surface and the other is the die. During analysis, strategically each boundary segment in the die, the corresponding boundary segment in the casting acts as a reference condition and vice versa. In detail, at the interface boundary, the reference temperature in the die is obtained by taking the averaged closest two nodal temperatures at the casting interface. This approximates the die reference

temperature at the interface. The same implementation is applied for the reference temperature in the casting by considering the averaged closest two nodal temperatures at the die interface.

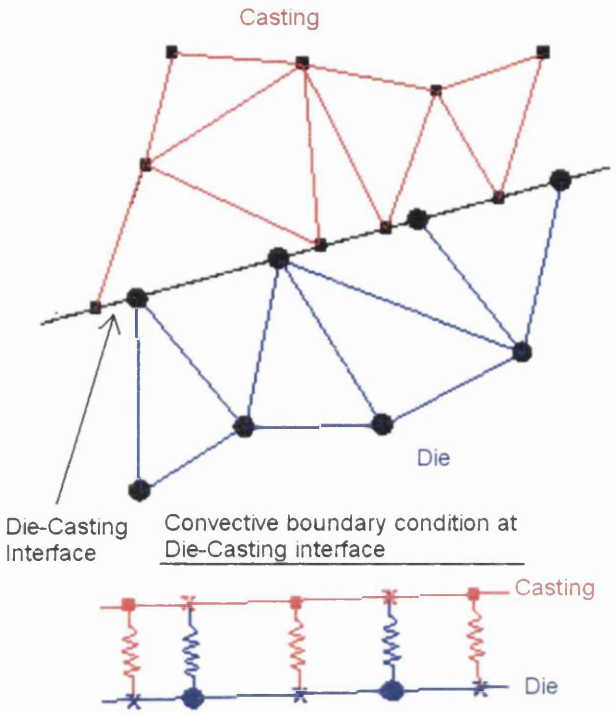

Figure 3.2

Schematic of interface model

Shape optimisation involves changes to geometry and consequent remeshing during the optimisation process. The success of an automatic remeshing procedure in the shape optimisation process is largely dependent on the selection of the mesh generator. In this research, the public domain Triangle 2D mesh generator has been used due to its robustness, efficiency and good quality meshes together with convenient integration with the GA and finite element analysis scheme [10]. However, in this work, FE mesh sensitivity studies have not been performed.

3.4 Validation

The Finite Element source code that was written by Manzari [9] to simulate the sand casting process was used as a starting point. This required modification to analyse the combined thermal and stress behaviour of the squeeze forming process and integrating this with the mesh generator and GA. The first stage will be concerned with validating the scheme as far as possible.

Although it is easy to validate the finite element analysis code itself, it is difficult to validate the overall scheme due to the sparsity of documented case studies with which to perform validation. Lewis et al. [9,11] used gradient-based optimisation to optimise the casting processes, where the case studies available at that time were principally obtained from researchers in the USA [12]. In the following works, firstly, the validation will be performed based on studies associated with traditional casting processes and this will be followed by exploring its application in the squeeze forming process.

To validate the application of the genetic algorithm optimisation approach, two casting optimisation studies have been undertaken. These have been derived from work on gradient based optimisation strategies where both focus on the sand casting process. These have been chosen since in each case, shape and process parameter settings are explored, thus providing opportunity to validate these features using the current genetic algorithm approach.

The main purpose of the work in [9] was to achieve directional solidification through sizing of the feeder system. The current work will achieve directional solidification through positioning of the cooling system. The case studies will infer validation of the scheme by successfully eliminating the hot spot from inside the casting to the feeder.

3.4.1 Axi-Symmetric Casting Process Example

In this section, the thermal optimisation of an axisymmetric casting is undertaken. It is based on the sand casting study [9], but it is presented as a gravity die-casting as shown in Figure 3.3. It represents an axisymmetric part casting within a steel die that incorporates a number of coolant channels as a method of heat removal. The aim of this case study is to achieve directional solidification in the casting and this will be successfully achieved by eliminating the hot spot from inside the casting to the feeder.

In this work, an Aluminium alloy (LM25) was used and the initial temperature of the casting metal was 730°C. The die was a carbon steel and this has an initial temperature of 300°C. These values are typical and have been drawn from industrial practice as reported for example in [13,14]. The heat transfer conditions in the coolant system corresponds to a heat transfer coefficient and reference temperature of 1000W/m^{2}K and 20°C respectively [Appendix II] with water used as coolant liquid and heat is removed from the external surfaces in accordance with a heat transfer coefficient to 25W/m^{2}K and an ambient temperature of 25°C representing free convection [9,15]. This is quite a high value, where a typical heat transfer coefficient value for natural convection to the surrounding is around 10W/m^{2}K. However, in this work, this value was employed since it is likely that some airflow around the die occurs. Besides, heat is extracted dominantly through the coolant channels. The constant conductivity values of 186.3W/mK and 50W/mK and densities of 2790kg/m^3 and 7850kg/m^3 [16,17] were assumed for the casting and steel die, respectively. The temperature dependent enthalpy curves for casting and die are itemised in Tables 3.1 and 3.2. Very good contact was assumed at the die and casting interfaces, hence an interfacial coefficient of 5000W/m^{2}K was applied [15,16].

Four coolant channels were used having a fixed geometry; only their position may be varied. Their initial locations are shown in Figure 3.3 to show the exact dimension of the coolant channels. However, for genetic algorithm-based optimisation, the initial positions of the design variables are selected randomly by the GA program from a large possible number of design solutions.

Temperature (°C)	Enthalpy (J/kg°K)
0	0
550	0.60×10^6
615	1.07×10^6
800	1.27×10^6

Table 3.1

Temperature dependent enthalpy curve for metal. (The tabulated results were obtained from [18])

Temperature (°C)	Enthalpy (J/kg°K)
0	0
200	0.08×10^6
400	0.19×10^6
800	0.54×10^6

Table 3.2

Temperature dependent enthalpy curve for die. (The tabulated results were obtained from [19])

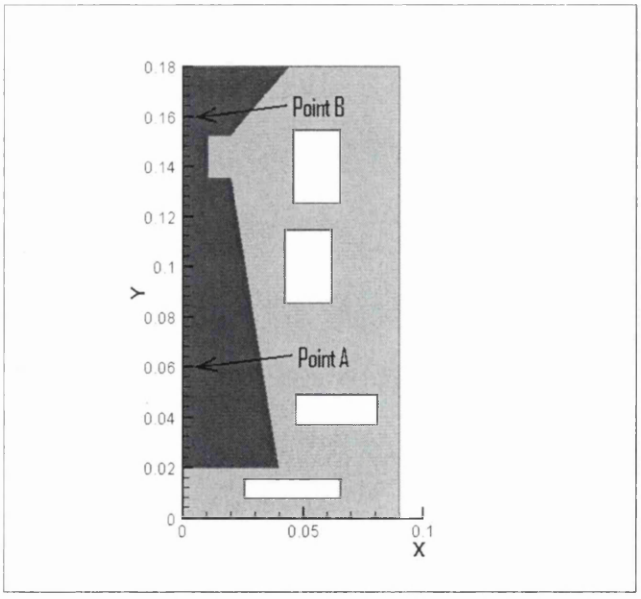

Figure 3.3

Location of Points A and B

3.4.1.1 Objective Functions

In this work, there are a number of objective functions that may be defined to optimise the system through the coolant system position. However, because the purpose of this section is to validate the thermal optimisation component, the functions for Case studies 1 and 2 have been chosen to be identical to those used in [9]. To achieve directional solidification, the objective function may be defined as minimising the following;

Case study 1

$$F(x) = T(A)-T(B)+200 \qquad (3.14)$$

where points A and B are located in the casting and feeder respectively as shown in Figure 3.3. This has been chosen to ensure directional solidification from the centre of the casting to the centre of the feeder. The objective function for Case study 2 was selected from [9], which is given as minimising the following, where instead of 200, the coefficient value is 30. This was chosen to see the difference in the results obtained from almost similar characteristics of the objective function for Case study 1, where the only difference is the coefficient values.

Case study 2

$$F(x) = T(A)-T(B)+30 \qquad (3.15)$$

For Case study 3, the objective function may be defined as minimising,

Case study 3

$$F(x)=\frac{1}{\Omega_C}\int_{\Omega c}[(T_{\max}-T_{ave})^2+(T_{\min}-T_{ave})^2]^{1/2}d\Omega \qquad (3.16)$$

where Ω_C is the casting domain. T_{max} and T_{min} are the maximum and minimum temperatures in the casting. T_{ave} is the average temperature in the casting, where it is calculated by summing up the average temperatures of the elements in the casting (T_C) and dividing this by the total number of elements as shown by the equation below,

$$T_{ave} = \frac{\sum_{i=1}^{NC} T_C}{NC} \qquad (3.17)$$

The first two objective functions have been developed to maintain a positive temperature gradient from the centre of the feeder to the centre of the casting during the solidification process. The constant terms (200 and 30) in equations 3.14 and 3.15 influence the temperature gradient that are set up within the casting. The Case study 3 (equation 3.16) implies a near simultaneous solidification through the entire casting section. This is in addition to the validation work and it is interesting to explore it since the achievement of near simultaneous solidification through a casting will also be beneficial since for a casting of near uniform section it also implies near identical cooling rates with consequent consistency of mechanical properties. Furthermore, if cooling rate can be controlled, this is particularly relevant to premium squeeze formed parts.

3.4.1.2 Design Variables and Constraints

Design variable constraints for the coolant channel position can be represented as follows and this assures that the coolant channels are located within the die space. The additional constraint of preventing coolant channels overlapping the part has not been included at this time.

x_i = X-coordinates of coolant channel i (i=1,2,…,4)

$y_{(j+4)}$ = Y-coordinates of coolant channel j (j=1,2,…,4)

Only inequality constraints are applied to the coolant channel position design. These constraints are of the form

$x_k - x_{min} \geq 0$

$x_{max} - x_k \geq 0$ (k=1,2,…,8)

3.4.1.3 Numerical Example of Axi-Symmetric Casting Process

Figure 3.4 shows the datum case in which no coolant channels are included. This shows the location of the final mushy zone in the casting which signifies the position of the last point to solidify and this contour is closely identical to that described in [9] for the sand casting process, only the duration is different due to the different thermophysical properties of the sand mould. This confirms the correct functioning of the thermal analysis. Figure 3.5 shows the corresponding result obtained in [9] for sand casting process, where the mushy zone remains in the casting. Figure 3.6 shows the location of the mushy zone inside the feeder and the final position of coolant channels for Case study 1. Figure 3.7 shows the location of the mushy zone inside the feeder after optimisation for the results obtained in [9]. Figure 3.8 shows the location of the mushy zone inside the feeder and final position of the coolant channels for Case study 2 and Figure 3.9 shows the location of the mushy zone inside the casting and final position of the coolant channels for Case study 3.

From Case study 1, it may be observed that the number of coolant channels was reduced to three from four to achieved directional solidification. From Case studies 1 and 2, it may also be observed that the same optimal solution or location of the mushy zone

was achieved through coolant channel positions that are located within the same die zone. Thus the different objective functions lead to similar cooling system designs and this is expected since the formulation of the objective functions for both case studies has almost similar characteristics, the only difference is the coefficient values. This implies that the obtained solutions in terms of mushy zone location are not sensitive to the choice of the defined objective function for Case studies 1 and 2.

Figures 3.10 and 3.11 show the location of the mushy zone inside the feeder and the final position of coolant channels for the proposed practical solution for Case studies 1 and 2. Figure 3.12 shows the location of the mushy zone inside the casting and final position of the coolant channels for the proposed practical solution for Case study 3. Clearly the 'practical solutions' reflect the results from the 'pure GA' optimisation solutions.

From Case study 3, the mushy zone remains inside the casting. This is because the formulation of the objective function was aimed at achieving near simultaneous solidification. However, the coolant channels were positioned to follow the contour of the casting.

For the three case studies, the duration was about the same, requiring about 12*s* to solidify under the configuration that was achieved for the final optimal solutions as shown in Figures 3.6, 3.8 and 3.9. Also, the objective function evaluations for the three case studies had a very small difference in terms of the calculation time.

The calculation itself was run entirely within memory and required 490 minutes on a Pentium 4 processor running at 2.80 GHz and 1.0GB of RAM. The solutions were achieved in 70 generations.

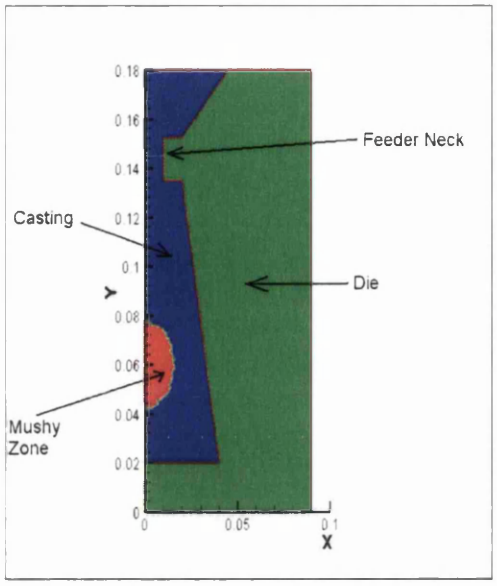

Figure 3.4

Location of the mushy zone using the die without coolant channels

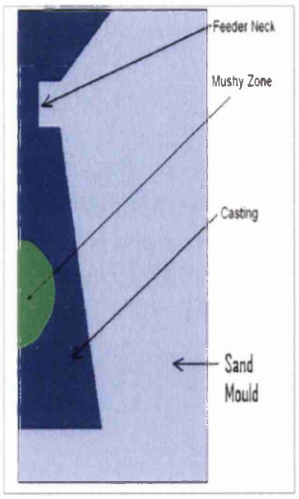

Figure 3.5

Location of the mushy zone in the casting before optimisation for sand casting process. [The picture was obtained from [9]]

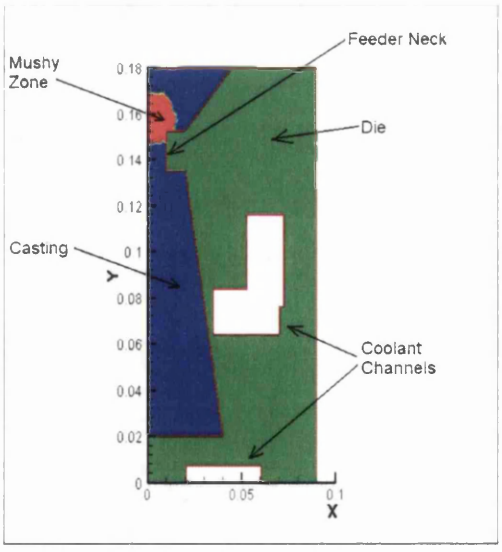

Figure 3.6

Location of the mushy zone in the feeder using the die with coolant channels for Case study 1

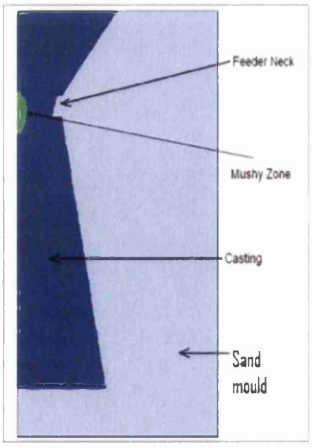

Figure 3.7

Location of the mushy zone in the feeder after optimisation for sand casting process. [The picture was obtained from [9]]

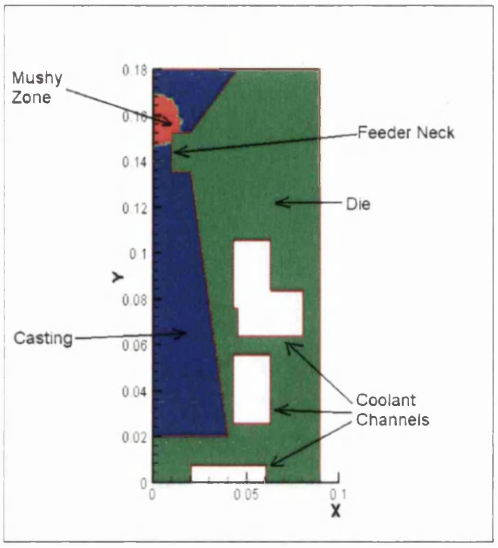

Figure 3.8

Location of the mushy zone in the feeder using the die with coolant channels for Case study 2

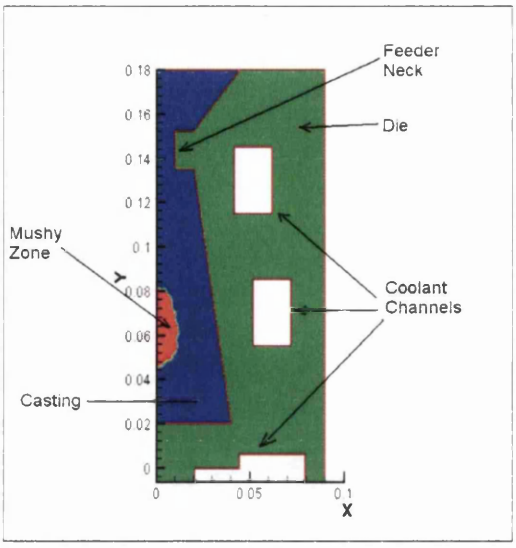

Figure 3.9

Location of the mushy zone in the casting using the die with coolant channels for Case study 3

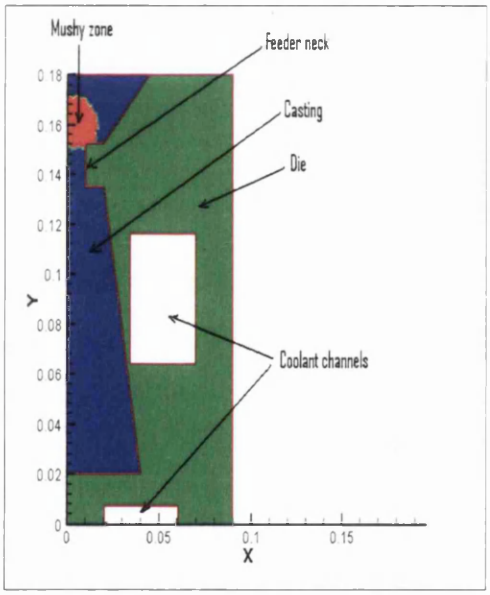

Figure 3.10

Location of the mushy zone in the feeder using the die with coolant channels for practical solution based on Case study 1

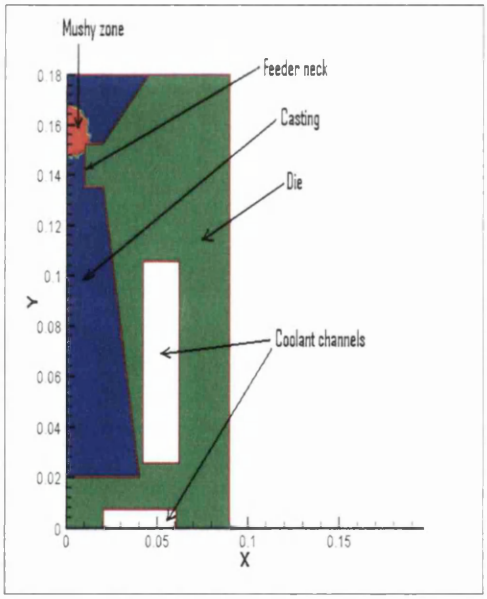

Figure 3.11

Location of the mushy zone in the feeder using the die with coolant channels for practical solution based on Case study 2

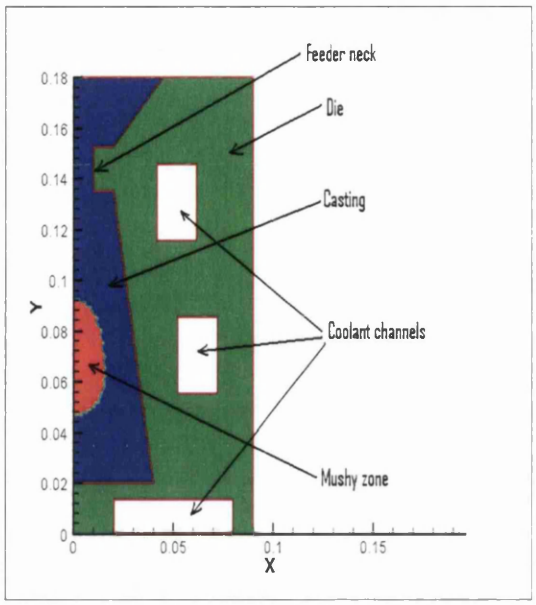

Figure 3.12

Location of the mushy zone in the feeder using the die with coolant channels for practical solution based on Case study 3

3.4.2 2D Casting Process Example

The thermal optimisation of a second 2D non-axisymmetric gravity die-casting is presented and the case study is shown in Figure 3.13. It represents a 2D part casting within a steel die that incorporates coolant channels as a method of heat removal. The aim of this case study is similar to the first, which is to achieve directional solidification in the casting and this will be successful if it eliminates the mushy zone from inside the casting. This is slightly different from the work done in [9] for gravity sand in which steel blocks form chills to provide local thermodynamic control. However the work in [9] will be used for qualitative validation reflected in similarity of solidification contour as a consequence of such thermodynamic control.

In this case, the initial temperature of the casting was 730°C and the casting material was aluminium LM25 whereas the die is a carbon steel having an initial temperature of 250°C [13,20]. The heat transfer conditions in the coolant system corresponds to a heat transfer coefficient and reference temperature of 1000W/m^{2}K and 20°C respectively [Appendix II] with water used as a coolant liquid and heat is removed from the external surfaces (excluding the exterior surface at the bottom of the die) in accordance with a heat transfer coefficient of 25W/m^{2}K and an ambient temperature of 25°C [9,15].

3.4.2.1 Objective Functions

In a first analysis and to achieve directional solidification, the objective function defined in equation 3.14 for Case study 1 above was used where points A and B are located in the casting and feeder respectively as shown in Figure 3.13.

In a second analysis, the objective function is similar to the objective function defined for Case study 3 above in equation 3.16.

This is similar to the first validation, however it tests the capability to optimise planar as opposed to axisymmetric shapes. It also explores more directly the possibility of achieving thermodynamic control through cooling system position.

3.4.2.2 Design Variables and Constraints

Design variables for the coolant channels position and constraints are similar to the ones described in the previous section.

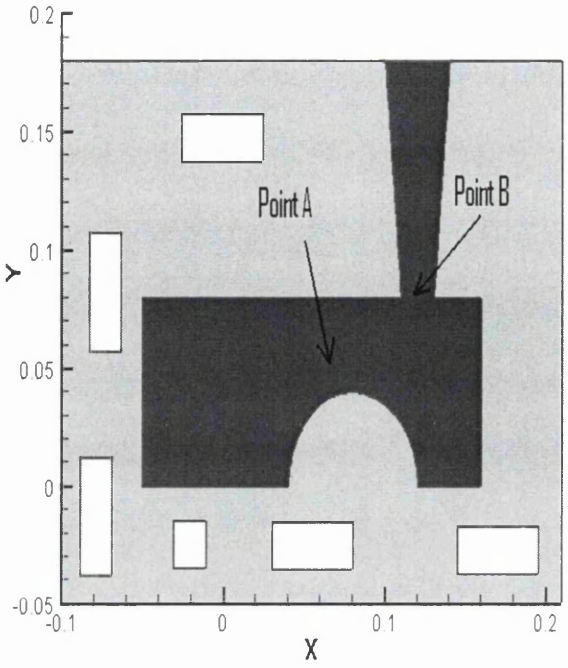

Figure 3.13

Location of Points A and B for 2D
casting process problem

3.4.2.3 Numerical Example of 2D Casting Process

Figure 3.14 shows the location of the mushy zone in the casting which signifies the position of the last point to solidify. This was obtained by using a die without coolant channels. Figure 3.15 shows the location of the mushy zone inside the feeder and final positions of the coolant channels for the first analysis run, corresponding to the objective function designated Case study 1. Figure 3.16 shows the location of the mushy zone, which was eliminated from inside the casting for the results obtained in [9]. From the two figures, the similarity of the positions of chills and the positions of the coolant channels can be observed. Figure 3.17 shows the location of the mushy zone and the final position of coolant channels for Case study 3.

For Case studies 1 and 3, the duration to achieve solidification was at t= 108s to reach the final optimal solutions as shown in Figures 3.15 and 3.17. Also, the objective function evaluations for the case studies had a very small difference in terms of the calculation time.

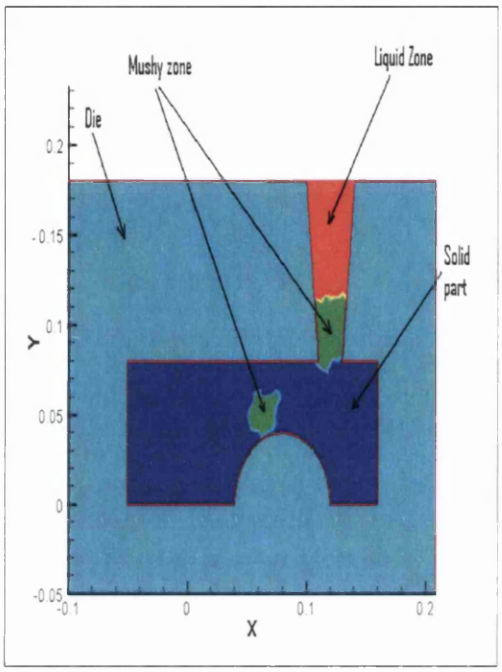

Figure 3.14

Location of the mushy zone (green) using the die without coolant channels

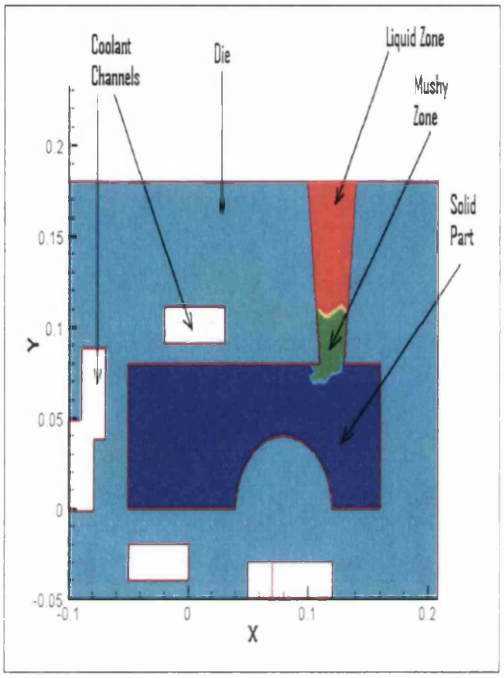

Figure 3.15

Location of the mushy zone (green) using the die with coolant channels for Case study 1

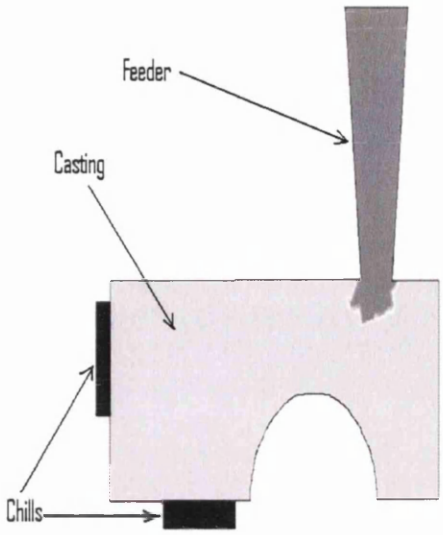

Figure 3.16

The mushy zone was eliminated from inside the casting for the result obtained from [9].

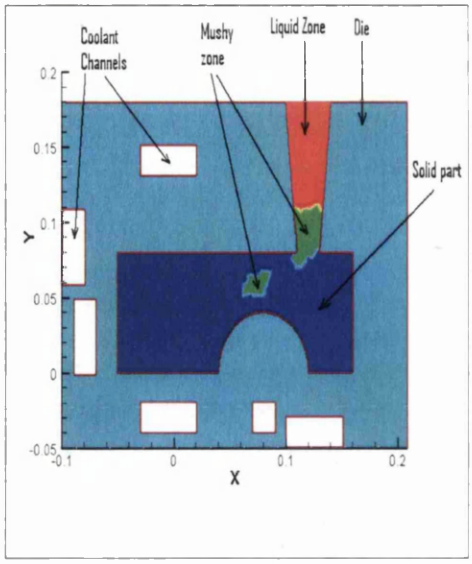

Figure 3.17

Location of the mushy zone (green) using the die with coolant channels for Case study 3

From the validation aspect, it can be seen that the agreement between the pattern of the coolant system design and the position of chills obtained in [9] is closely similar. This confirms that the design solution is good and this also applies to the design solution for Case study 3, where the coolant channels are positioned to nearly follow the geometry of the casting. However, the solution obtained for simultaneous solidification for the objective function designated Case study 3 may not be so good since the smaller gradients also lead to internal freeze off as opposed to final freeze off in the filling system.

3.5 Simulating Solidification in the Squeeze Forming Process

Squeeze forming is being applied to produce complex shape components and has significant benefits over other forming processes as discussed in Chapter two. Also there are a number of parts that exhibit rotational symmetry which are commonly being manufactured in the industry, thus, the axisymmetric model of the squeeze forming process will be used in the following case studies.

The aim of this section is to explore techniques to automatically optimise the squeeze forming process from a thermodynamic view point through appropriate positioning the coolant channels in the die and to explore the influence of process parameters and operation on their positioning. This will include for instance the effect of pressurisation within the cycle and the impact of a cyclic analysis that captures 'process warm up'.

There are a number of process parameters that may be explored to optimise the squeeze forming process. For a prescribed part shape these include overall die dimensions and the cooling system size and position. The current work focuses on the latter and will investigate a method whereby coolant channel position may be optimised, subject to a prescribed heat transfer coefficient that is determined by the flow regime within the coolant channels.

3.5.1 Objective Functions

The axisymmetric squeeze formed part is shown in Figure 3.18 and represents a wheel component. Based on industrial information [21], the initial temperature of the casting was 700°C. The casting material is Aluminium LM25 whereas the die is a steel H13. This has an initial temperature of 200°C, the heat transfer conditions in the coolant

system corresponds to a heat transfer coefficient and reference temperature of 1000W/m^{2}K and 100°C respectively [Appendix II]. The latter is appropriate for oil as a coolant, often supplied at a preset temperature in the cooling system. Heat is removed from the external surfaces in accordance with a heat transfer coefficient to 25W/m^{2}K and an ambient temperature of 25°C [9,15]. The constant conductivity values of 186.3W/mK and 25W/mK and densities of 2790kg/m^3 and 7800kg/m^3 were assumed for the casting and steel H13 die [16,22], respectively. The temperature dependent enthalpy curves for casting and steel H13 die are itemised in Tables 3.3 and 3.4. In this example, a number of coolant channels were given a priori. Six coolant channels were used having a fixed geometry; only their position may be varied. These are shown in Figure 3.18. Very good contact is assumed at the die and casting interfaces, hence an interfacial coefficient of 5000W/m^{2}K [15,16] was applied.

Temperature (°C)	Enthalpy (J/kgK)
0	0
550	0.60×10^6
615	1.07×10^6
800	1.27×10^6

Table 3.3

Temperature dependent enthalpy curve for casting. (The tabulated results were obtained from [18])

Temperature (°C)	Enthalpy (J/kgK)
0	0
200	1.424×10^5
400	2.488×10^5
800	5.696×10^5

Table 3.4

Temperature dependent enthalpy curve for steel H13 die. (The tabulated results were obtained from [18])

There are a number of objective functions that may be defined to optimise coolant system position. To attempt to achieve near simultaneous solidification of the casting, the objective functions may be defined as minimising the temperature differences at strategic

points within the casting. A number of points may be chosen for this, however for the purpose of illustration, two case studies are defined below.

Case study 4

$$F(\mathbf{x})=(T_A-T_B)^2 \tag{3.18}$$

Case study 5

$$F(\mathbf{x})=(T_C-T_D)^2 \tag{3.19}$$

The locations of points A, B, C and D are shown in Figure 3.18 and these are defined in order to try to achieve near simultaneous solidification in the casting by defining only two positions in the casting component as control points. Following on from the need to achieve near simultaneous solidification, the objective function defined for Case study 3, equation 3.16 may also be considered. As explained above, this attempts to achieve uniform solidification in a global rather than local (two point) sense.

Casting processes stabilise as the cycle is repeated and the die achieves a stable thermal history. Optimisation studies that include both single and cyclic simulations will be investigated. First, the non-cyclic optimisation of the squeeze forming process will be explored and this will be followed by optimisation that includes a cyclic analysis in order to show how coolant system design responds as the die temperature stabilises. Comparison will be done for cycles 1, 5 and 10. At each cycle, the temperature distribution in the die from the previous cycle was used for the thermal analysis for the next cycle. The initial temperature distribution in the casting for every cycle was held constant at 700°C. In the last section of this chapter, the impact of interfacial heat transfer coefficient changes during the cycle will be performed in order to approximate pressure

effects and how this may affect the coolant system position. This was calculated for a planar 2D model for the same section geometry as the wheel component. The same initial and boundary conditions as the axisymmetric problem were applied.

3.5.2 Design Variables and Constraints

Figure 3.19 shows the numbering of coolant channels. Design variables for the coolant channels position and constraints are similar as described in the previous section.

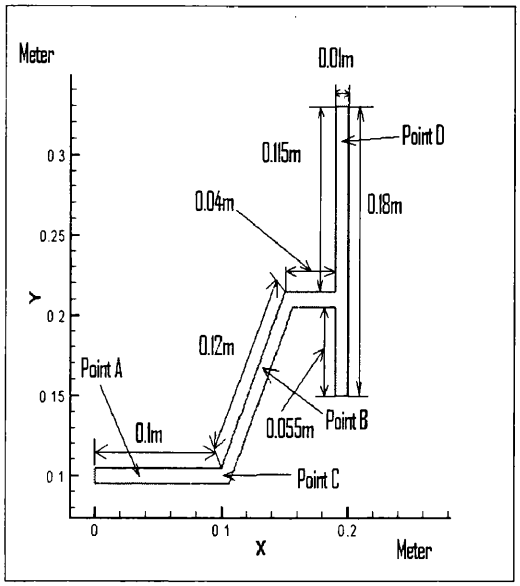

Figure 3.18

Location of points A, B, C and D and also the dimension of the casting

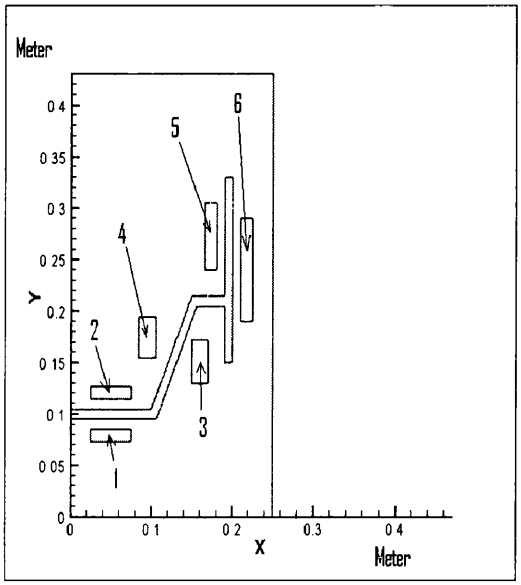

Figure 3.19

Coolant channels numbering

3.5.3 Non Cyclic Optimisation

The thermal optimisation of an axisymmetric squeeze formed part is presented. Figure 3.20 shows the transient thermal solution in the die (left) and casting (right) at t=50s for the initial positions of coolant channels. This is chosen because at 50s all the casting will

be solid. Figures 3.21 and 3.22 show the transient thermal solutions in the die (left) and casting (right) at t=50s and optimal positions of coolant channels for Case studies 4 and 5. The minimum objective function values obtained for both case studies were 0.01°C and 0.329°C respectively, where the obtained objective function values almost reached the global optimum which is at 0°C. Figures 3.23 and 3.24 show the iso-solidification contour in the casting for Case studies 4 and 5, where the casting solidified faster for Case study 5 when compared to Case study 4 and this is because one of the coolant channels was positioned very near to the casting. Figure 3.25 shows how the objective function decays as successive generations are processed, achieving a near zero value for the function.

Figure 3.26 shows the transient thermal solutions at t=50s and optimal positions of coolant channels for Case study 3. It can be seen from previous case studies that the control provided by the 2 point difference function does not achieve near simultaneous solidification. Even though, one of the case studies nearly achieved the objective, the high temperature distribution was not fully concentrated surrounding the casting. This can be seen for the results obtained for Case study 5, where the temperature distribution in the casting was not uniform, especially in the right region where one of the coolant channels was positioned near the part. For the results obtained for Case study 4, the temperature distribution in the casting was more uniform than the results obtained for Case study 5. However, the result obtained for Case study 3 was the best. Thus to achieve near simultaneous solidification in the casting, there is a need to use the objective function which reflects the whole domain, rather than focusing between the two points in the casting.

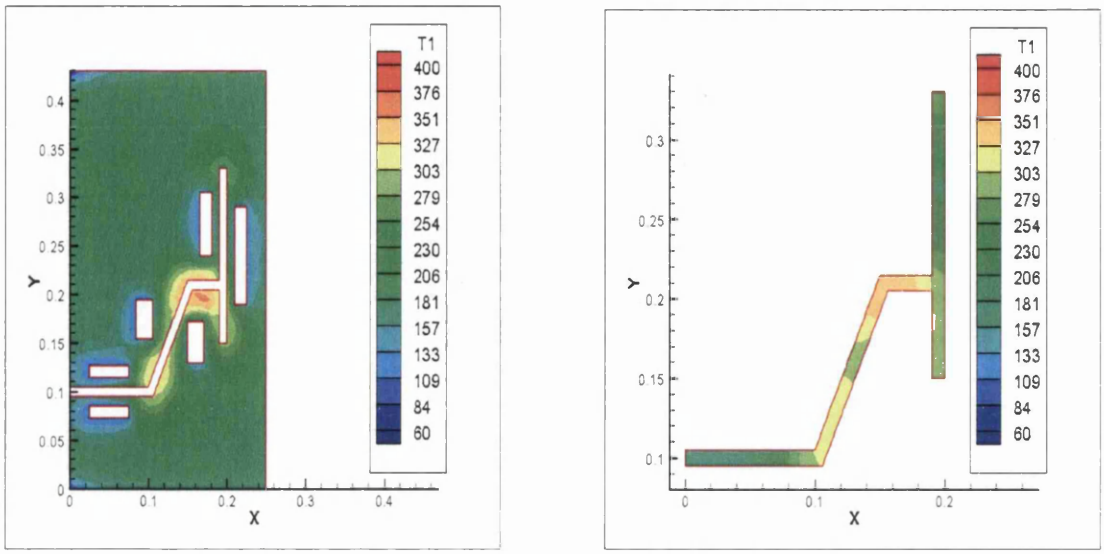

Figure 3.20

Temperature distribution in the die and casting at t=50s for the initial position of coolant channels

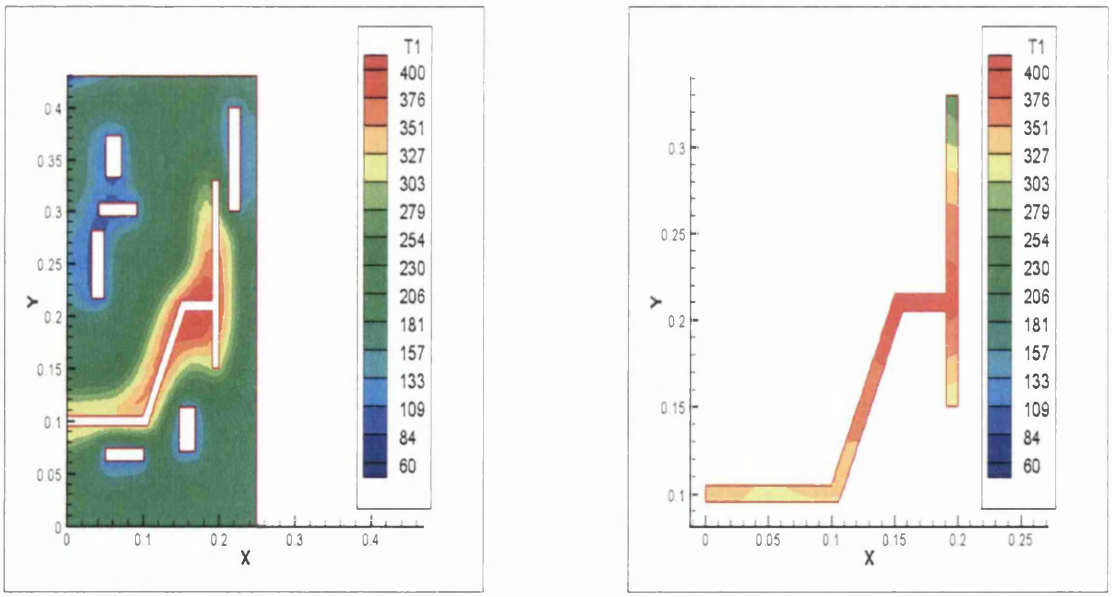

Figure 3.21

Temperature distribution in the die and casting at t=50s and the optimum position of coolant channels for Case study 4

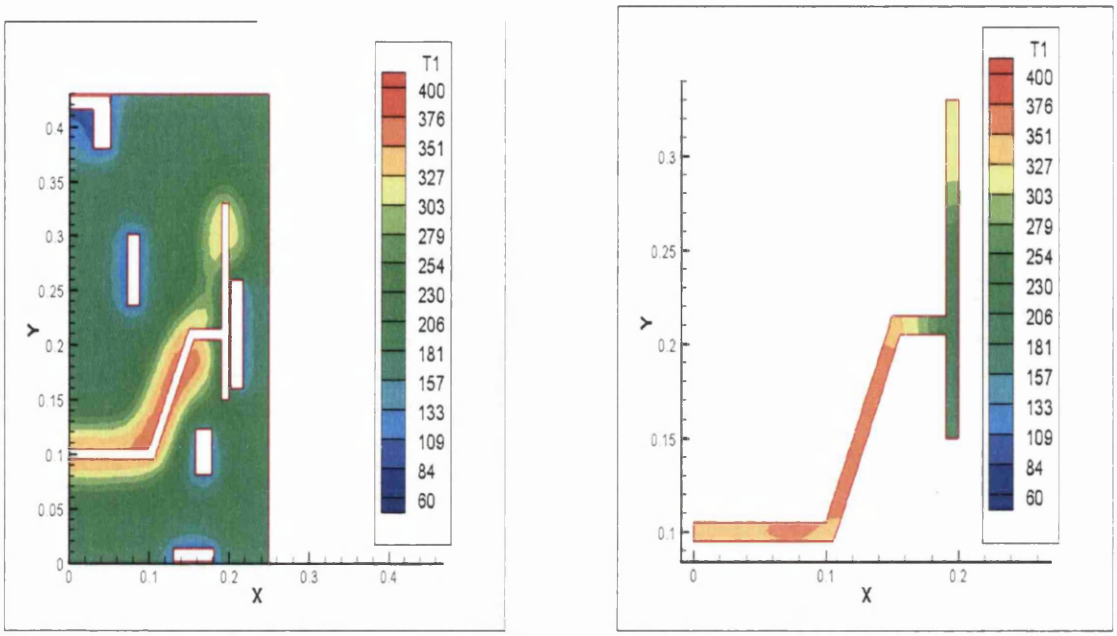

Figure 3.22

Temperature distribution in the die and casting at t=50s and optimum position of coolant channels for Case study 5

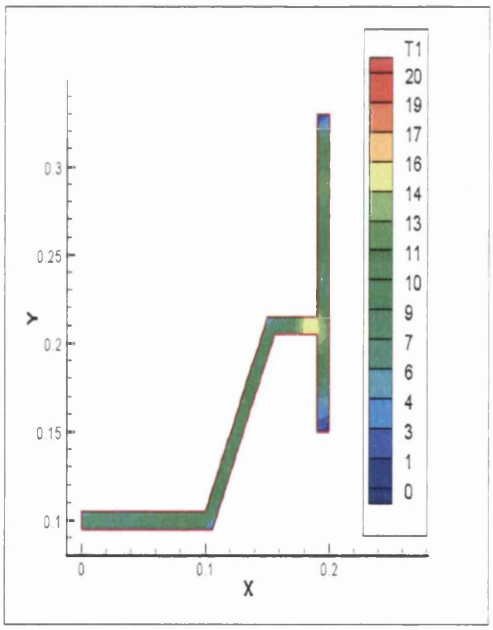

Figure 3.23

Iso-solidification contour in the casting for Case study 4

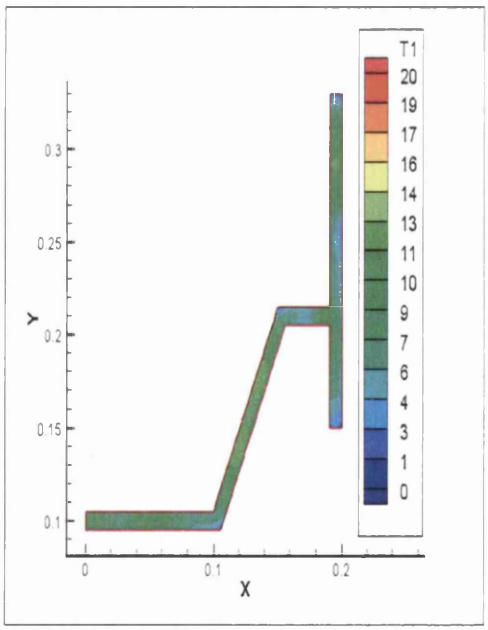

Figure 3.24

Iso-solidification contour in the casting for Case study 5

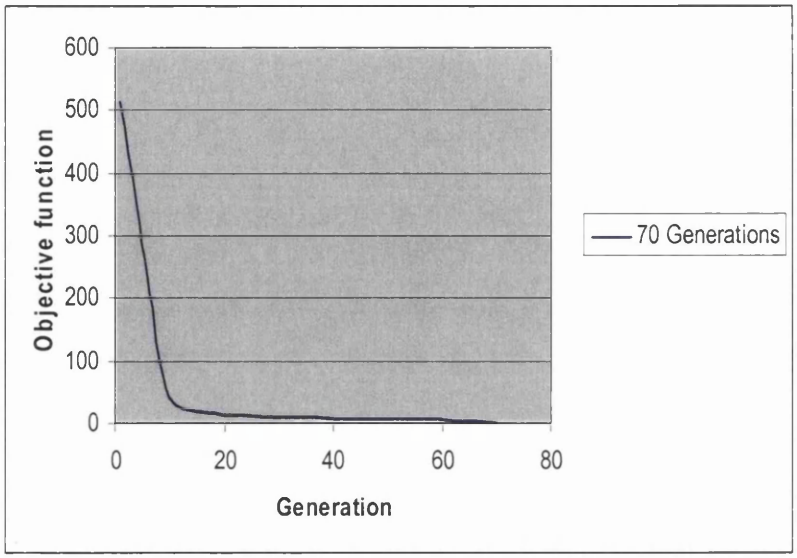

Figure 3.25

The graph of the objective function vs generation
for 70 generations for Case study 5

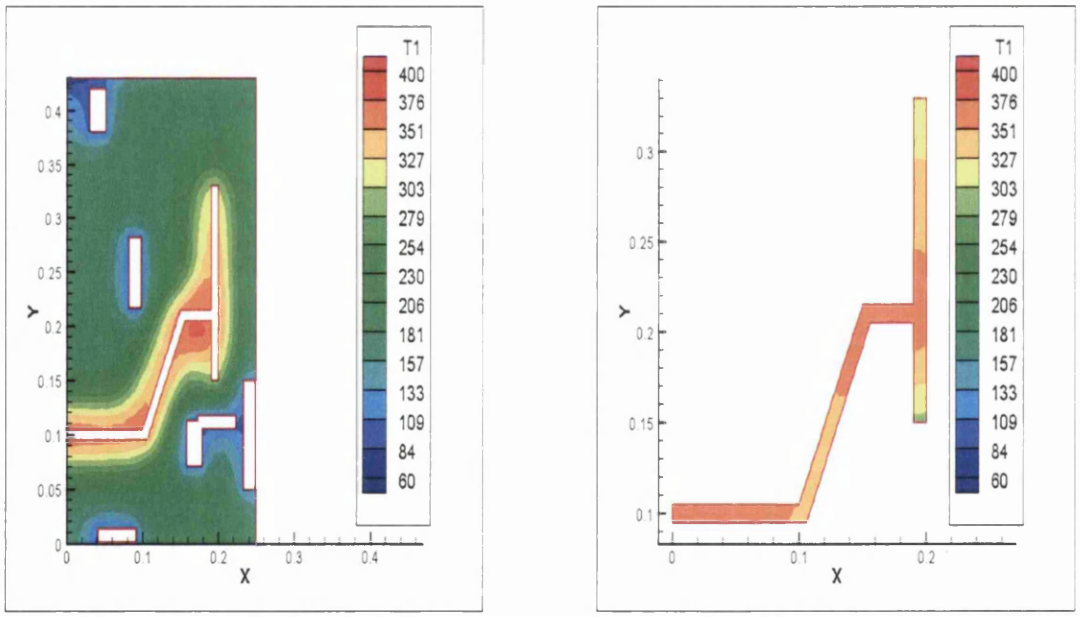

Figure 3.26

Temperature distribution in the die and casting at
t=50s and the optimum position of coolant
channels for Case study 3 for the first cycle

3.5.4 Cyclic Analysis

It is also acknowledged that a die undergoes a cyclic thermal process during the normal stable casting cycle. Practically, there is also a thermal startup. In this instance a uniform temperature in the die starts the analysis, then the die temperature is updated to achieve a stable value. This occurs at typically at 10-20 cycles and the temperature at a point in the die during a simulation conducted over 20 cycles is shown in Figures 3.27 and 3.28. The duration for each cycle was assumed to be 50*s* determined principally by the complete solidification of the part [23]. Figure 3.27 shows the location of a point E in the die which will be used to show the stabilisation process. Figure 3.28 shows the temperature history at point E for the thermal cyclic process up to the twentieth cycle. It was observed that the temperature increased rapidly at the initial cyclic stage and progressively developed towards the steady state after about the tenth stage. This is quite similar to the work done in [24] that focuses on the gravity die casting process. In this work, the steady state temperature in the part was reached after the sixth cycle whereas Davey and Hinduja [25] found that the stabilisation of pressure die-casting process occurred after only 3 cycles. At GKN, they expect typically 10 cycles to achieve some stabilisation. A few other points near the casting were tested and these yielded the same result pattern, suggesting that a stable thermal excursion within the die is achieved at typically 10 cycles. However, in this work, the cyclic analysis excluded the open time and the effect of spraying a release agent onto the die. The latter has only a small effect on temperature local to the die surface and is generally minimal due to the large thermal mass of die. An optimal design based on a uniform die starting temperature may not be

optimal where a cyclic analysis is used where the die temperature becomes non-uniform and this will be discussed below.

Figures 3.29 and 3.30 show the transient thermal solutions in the die and casting at t=50s for Case study 3 for the fifth and tenth cycles. To facilitate comparison and to illustrate how coolant position design changes when die cyclic stabilisation occurs, for the Case study 3, Figures 3.31 and 3.32 show the transient thermal solutions in the die and casting respectively at t=50s for the first and tenth cycles. Figures 3.33 and 3.34 show the transient thermal solutions in the die and casting respectively at t=50s for the fifth and tenth cycles. It can be seen that the trend of coolant system position tends to converge on position after about 10 cycles.

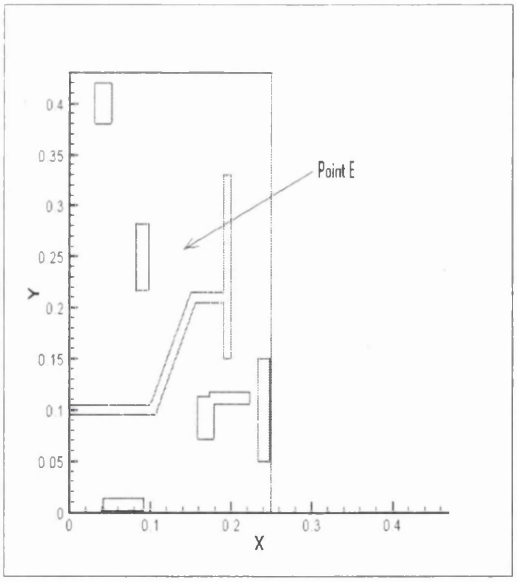

Figure 3.27

The location of point E

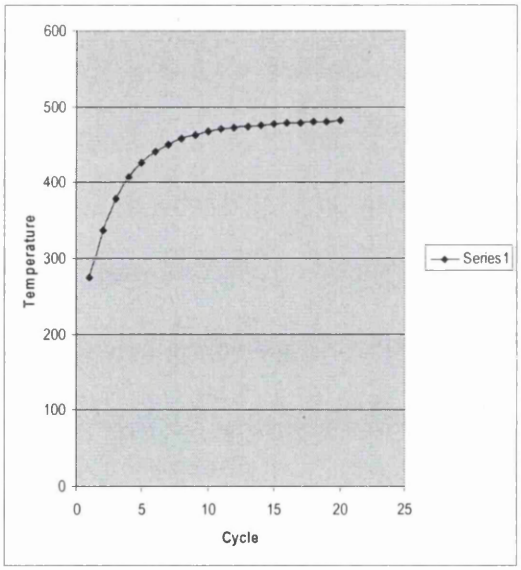

Figure 3.28

The temperature history at point E from cycle 1 to 20

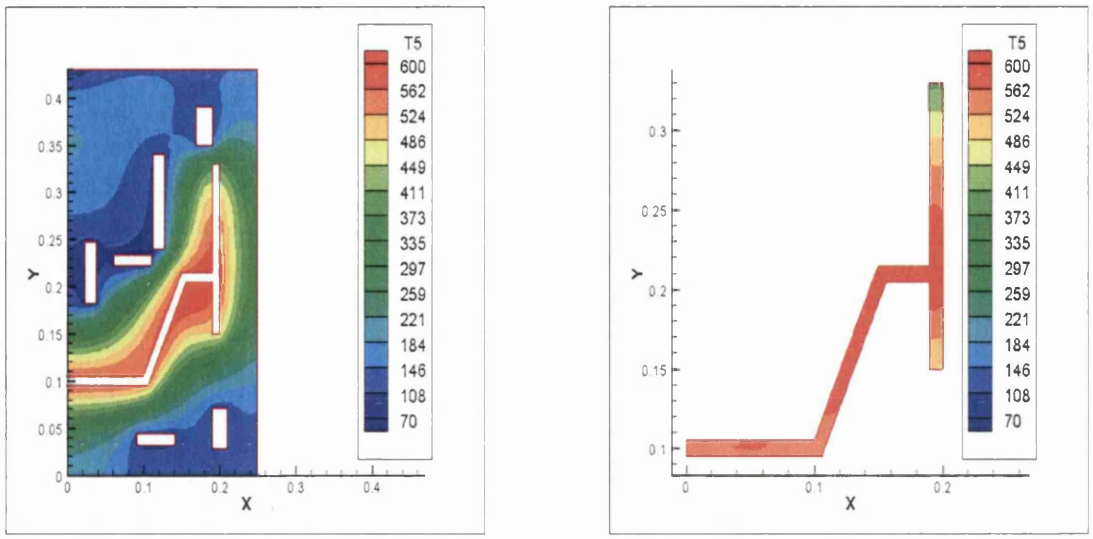

Figure 3.29

Temperature distribution in the die and casting at t=50s and the optimum position of coolant channels for Case study 3 for the fifth cycle

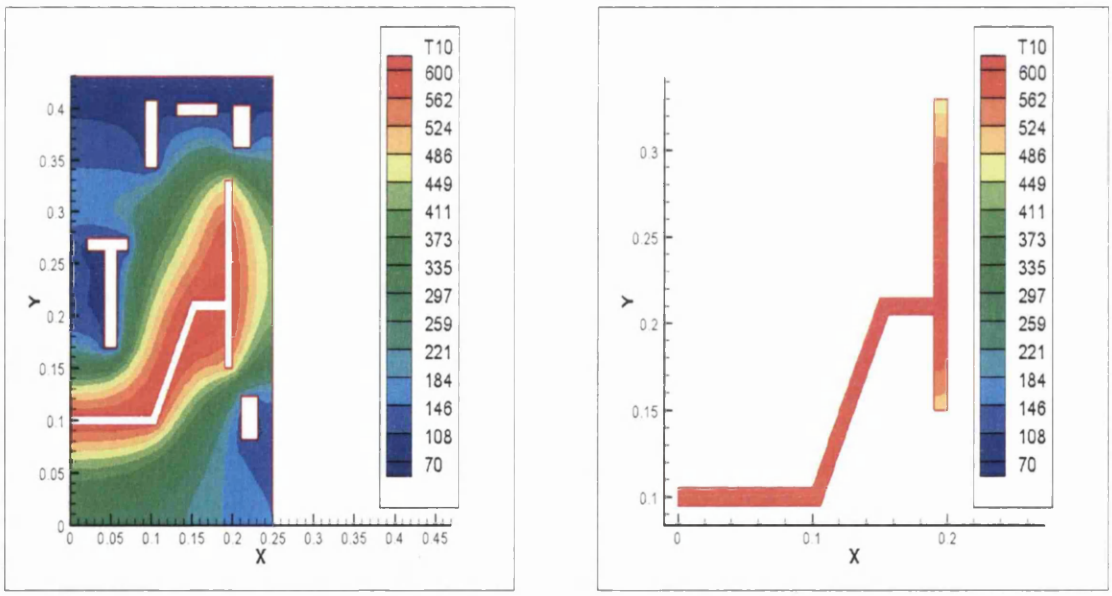

Figure 3.30

Temperature distribution in the die and casting at t=50s and the optimum position of coolant channels for Case study 3 for the tenth cycle

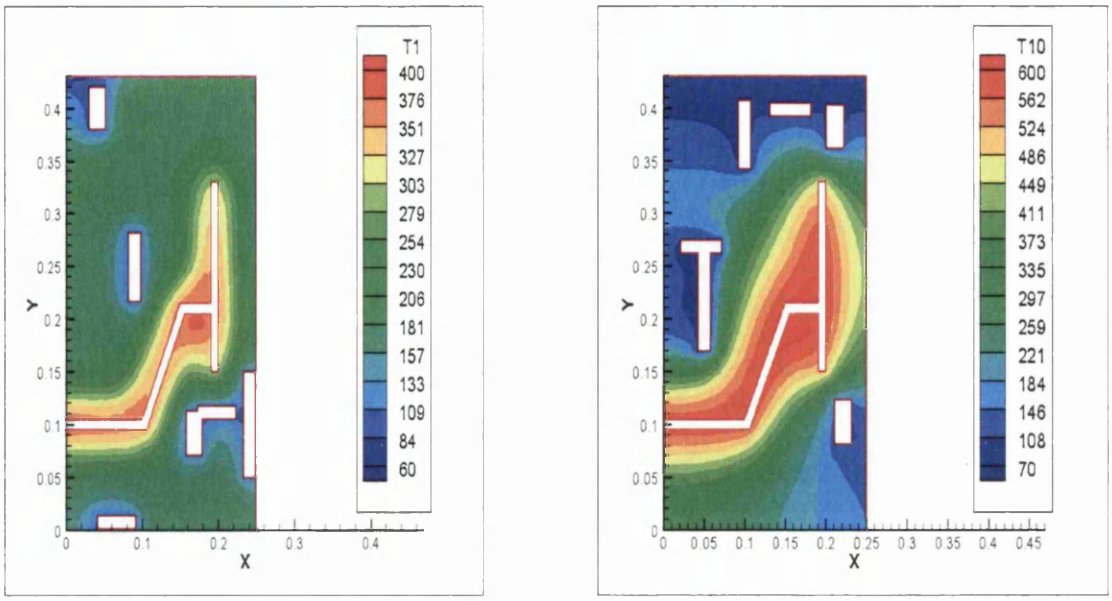

Figure 3.31

Temperature distribution in the die at t=50s for the optimum positions of coolant channels for Case study 3 for the first cycle (left) and tenth cycle (right)

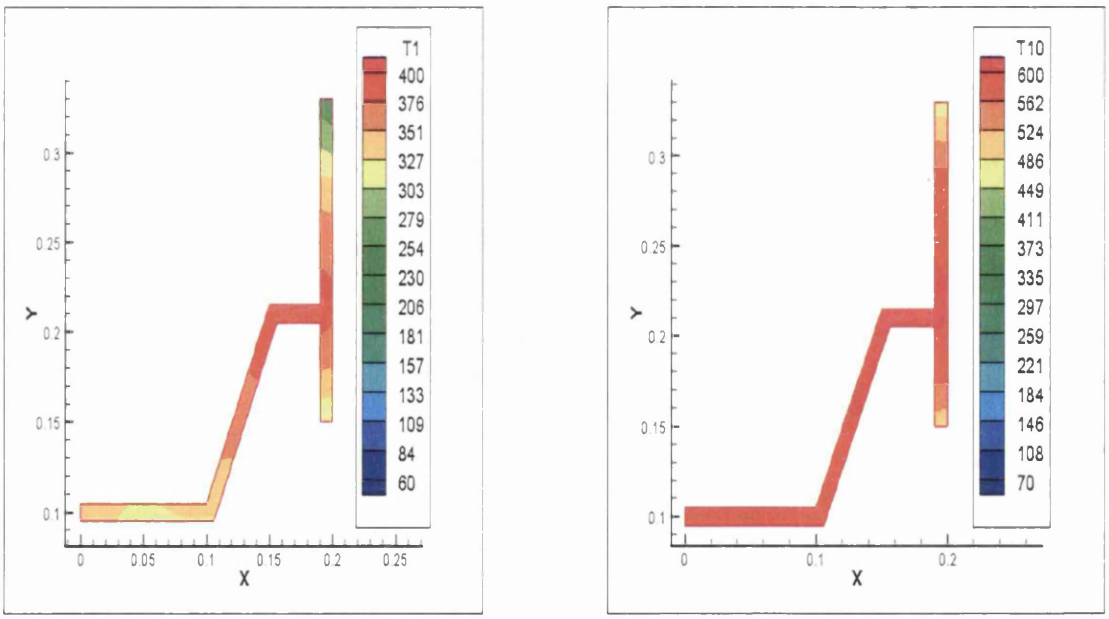

Figure 3.32

Temperature distribution in the casting at t=50s for the optimum positions of coolant channels for Case study 3 for the first cycle (left) and tenth cycle (right)

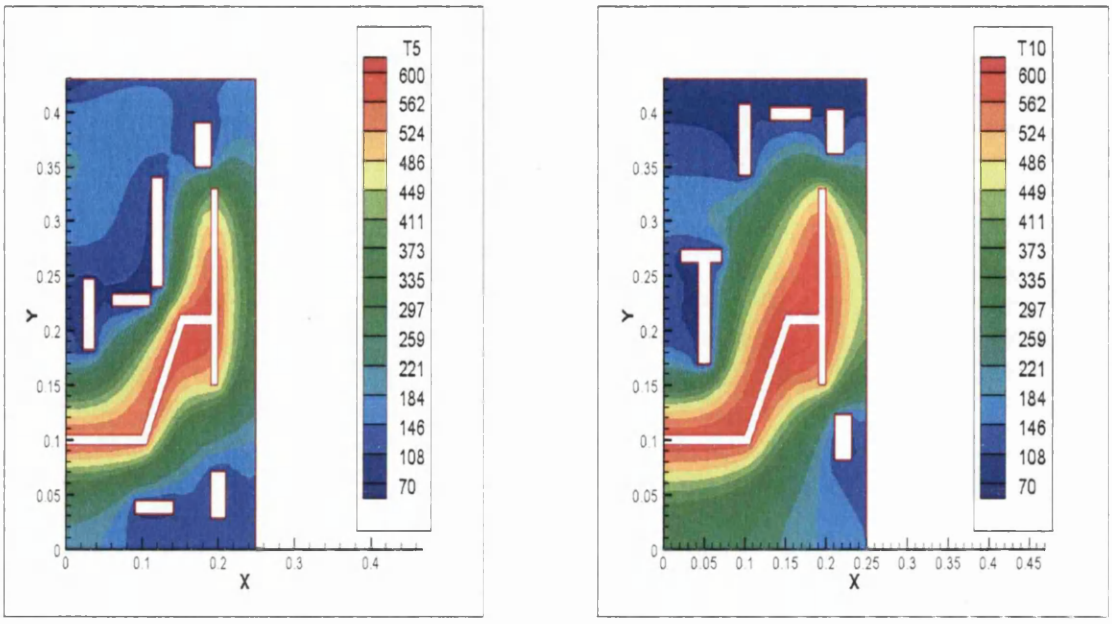

Figure 3.33

Temperature distribution in the die at t=50s for the optimum positions of coolant channels for Case study 3 for the fifth cycle (left) and tenth cycle (right)

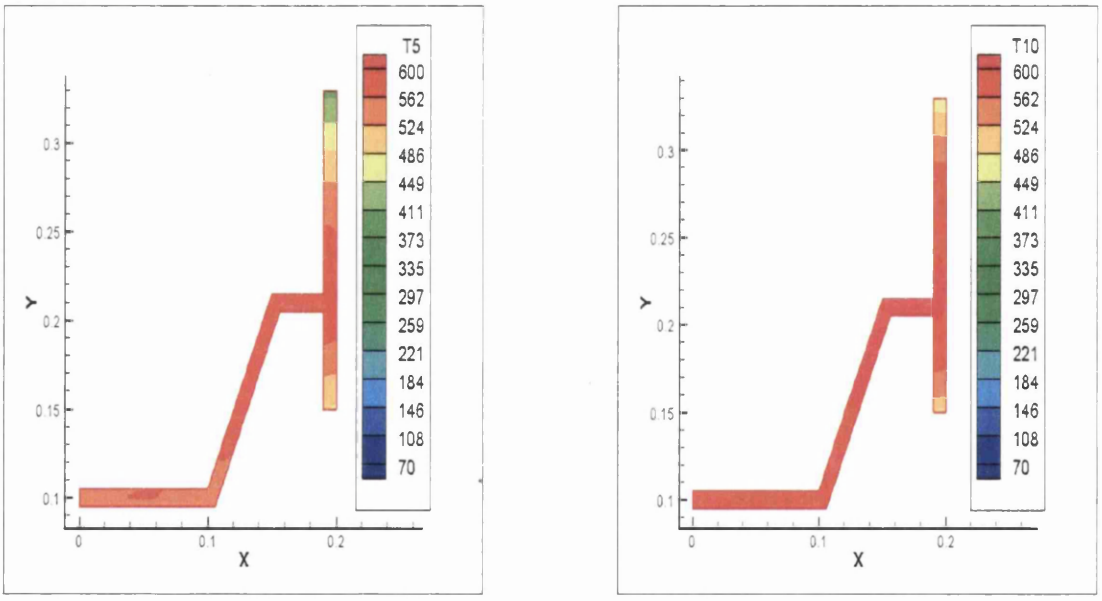

Figure 3.34

Temperature distribution in the casting at t=50s for the optimum positions of coolant channels for Case study 3 for the fifth cycle (left) and tenth cycle (right)

From the three cases, it can be seen that the coolant channels were positioned away from the casting in a way that they control the temperature enclosing the casting as opposed to the initial design where the coolant channels were positioned near the casting. It can also be seen from the three case studies, the design based on a non cyclic analysis gives a very different result from a design based on a cyclic analysis. Also, the cyclic calculation yields higher temperature at the same time and that in order to achieve an ejection temperature, the cooling duration needs to be longer.

Figure 3.35 shows the temperature distribution in the die and casting for the proposed practical solution for Case study 3 for the tenth cycle, where the three coolant channels at the top section of the die were combined together to become a single coolant channel. Clearly the 'practical solution' reflects the result from the 'pure GA' optimisation solution.

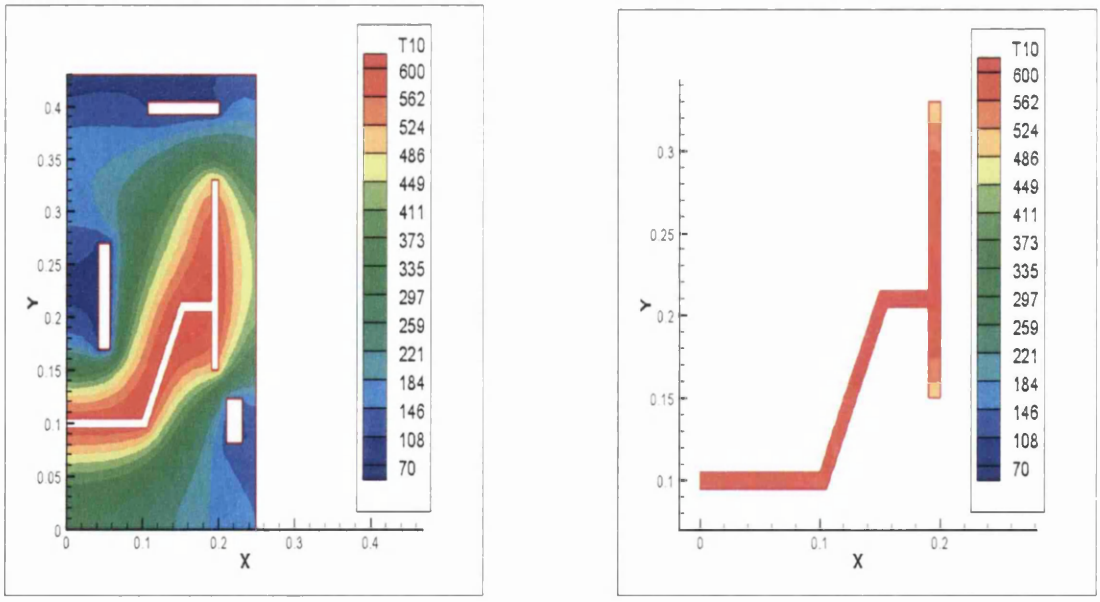

Figure 3.35

Temperature distribution in the die and casting at t=50s for the practical solution based on the Case study 3 for the tenth cycle

3.5.5 Pressure Relaxation Effects

As explained in [26], as the metal solidifies, develops structure and shrinks, it is likely that the pressure between the casting and die wall will fall away. Calculation of this history will require a simulation of structural evolution and this is beyond the scope of the current study since even one cycle will require a long calculation time. However its effect may be evaluated by changing the level of interfacial heat transfer coefficient during the cycle and observing its effect on the solidification response. Determining the precise time at which to perform this relaxation is difficult, but its effect may be observed through choosing a time at which this could occur. In this instance, relaxation was applied at 30*s* for a simulation duration of 50*s*. This was chosen since the whole domain of the casting can be seen to be below the solidus temperature.

The heat transfer coefficient is changed during the cycle, effectively representing a relaxation in pressure. This relaxation was modeled by assuming the heat transfer coefficient reduced to 500W/m^{2}K from the initial level of 5000 W/m^{2}K. This was based on experimental work that is discussed fully in [15]. Figure 3.36, 3.38, 3.40, 3.42 and 3.44 show the temperature distributions in the die at t=50*s* for first, second, third, fourth and fifth cycles respectively for cases without relaxation (left) and with relaxation (right) after optimisation of the positions of the coolant channels. Figure 3.37, 3.39, 3.41, 3.43 and 3.45 show the corresponding temperature distributions in the casting.

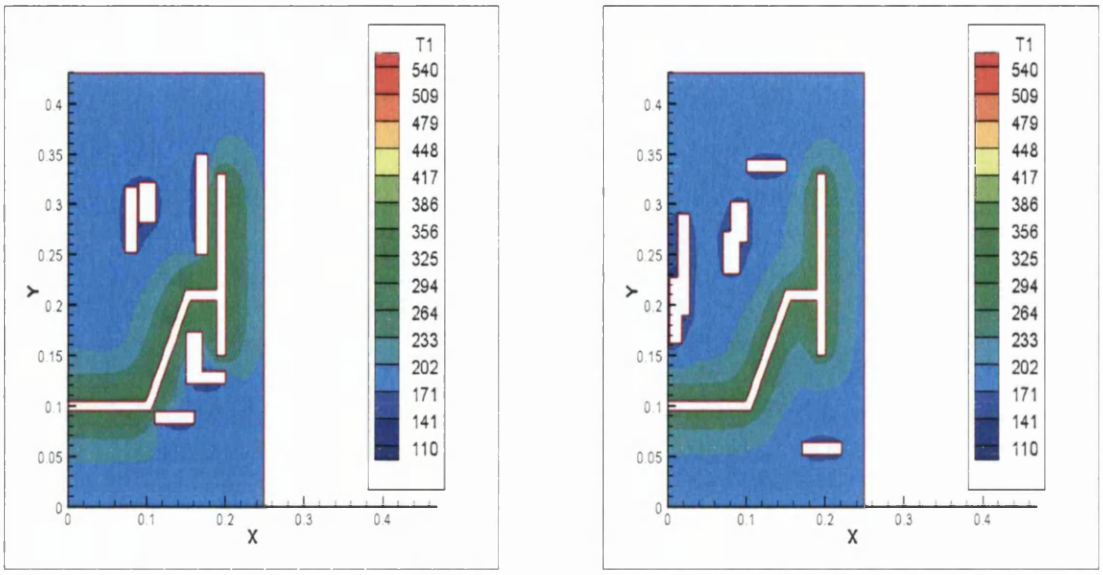

Figure 3.36

Temperature distributions in the die at t=50s for the first cycle for without relaxation (left) and with relaxation (right)

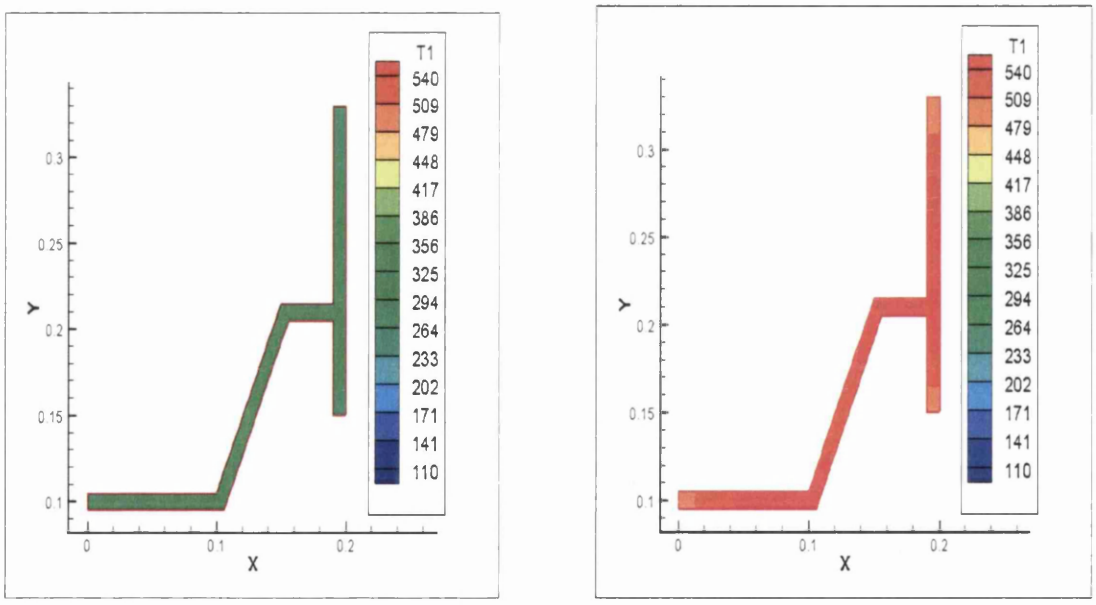

Figure 3.37

Temperature distributions in the casting at t=50s for the first cycle for without relaxation (left) and with relaxation (right)

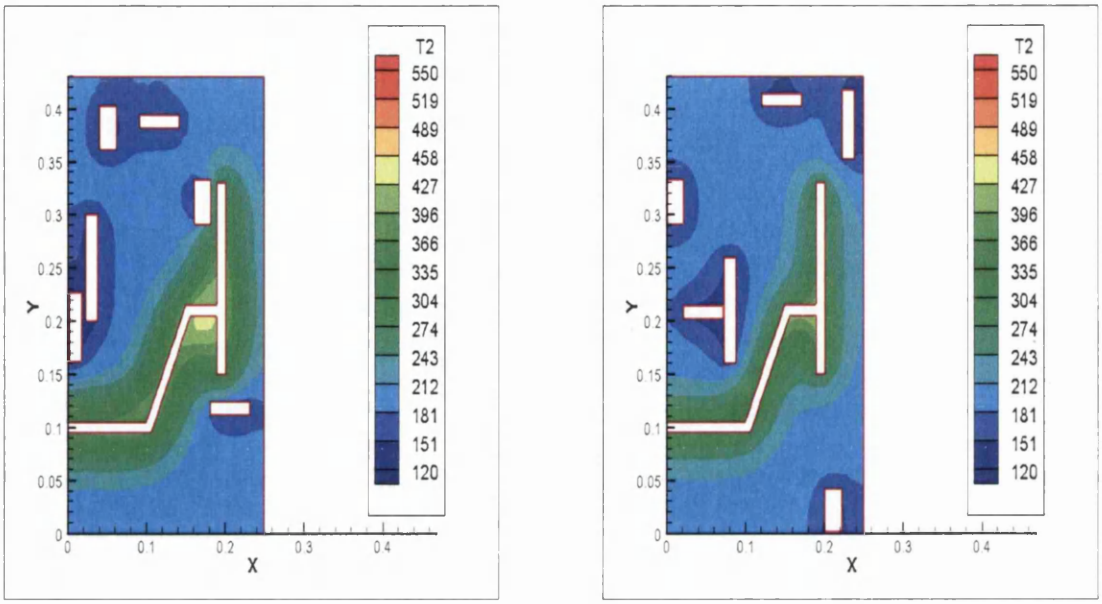

Figure 3.38
Temperature distributions in the die at t=50s for the second cycle for without relaxation (left) and with relaxation (right)

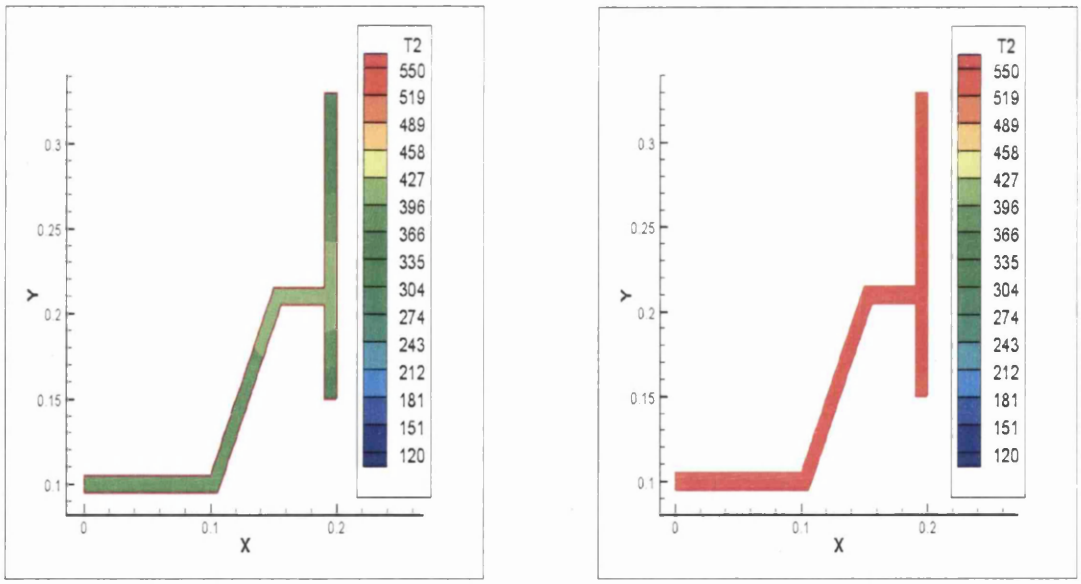

Figure 3.39

Temperature distribution in the casting at t=50s for the second cycle for without relaxation (left) and with relaxation (right)

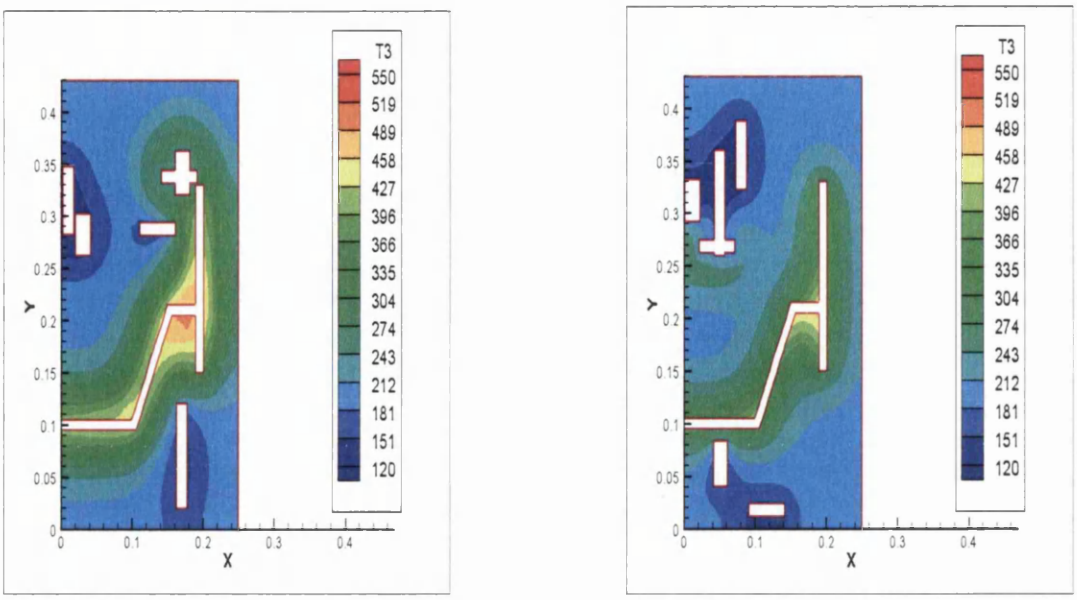

Figure 3.40

Temperature distribution in the die at t=50s for the third cycle for without relaxation (left) and with relaxation (right)

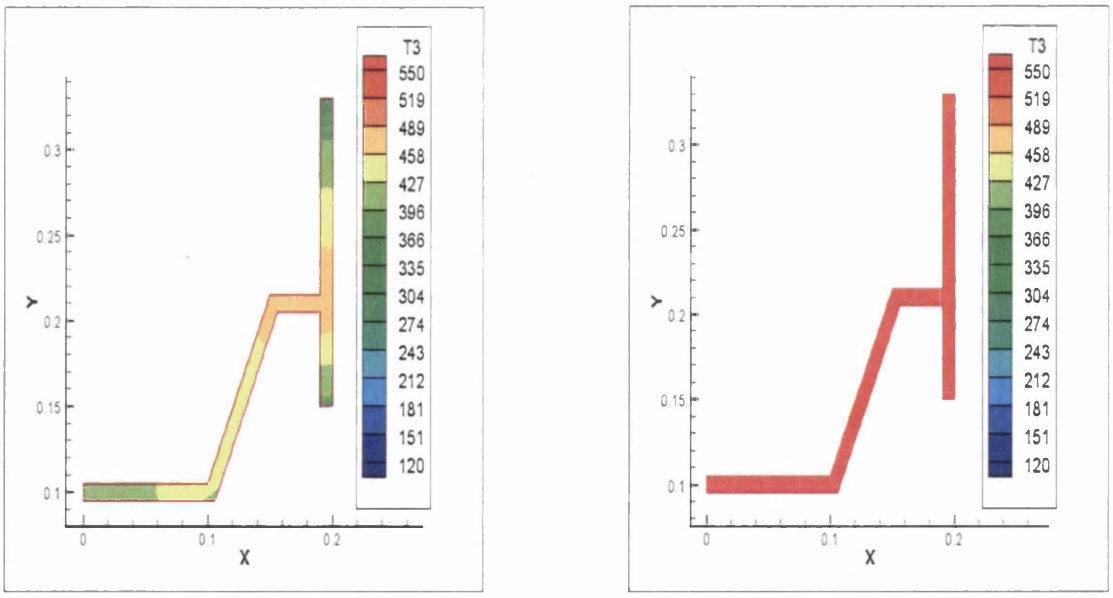

Figure 3.41

Temperature distribution in the casting at t=50s for the third cycle for without relaxation (left) and with relaxation (right)

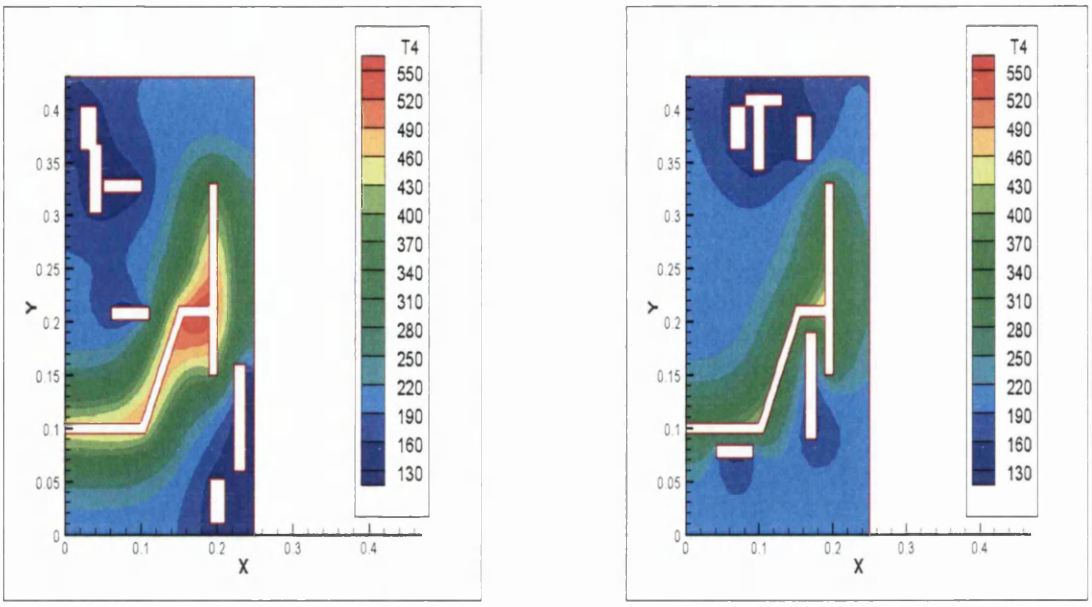

Figure 3.42

Temperature distribution in the die at t=50s for the fourth cycle for without relaxation (left) and with relaxation (right)

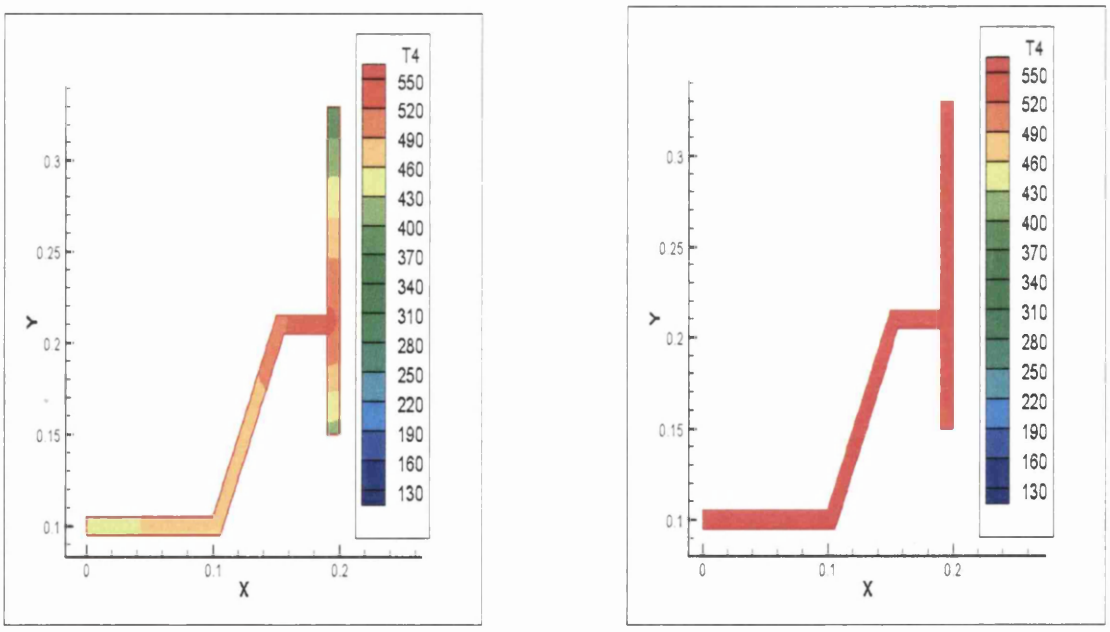

Figure 3.43

Temperature distribution in the casting at t=50s for the fourth cycle for without relaxation (left) and with relaxation (right)

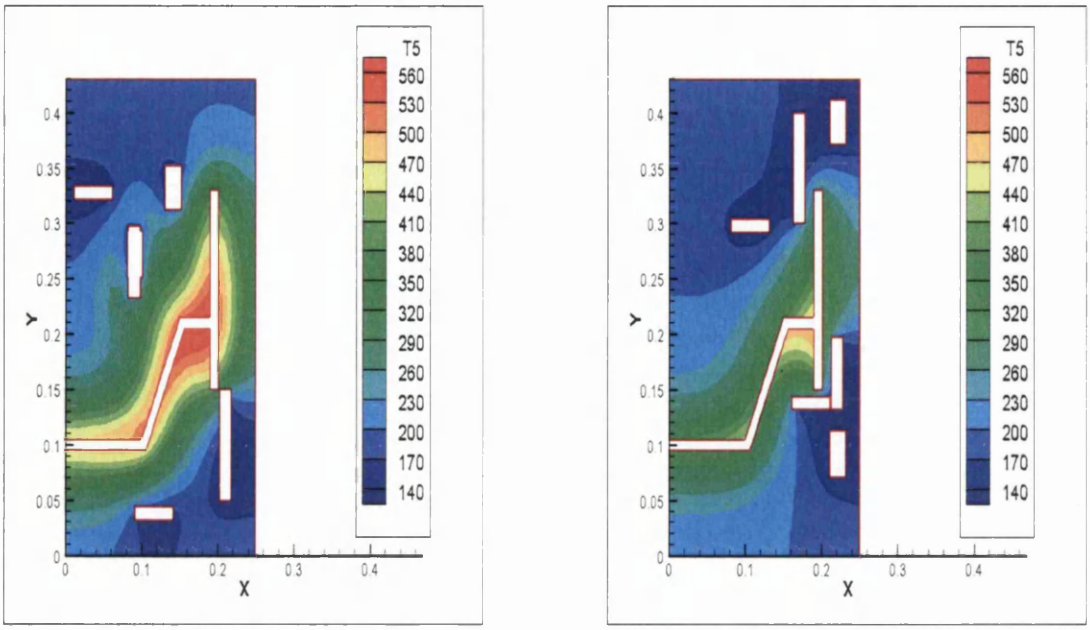

Figure 3.44

Temperature distribution in the die at t=50s for the fifth cycle for without relaxation (left) and with relaxation (right)

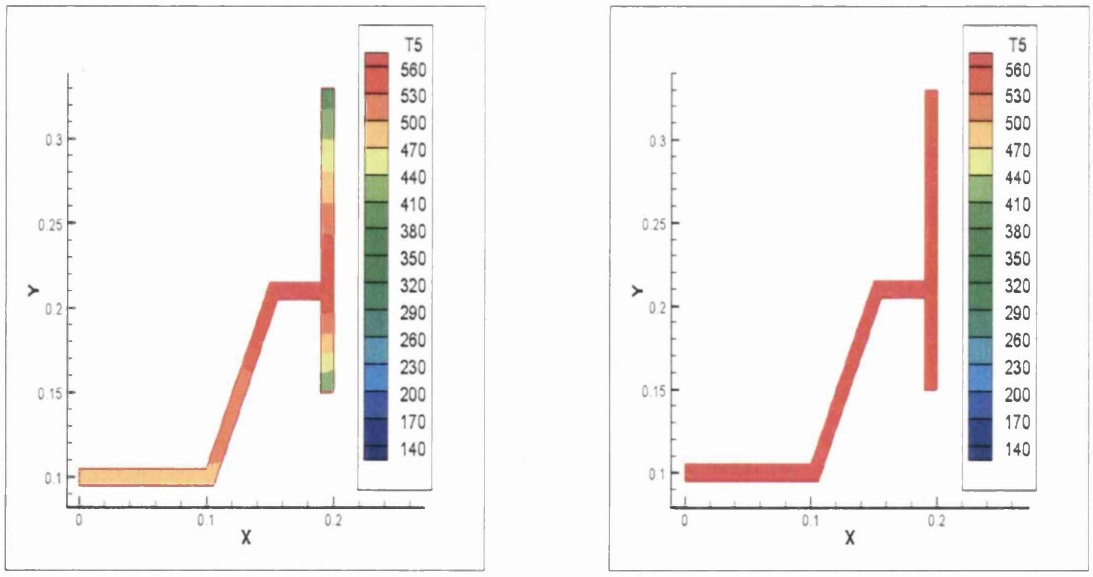

Figure 3.45

Temperature distribution in the casting at t=50s for the fifth cycle for without relaxation (left) and with relaxation (right)

From the above figures, it can be seen that the effect of the changes of interfacial heat transfer coefficient has a very significant influence on the temperature distribution in the die and casting. Die temperatures are generally lower since heat is not extracted from the casting and conversely the casting is at a higher, and fortuitously more uniform temperature. This highlights the need for pressure control within the cycle. However the timing of this pressure control cycle has not been explored further at this time, but will be proposed as further work that needs to be carried out in any subsequent study.

3.6 Comparison of the Coolant Channel System Design

In this section, the comparison of the coolant channel system design between the results obtained from the optimisation software and the coolant channel design which is implemented in the industry (GKN Squeezeform) is discussed. For the design implemented in the industry, the die consists of a number of blocks, as opposed to only a one piece die. Besides, the initial temperature distribution in the casting is not uniform and can be obtained from a mould filling analysis. Moreover, the shape of the part and coolant channels and also a number of the coolant channels employed are slightly different. However, to facilitate the comparison, this section is devoted to discuss the configuration of the coolant channels system design in general and to contrast solution derived from an optimisation study with that based on practical experience.

Figure 3.46 shows the thermal analysis in the casting and die, where (a) shows the temperature distribution after filling and (b) shows the temperature distribution after 16*s*.

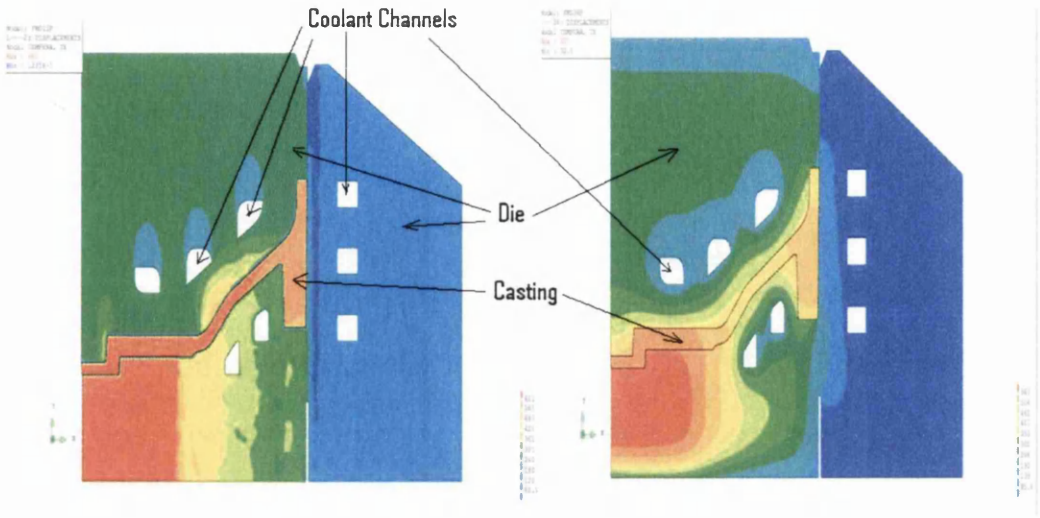

(a) (b)

Figure 3.46

Thermal analysis after filling the die; Temperature distribution after filling (a) and temperature distribution after 16*s* (b). (From GKN)

From Figure 3.46, the non-uniformity of temperature distribution can be observed especially in the middle section of casting. In contrast, the results obtained from the practical solution as shown by Figure 3.35 demonstrated more uniform temperature distributions in the casting. This reflects that the practical solution which is based on the result obtained from pure optimisation solution is more efficient in terms of achieving solidification control in the casting as compared to the GKN scheme (based on intuition).

3.7 Closure

Genetic algorithm based optimisation has been successfully integrated with automatic remeshing procedure and Finite Element analysis to design the thermodynamic control in casting and squeeze forming processes. It can be seen that from the validation against other casting studies, the results show similar agreement with the results obtained in

previous work of similar geometries for 2D planar and axisymmetric problems, where the mushy zone is located inside the feeder.

For the squeeze forming process, the optimal solutions obtained for the formulation of the objective functions between two points has successfully achieved a near global optimal solution reflected in a near zero residual for the objective function. However, to achieve near simultaneous solidification in the squeeze cast component, the consideration from the whole casting domain is required in order to ensure such objective to be achieved successfully. In this work, following a cyclic analysis, the process starts to stabilise after the tenth cycle. The optimal cooling design solution obtained for a cyclic analysis are different from the non-cyclic analysis, thus, suggesting that the design analysis must consider cyclic analysis in order to mimic the actual process in industry. Also a simplified exploration of the pressure relaxation aspect is shown to be critically important to the process due to the direct influence it has on the temperature distribution in the casting and die. Detailed investigation is still required and is outside the scope for now, it will not be explored further in this thesis, but is a recommendation for future work.

The next chapter will explore the application of multi-objective optimisation involving process simulation of the squeeze forming process using Genetic Algorithms. The aim of this chapter is to obtain optimised design by considering different conflicting requirements involving thermal and mechanical aspects.

References

1. Michalewicz Z. Genetic algorithms + data structures = Evolution programs. New York:Springer-Verlag,1996.

2. Goldberg E. Genetic algorithms in search, optimization and machine learning, Reading, UK : Addison Wesley, 1989.

3. Mitchell M. An Introduction to genetic algorithms, Cambridge, London : MIT press, 1996.

4. Beck T. Evolutionary algorithms in theory and practice : evolution strategies, Evolutionary programming, genetic algorithms. Oxford,UK: Oxford University Press,1996.

5. http://www.magmasoft.com/ (2003)

6. http://www.calcom.ch/index.html/ (2003)

7. Lewis RW, Morgan K, Thomas HR and Seetharamu KN. The finite element method in heat transfer analysis. Chichester: Wiley,1996.

8. O.C. Zienkiewicz, 'The fnite element method' Berkshire,UK: McGraw Hill, 1977.

9. Lewis RW, Manzari MT and Gethin DT. Thermal optimisation in the sand casting process. *Engineering Computations*. 2001; **18 (3/4)**: 392-416.

10. www.cs.cmu.edu/~quake/triangle.html (2003)

11. Lewis RW, Manzari MT, Ransing RS and Gethin DT, 'Casting shape optimisation via process modelling', *Materials and Design*, **21**, 381-386 (2000).

12. Tortorelli DA, Tomasko JA, Morthland TE and Dantzig JA, 'Optimal design of nonlinear parabolic systems. Part II: variable spatial domain with applications to casting

optimisation', *Computer Methods in Applied Mechanics and Engineering*, Vol. 113, pp. 157-72.

13. C.S. Lim, A.J. Clegg and N.L. Loh, 'The reduction of dendrite arm spacing using a novel pressure-assisted investment casting approach' *Journal of Material Processing Technology*, 1997;**70**, 99-102.

14. Lee JH, Kim HS, Won CW and Cantor B, ' Effect of the gap distance on the cooling behavior and the microstructure of indirect squeeze cast and gravity die cast 5083 wrought Al alloy', *Materials Science and Engineering* **A338**, 182-190 (2002).

15. Anderson JT. A theoretical and experimental investigation into the investment and gravity die casting processes. M.Phil Thesis, Swansea University, 1995.

16. K. Ravindran and R.W. Lewis, 'Finite element modelling of solidification effects in mould filling', *Finite Elements in Analysis and Design*, 1998;**31**, 99-116.

17. Callister WD. Materials Science and Engineering, An Introduction. New York: John Wiley & Sons, Inc, 1997.

18. Lewis RW and Ransing RS, 'The optimal design of interfacial heat transfer coefficients via a thermal stress model', *Finite Elements in Analysis and Design*, 34, 193-209 (2000).

19. www.thermocalc.com/ (2003)

20. M.S. Young and A.J. Clegg, 'Process optimisation for a squeeze cast magnesium alloy metal matrix composite' *Journal of Material Processing Technology*, 2005;**168**, 262-269.

21. www.gknplc.com/ (2003).

22. http://www.bucorp.com/Products/HotWorkSteels/DataSheets/Orvar_Superior.pdf (2003).

23. Gethin DT, Lewis RW and Tadayon MR. 'A finite element approach for modeling metal flow and pressurized solidification in the squeeze casting process' *Int. j. numer. Methods eng.* 1992;**35**:939-950.

24. Sulaiman SB. An analysis of thermal behaviour and molten metal flow with expert system applications in pressure diecasting. Ph.D. Thesis, Swansea University, 1992.

25. Davey K and Hinduja S. 'Modelling the transient thermal behavior of the pressure die-casting process with the BEM', *App. Math. Modelling.* 1990;**14**:394-409.

26. Postek EW, Lewis RW, Gethin DT and Ransing RS, 'Influence of initial stresses on the cast behaviour during squeeze forming processes', *Journal of Material Processing Technology*, 2005;**159**, 338-346.

Chapter 4

Multi-Objective Optimisation

4.1 Introduction

Chapter 3 presented and explored the application of genetic algorithms to optimise the thermal design of the casting and squeeze casting process. A number of objective functions were tested, including functions that may be used to achieve near simultaneous solidification of the cast part. In this chapter, multi-objective optimisation of the squeeze forming process involving both thermal and mechanical aspects will be explored. The exploration again deals with the positions of the coolant channels, where their positions are not only crucial in controlling the solidification process, but also impact on the stress distribution in the die and the cast component. The impact on stress evolution in the cast part is excluded from the current work due to the extreme computational effort that is needed, even for a single cooling cycle [1]. Thus the current chapter will focus on die thermal stress evolution only since this is also important with respect to die life through

cyclic thermal loading. Stress will also be induced in the die due to pressurisation by the squeezing action. This has been excluded from the current work, but its significance is demonstrated in Appendix III where it can be seen that for the geometry considered, thermal and pressure induced stresses are of the same order.

The aim of this chapter is to explore the application of genetic algorithms to optimise two objective functions that describe thermal behaviour in the casting and stress evolution in the die. Thus the genetic algorithm will be integrated with a coupled Finite Element Analysis of the thermomechanical behaviour of the squeeze forming system.

In the previous chapter, the optimum positions of coolant channels were achieved while considering the thermal aspect only. Both directional and near simultaneous solidification in the cast part were considered. It is likely that this optimum solution will not be appropriate when the stress evolution in the die is taken into account due to the conflicting requirements that are present in the formulation of potential objective functions.

In the following sections, a single objective function will be explored first to achieve an optimum mechanical design of the die due to thermal loading, excluding the application of pressure in the pressing cycle. By using von Mises stress, a number of objective functions will be explored aimed at achieving a near uniform stress distribution throughout the die. This will be followed by exploring multi-objective optimisation. It should be noted that positioning the cooling channel affects the stress that is derived from the thermal field and is also influenced by the modification that is made to the die structure.

The settings of the Genetic Algorithm operators and parameters are shown in Table 4.1 (Appendix I). These have been chosen because of GENOCOP application experience which are based on a number of trials that have proven to be effective through examples as discussed in [2]. The correctness of these parameters was established in Chapter 3, section 3.5 in which it was shown that the objective function was satisfied, achieving a global optimum solution denoted by a residual that was in all cases close to zero. Since the GA operators and parameters used in this example effectively achieved near the global optimum solution, the same parameter settings have been used in this chapter.

For the data transfer between the thermal and structural analyses for die thermal stressing, the same finite element mesh has been implemented for both problems. By doing so, imbalances during the data exchange can be avoided, where the imbalances are often a function of mesh quality and interpolation method [3].

The first stage in the mechanical analysis was concerned with node and element renumbering because the mechanical analysis applies to the die components only. The thermal field was then applied to the new element/nodal assignment and the mechanical boundary conditions applied to represent centerline symmetry and rigid vertical fixing at the base of the die. In this research, the die is considered as a single piece rather than a number of blocks. For the zero initial stress state, the manufacturing temperature was 25°C and this was used as the reference temperature. For accurate modeling of the squeeze forming process, the contact boundary condition at the die-cast interface has to be considered to simulate the interaction between them. This includes the normal and tangential forces that are present and also the relaxation that takes place in the cast part.

However, this modeling is very complex to simulate due to the material and geometrical nonlinearities that are present and therefore was not considered in this work.

probability of uniform mutation	0.0
probability of non-uniform mutation	2.0
probability of boundary mutation	0.0
probability of arithmetic crossover	0.25
probability of simple crossover	10.0
rank selection pressure	0.2
probability of heuristic crossover	0.0
probability of cloning	0.0
Number of chromosomes	70
Number of genes	12

Table 4.1

The Genetic Algorithms operators and parameters that have been used

4.2 Nonlinear Optimisation

There are a number of process parameters that may be explored to optimise the squeeze forming process. For a prescribed part shape these include overall die dimensions, the cooling system position and size, preheating, metal pour temperatures, pressing cycle timings and heat transfer coefficient. The current work focuses on the cooling system design and will investigate a method whereby coolant channel position may be optimised, subject to a prescribed heat transfer coefficient that is determined by the flow regime within the coolant channel.

Mathematically, non linear optimisation of the coolant channel system can be defined as follows,

Min $f(\mathbf{x})$

Subject to $\mathbf{x} \in \Omega$

$\mathbf{x}=[\mathbf{x}_1,\mathbf{x}_2,\ldots,\mathbf{x}_S]^T$

where $f(\mathbf{x})$ is a non-linear objective function, $\mathbf{x}$ the design variables and Ω is the feasible decision space.

4.3 Single Objective Optimisation for Die Thermal Stressing

Before exploring the application of genetic algorithms to the multi-objective optimisation, which is the main objective of this chapter, single objective optimisation will be explored first where it will act as a good indicator to ensure the success of the multi-objective optimisation of the squeeze forming process. To achieve this required development of code to analyse thermomechanical behaviour. Although there are a number of sophisticated commercial codes available [4,5] these have not been adopted since they cannot be interfaced readily with the GA optimisation procedures. Thus it was necessary to develop a simple code with 'just adequate capability' to facilitate exploration of the application of GA's to achieve thermomechanical optimisation. The correctness of this code was tested through comparison with a benchmark finite element analysis for a simple cylinder. Figure 4.1 shows the finite element mesh in the cylinder and also the applied thermal boundary conditions that were used for validation. The initial temperature in the cylinder was 200°C. Figure 4.2 shows the temperature distribution in the cylinder at t=50s which was used for thermal stress evaluation in the

cylinder. The mechanical boundary conditions were applied to represent centerline symmetry and rigid fixing at the base of the die. The results for thermal stresses in the domain are shown in Figure 4.3 and these may be compared directly with the results obtained from ELFEN software [6] for the same temperature distribution in the same domain and also the boundary conditions. It can be seen that the results show close agreement. The effective stresses at selected nodes (Nodes A,B and C) as shown in Figure 4.1 are listed in Table 4.2 and again the comparison at the nodes also shows close agreement and this applies to other nodes as well.

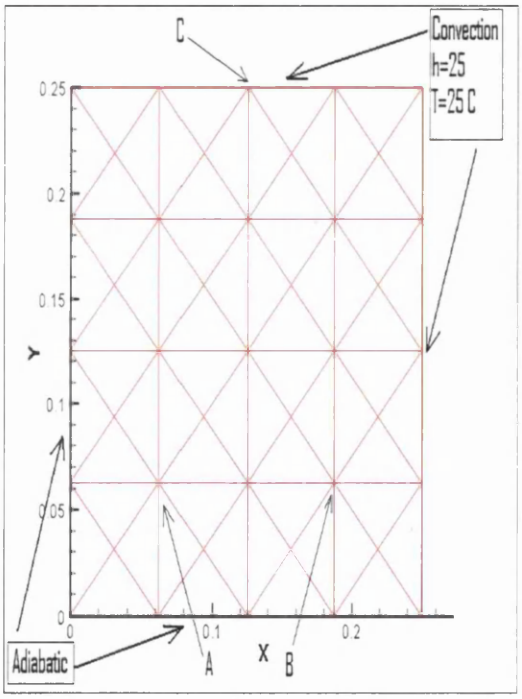

Figure 4.1

Finite element mesh in the cylinder and the applied boundary conditions

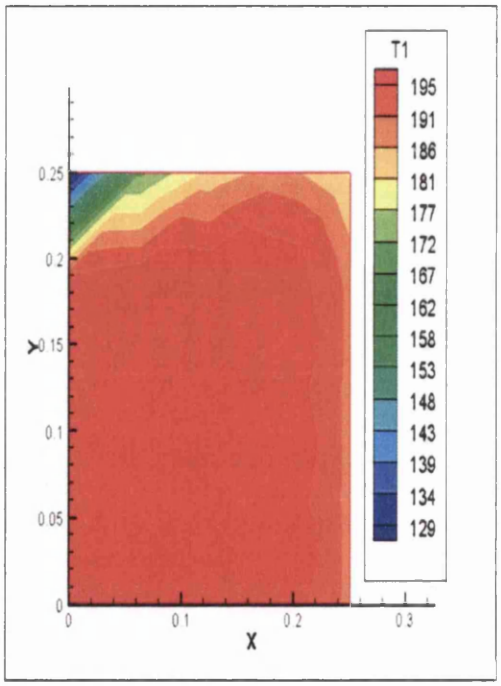

Figure 4.2

Temperature distribution in the cylinder at t=50s

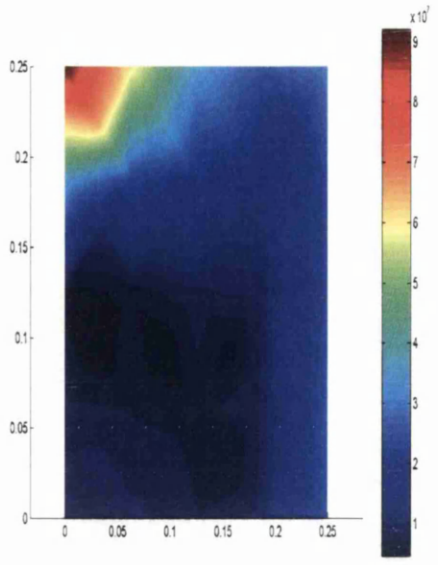

Figure 4.3

Effective stress in the die at t=50s for the results obtained from the code

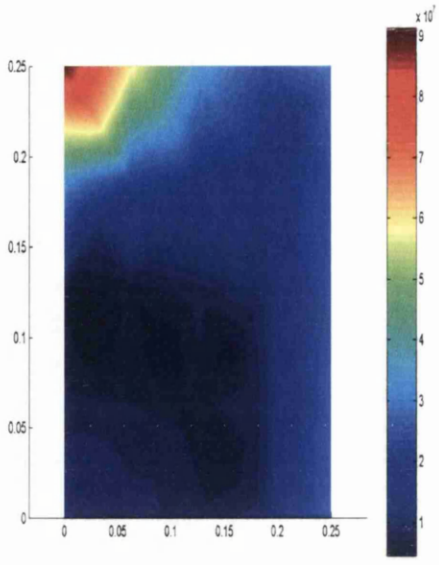

Figure 4.4

Effective stress in the die at t=50s for the results obtained from ELFEN software

	Code (MPa)	ELFEN (MPa)
Point A	7.12	7.21
Point B	8.99	8.95
Point C	33.9	33.6

Table 4.2

The comparison of the effective stress at selected points for the results obtained from the code and ELFEN software

4.3.1 Objective Functions

There are a number of objective functions that may be defined to optimise coolant system position to achieve a near uniform von Mises stress distribution in the die. Von Mises stress has been chosen since it represents a local stress level, but does not differentiate between compressive or tensile components in the die. Two forms of objective function

may be chosen that approximate the achievement of near uniform von Mises stress, identified as Case studies 6 and 7.

Case study 6

$$F_1(\mathbf{x}) = \left\{ \frac{1}{\Omega_D} \int_{\Omega_D} \left[(\sigma_{max} - \sigma_{ave})^2 + (\sigma_{ave} - \sigma_{min})^2 \right]^{\frac{1}{2}} d\Omega \right\} / 10^5 \qquad (4.1)$$

where Ω_D is the domain of the die. σ_{max} and σ_{min} are the maximum and minimum von Mises stresses and σ_{ave} is the average value in the die,

$$\sigma_{ave} = \frac{\sum_{i=1}^{ND} \sigma_e(\mathbf{x})}{ND} \qquad (4.2)$$

where $\sigma_e(\mathbf{x})$ is the average von Mises stress for each element in the die and ND is the total number of elements in the die. The idea behind the formulation of the above objective function is to drive the maximum and minimum von Mises stresses towards the average value in the die in order to try to attempt to achieve near uniform stress in the die. The objective function has a similar characteristic to the one developed to achieve near simultaneous solidification in the cast part as described in Chapter 3.

To facilitate a comparison, a second objective function may also be defined and this is designated Case study 7.

Case study 7

The objective function is defined as follows:

$$F_2(\mathbf{x}) = \sum_{i=1}^{ND} \left[(\sigma_e(\mathbf{x}) - \sigma_{ave})^2 \right] / 10^6 \qquad (4.3)$$

For Case study 6, the objective function was developed to minimise the von Mises stress range. For Case study 7, the objective function was aimed to achieve a more uniform stress distribution, rather than minimising the stress range. Although both drive the solution in the same direction, a different result is expected. This is because different expressions of the formulation of objective function will have different effects on the optimal solutions due to the sensitivity of the Genetic Algorithm to the defined objective functions.

4.3.2 Design Variables and Constraints

Figure 4.5 shows a section through the axisymmetric squeeze formed part that was presented in Chapter 3 and also the corresponding finite element mesh. Again the design variables focus on the coolant channel position and their initial position and numbering are also shown in this figure.

The design variables for the coolant channel position can be represented as follows and ensures that the coolant channel is located within the die space. Further constraints may be applied to ensure that they do not overlap the cast part and also the use of block components to build the die could also be implemented as part of the model build constraints. To do so for arbitrary and complex shaped components will require substantial coding developments in order to detect clashes and then to take appropriate action, consequently this has not been done in this work, but remains as a future challenge.

x_i = X-coordinates of coolant channel i (i=1,2,…,6)

$y_{(j+6)}$ = Y-coordinates of coolant channel j (j=1,2,…,6)

To allow the coolant channels to move flexibly in the die, only inequality constraints are applied. These constraints are of the form

$x_k - x_{min} \geq 0$

$x_{max} - x_k \geq 0$ (k=1,2,...,12)

where k represents the design variable, x_{max} represents the maximum value of the design variable constraint and x_{min} represents the minimum value of the design variable constraint.

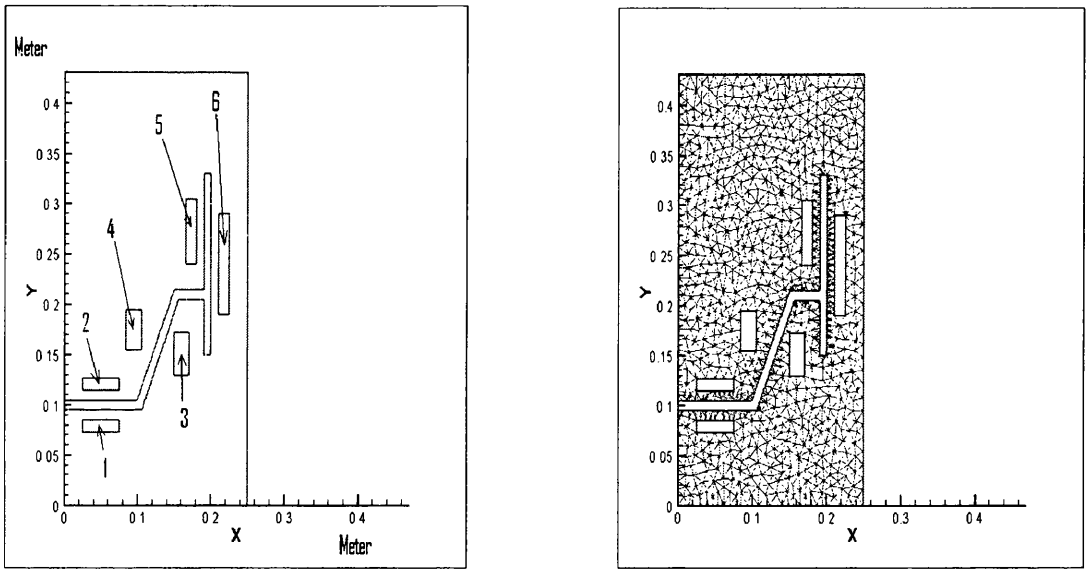

Figure 4.5

Squeeze casting part design and initial coolant channel position and numbering and the finite element mesh

The design variables and constraints defined in this section will be applied to all numerical examples for single and multi objective optimisation case studies presented in this chapter.

4.3.3 Numerical Example

For the case studies, the cast material is Aluminium LM25 whereas the die is a tool steel H13, their relevant mechanical properties are set out in Table 4.3. The thermal properties were explained in Chapter 3. The zero stress temperature is close to the temperature at which the die was manufactured at which point the residual stress within the die material was also assumed to be zero. The initial temperature of the cast metal was 700°C [7] throughout and this, is assumed to approximate the metal temperature at the end of the displacement part of the cycle. The die has an uniform initial temperature of 200°C. The heat transfer conditions in the coolant system corresponds to a heat transfer coefficient and reference temperature of 1000W/m^{2}K [Appendix II] and 100°C respectively and heat is removed from the external surfaces in accordance with a heat transfer coefficient to 25 W/m^{2}K and an ambient temperature of 25°C [8,9]. Very good contact is assumed at the die to cast interface, hence an interfacial heat transfer coefficient of 5000 W/m^{2}K [9,10] was applied.

Mechanical Properties	
Young's Modulus (N/m2)	2.10×10^{11}
Poisson's Ratio	0.3
Thermal expansion coefficient (per °C)	0.12×10^{-4}
Zero stress temperature (°C)	25

Table 4.3

The mechanical properties of a tool Steel H13 [11]

The temperature distribution in the die was used for the calculation of thermal stresses for the structural evaluation. All axial displacements were constrained at the

bottom of the die reflecting its fixture in the squeeze forming press and symmetry was applied on the rotational axis.

Due to the transient nature of the cooling process, there will be a consequent variation in stresses within the die and ideally, the coolant channel positions will respond to minimise stresses throughout the cooling cycle. Practically this is not easy to achieve[1] and so the optimisation has been applied for a stress state achieved after a cooling time of 50*s*. This has been chosen since the time was used in the work in [12] for an almost similar geometry for the pressurised solidification duration. The exact duration for the pressurised solidification in the work [12] was 57*s*, however, due to the slightly different initial conditions, 50*s* has been selected in this work. All of the casting is predicted to be solid after just 15*s*. This is slightly different from the result obtained in [13], since the boundary condition of the coolant channels was considered as a fixed temperature prescription of 280 °C.

Figure 4.6 shows the von Mises stress distribution in the die for the optimum position of coolant channels derived from the single-objective function defined as Case study 6. Figure 4.7 shows the von Mises stress distribution in the die for the optimum position of coolant channels obtained from Chapter 3 to achieve near simultaneous solidification for the first cycle. It can be seen from both Figures that higher von Mises stresses are developed near the corners of the part and coolant channels. Indeed, high stress level can be observed from both Figures. This is due to the fact that in this work, the die is constructed from single piece. The use of block components to build the die will probably lead to some relaxation since each block can move relative to each other. However, this is not considered in this work because to deal with this accurately will require

[1] It may be approximated through switching coolant channels on and off during the cooling process

consideration of contact and fixing models between the blocks. Figure 4.8 shows the corresponding finite element mesh in the die for the Case study 6. Figure 4.9 and 4.10 show the temperature distribution in the die and cast part respectively at t=50s. It can be seen from Figure 4.10 that the temperature distribution in the cast part was not uniform and this will lead to more complex non uniform solidification history. Also, as indicated, one of the coolant channels was positioned within the geometry of the cast part. This is impractical, but could be interpreted as a requirement for two smaller coolant ducts to be placed either side of the component. Under these circumstances, any mesh conflict was edited from the domain. This geometrical conflict could be eliminated through imposing additional constraints on coolant duct position. When overlapping between the coolant and part geometry occurs, the mesh belongs to the incorrect domain as shown in Figure 4.11. However, the unwanted mesh attached to the cast part was deleted by hand for the purpose of graphical presentation. The correctness of the predicted results is not affected.

Figure 4.12 shows the stress levels at nodes in the die at t=50s for the optimum solution obtained in Case study 6. The X-axis represents the node number in the die and the y-axis represents the von Mises stress value and the horizontal line represents the average value. Figure 4.13 shows the stress distribution in the die at t=50s for the optimum solution obtained in Chapter 3 to achieve near simultaneous solidification in the cast part for the first cycle. It can be seen from these figures, the result obtained for Case study 6 not only lowered the fluctuation of the von Mises stress distribution, but also reduced the average von Mises stress value in the die. The ideal solution is where the residual of the fluctuation of von Mises stress distribution and the average von Mises stress are close to zero.

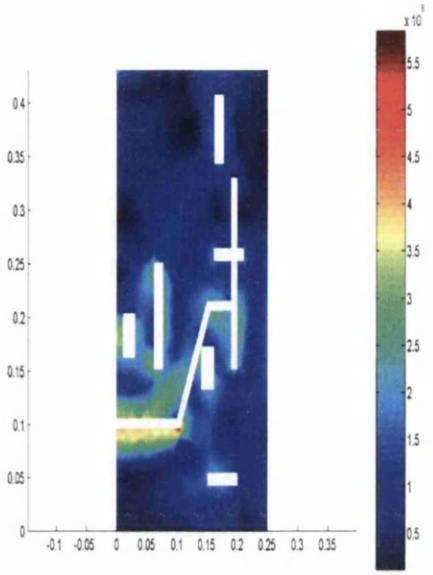

Figure 4.6

Von Mises stress in the die at t=50s for the single-objective optimum solution for Case study 6

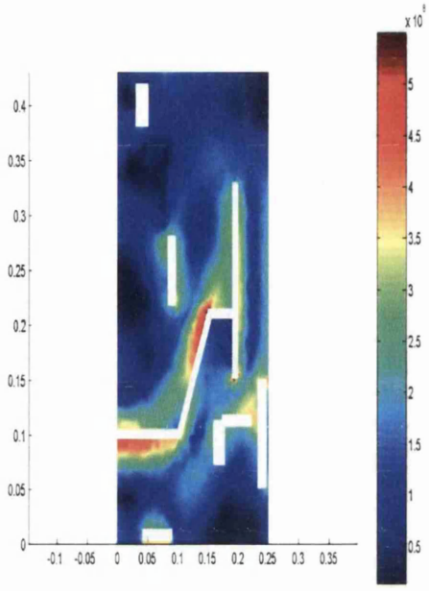

Figure 4.7

Von Mises stress in the die at t=50s for the optimum solution obtained in Chapter 3 for Case study 3

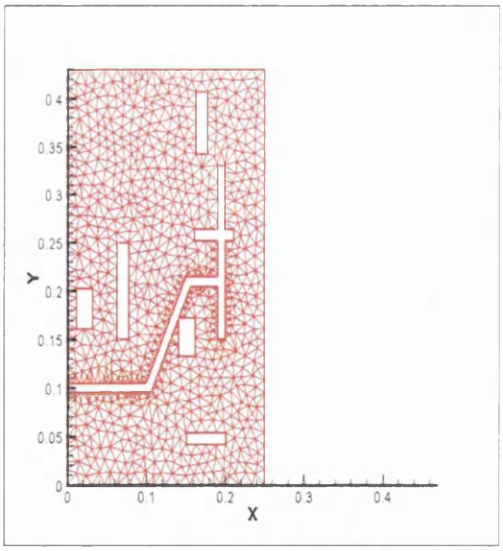

Figure 4.8

The corresponding finite element mesh in the die

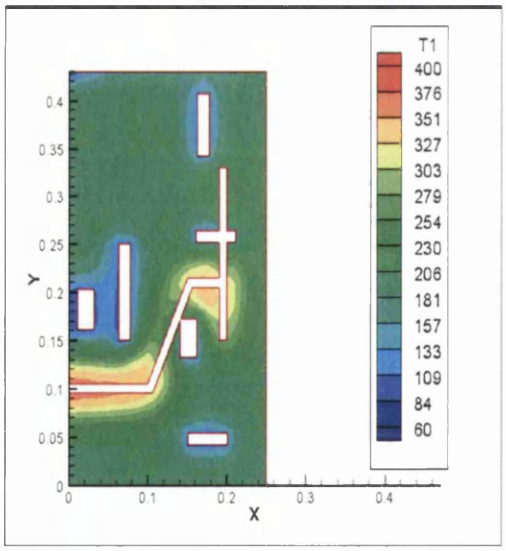

Figure 4.9

Temperature distribution in the die at t=50s for the single-objective optimum solution for Case study 6

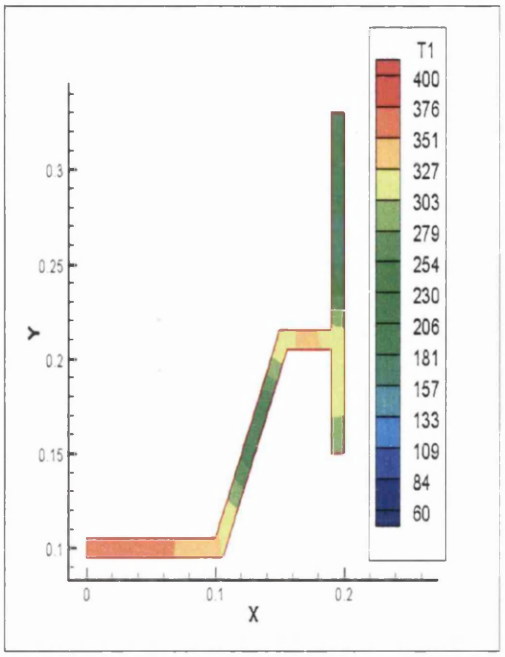

Figure 4.10

Temperature distribution in the casting at t=50s for the single-objective optimum solution for Case study 6

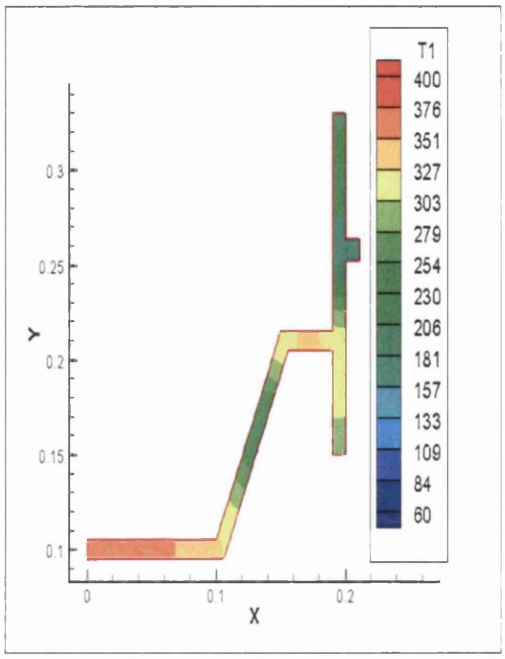

Figure 4.11

Temperature distribution in the casting without editing at t=50s for the single-objective optimum solution for Case study 6

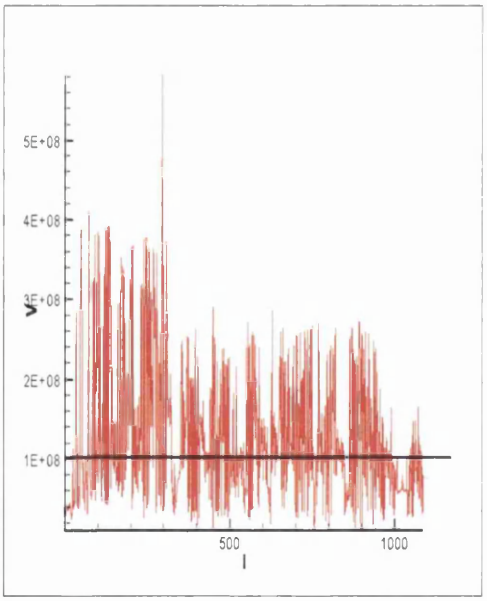

Figure 4.12

Stress distribution in the die at t=50s for the optimum solution obtained for Case study 6

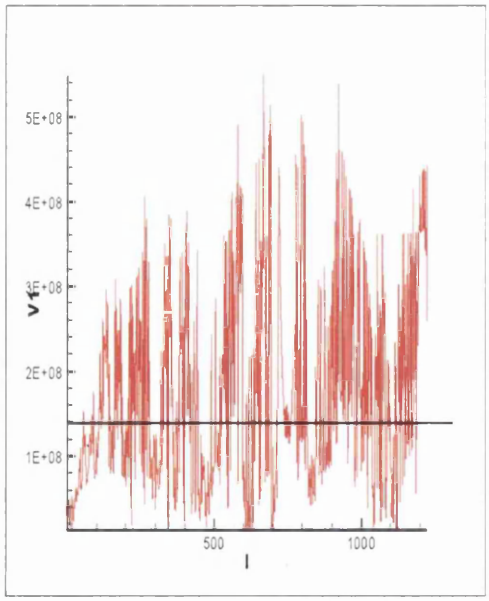

Figure 4.13

Stress distribution in the die at t=50s for the optimum solution obtained in Chapter 3 for Case study 3

Figure 4.14 shows the von Mises stress distribution in the die for the optimum position of coolant channels for the objective function defined as Case study 7. Figures 4.15 and 4.16 show the temperature distributions in the die and cast part respectively. Figures 4.17 and 4.18 show the stress distributions in the die at t=50s for the optimum solutions obtained in Case study 7 and also from Chapter 3. Again, the result obtained for Case study 7 are better when compared with the result obtained in Chapter 3 in terms of reducing the fluctuation and also the average von Mises stress value.

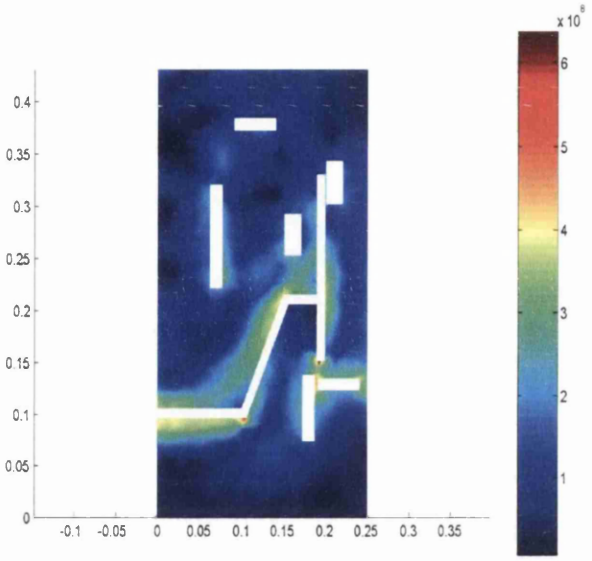

Figure 4.14

Von Mises stress in the die at t=50s for the single objective optimum solution for Case study 7

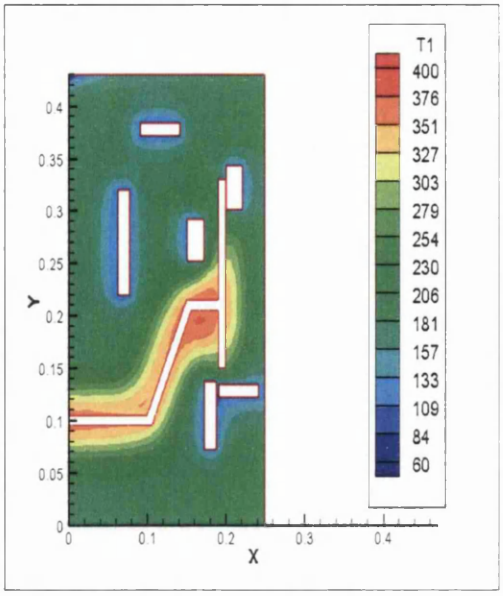

Figure 4.15

Temperature distribution in the die at t=50s for the single-objective optimum solution for Case study 7

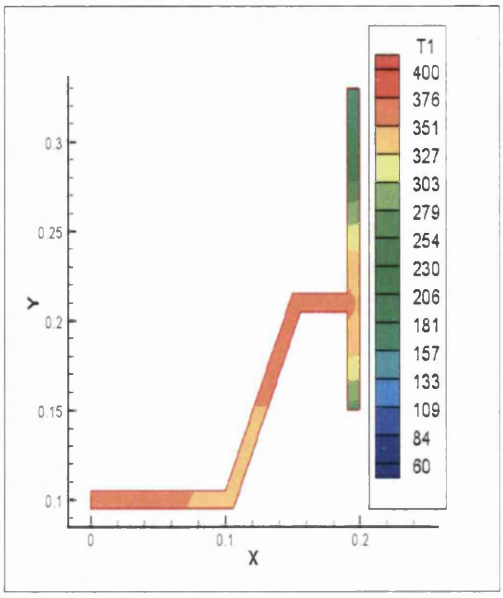

Figure 4.16

Temperature distribution in the casting at t=50s for the single-objective optimum solution for Case study 7

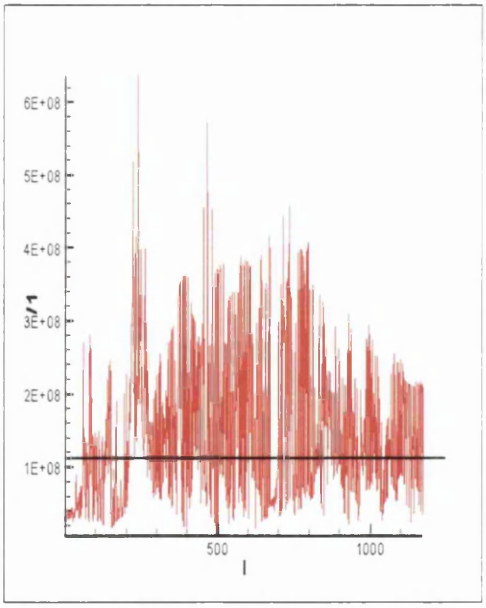

Figure 4.17

Stress distribution in the die at t=50s for the optimum solution obtained for Case study 7

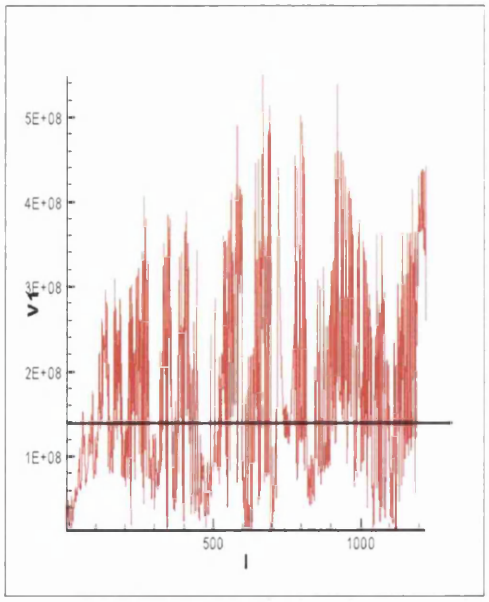

Figure 4.18

Stress distribution in the die at t=50s for the optimum solution obtained in Chapter 3 for Case study 3

Although temperature non-uniformity in the cast part was still observed, a better result is obtained using the objective function for Case study 7, where a more uniform temperature distribution in the part can be observed when compared with Case study 6. However, the Case study 6 gave the best average stress function as compared to Case study 7.

It can be seen that preceding examples show how the conflict between optimisation based on thermal and stress based criteria. Therefore, in the following examples, the mutli-objective optimisation will be attempted by considering both aspects.

4.4 Multi-Objective Optimisation

Multi-objective optimisation is often required as part of the design process, especially in applications that feature process simulation. In all cases, the attraction is the prospect of obtaining a good (or even best) solution with respect to different and often conflicting requirements. In this section, the conflicting requirements involve the thermal and mechanical aspects which will be set out below.

4.4.1 Objective Functions

There are a number of objective functions that may be defined and tested to optimise coolant system position. To achieve multi-objective optimisation, the objective function may be defined as minimising the following, where $F_1(\mathbf{x})$ represents the objective function for thermal analysis and $F_2(\mathbf{x})$ represents the objective function for mechanical analysis;

$$F(\mathbf{x}) = F_1(\mathbf{x}) + F_2(\mathbf{x}) \tag{4.4}$$

The objective functions chosen build on those defined in Chapter 3 and in section 4.3.

Two case studies have been considered as set out below.

Case study 8

In Case study 8, $F_1(\mathbf{x})$ is defined as

$$F_1(\mathbf{x}) = \frac{1}{\Omega_C} \int_{\Omega_C} [(T_{\max} - T_{\text{ave}})^2 + (T_{\min} - T_{\text{ave}})^2]^{1/2} d\Omega \tag{4.5}$$

where Ω_C is the cast part domain. T_{max} and T_{min} are the maximum and minimum temperatures in the cast part. T_{ave} is the average temperature in the cast part,

$$T_{ave} = \frac{\sum_{i=1}^{NC} T_C}{NC} \tag{4.6}$$

where T_C is the average temperature of the cast element and NC is the total number of elements in the cast.

$F_2(\mathbf{x})$ can be described as

$$F_2(\mathbf{x}) = \left\{ \frac{1}{\Omega_D} \int_{\Omega_D} [(\sigma_{\max} - \sigma_{\text{ave}})^2 + (\sigma_{\text{ave}} - \sigma_{\min})^2]^{\frac{1}{2}} d\Omega \right\} / 10^5 \tag{4.7}$$

where Ω_D is the die domain. σ_{max} and σ_{min} are the maximum and minimum von Mises stresses in the cast part. σ_{ave} is the average von Mises stress in the die and it is given by

$$\sigma_{\text{ave}} = \frac{\sum_{i=1}^{ND} \sigma_e(\mathbf{x})}{ND} \tag{4.8}$$

where $\sigma_e(\mathbf{x})$ is the average von Mises stress for each discretised element in the die and ND is the total number of elements in the die.

The division by 10^5 is necessary to balance the value of $F_1(\mathbf{x})$. It acts as a scaling factor between the very large stress related and smaller temperature related values.

Case study 9

For Case study 9, $F_1(\mathbf{x})$ has the same definition as described in Case study 8. However, $F_2(\mathbf{x})$ is defined as and has been scaled by 10^6 to maintain compatibility with the thermal function.

$$F_2(\mathbf{x}) = \sum_{i=1}^{ND} \left[(\sigma_e(\mathbf{x}) - \sigma_{ave})^2 \right] / 10^6 \qquad (4.9)$$

where $\sigma_e(\mathbf{x})$ is the average von Mises stress for each discretised element in the die and ND is the total number of elements in the die. Again, σ_{ave} is the average of von Mises stress in the die.

The constraints on coolant channel position that have been discussed already were also applied.

4.4.2 Numerical Example

Figure 4.19 shows the von Mises stress distribution in the die for the optimum position of coolant channels for Case study 8 where the range of the von Mises stress was 484MPa. Although this is a high stress level it remains within the yield stress limit for a tool steel H13 die that is typically 1180 MPa at 150°C [11]. Figures 4.20 and 4.21 show the temperature distributions in the die and cast part respectively at t=50s. For the stress

analysis, for the case where the coolant channel is over the cast part, the mesh belongs to the die and therefore the stress solution is valid.

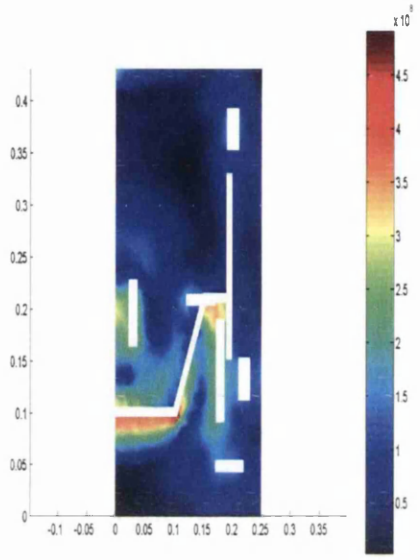

Figure 4.19

Von Mises stress in the die at t=50s for the multi-objective optimum solution for Case study 8

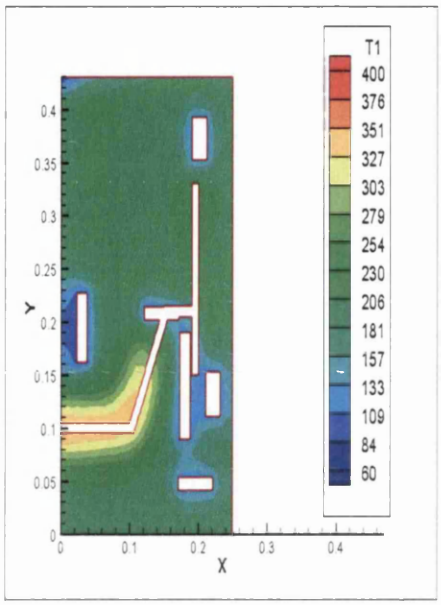

Figure 4.20

Temperature distribution in the die at t=50s for the multi-objective optimum solution for Case study 8

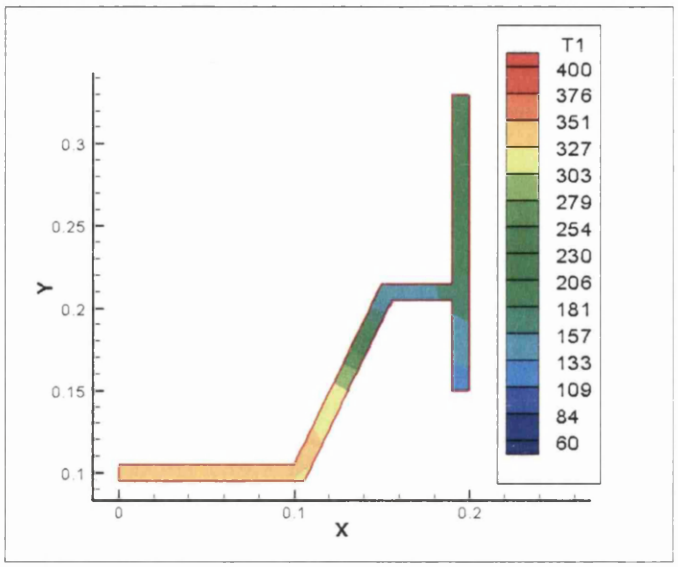

Figure 4.21

Temperature distribution in the casting at t=50s for the multi-objective optimum solution for Case study 8

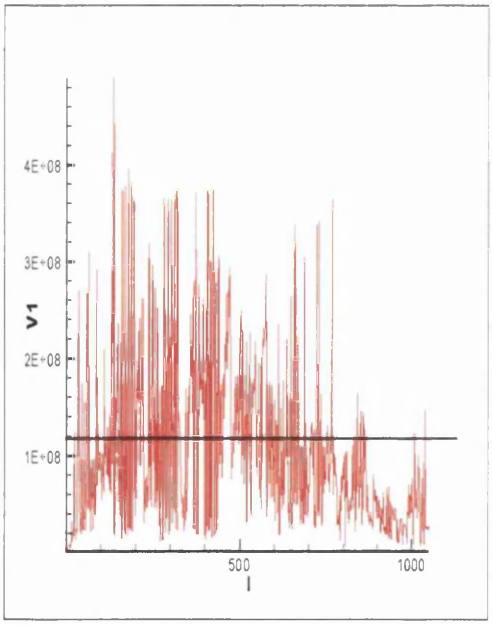

Figure 4.22

Stress distribution in the die at t=50s for the optimum solution obtained for Case study 8

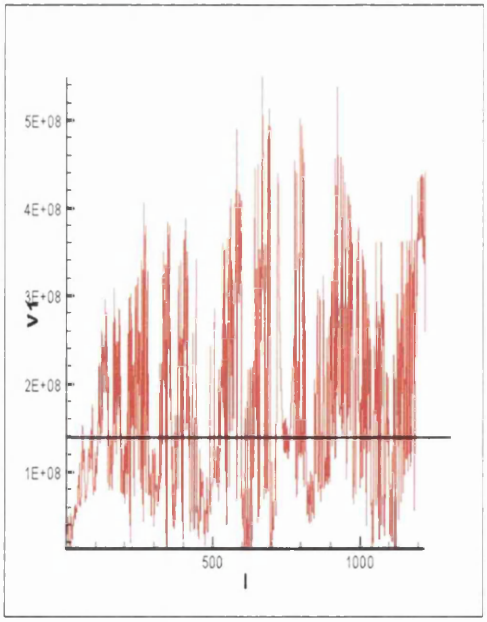

Figure 4.23

Stress distribution in the die at t=50s for the optimum solution obtained in Chapter 3 for Case study 3

Figures 4.22 and 4.23 show the stress distributions in the die at t=50s for the optimum solutions obtained in Case study 8 and also from Chapter 3. Again, the comparison has been done with the result obtained in Chapter 3. It can be seen that the result obtained from Case study 8 was better than the result obtained in Chapter 3 based on the reduction of the average von Mises value and also the fluctuation in the stress distribution.

Figure 4.24 shows the von Mises stress distribution in the die for the optimum positions of coolant channels for Case study 9 where the von Mises stress exhibited a maximum value of 558MPa. Figure 4.25 and 4.26 show the temperature distributions in the die and cast part respectively at t=50s.

It can be seen that the von Mises stress range obtained for Case study 8 was lower than the von Mises stress range for Case study 9, thus, showing the effectiveness of the formulation of the objective function for Case study 8 to minimise the von Mises stress range in the die. Generally, Case study 9 gives a lower level through the die, the high value is rather local.

Figures 4.27 and 4.28 show the stress distributions in the die at t=50s for the optimum solutions obtained in Case study 9 and also from Chapter 3. The result obtained in Case study 9 was better than the result obtained in Chapter 3 in reducing the von Mises stress distribution fluctuation and also the average von Mises stress value.

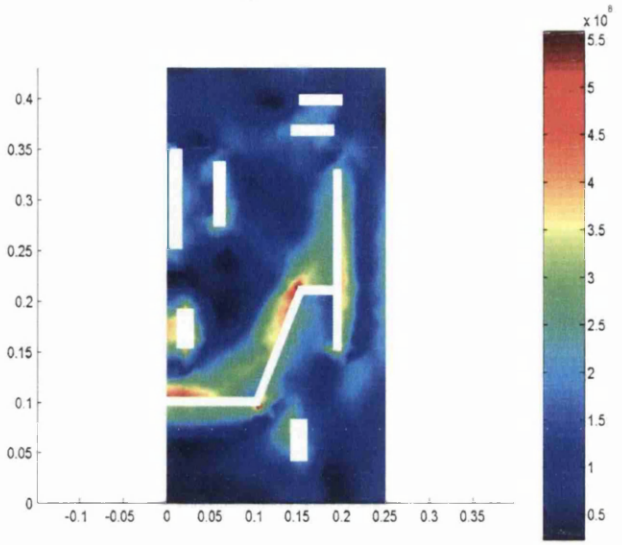

Figure 4.24

Von Mises stress in the die at t=50s for the multi-objective optimum solution for Case study 9

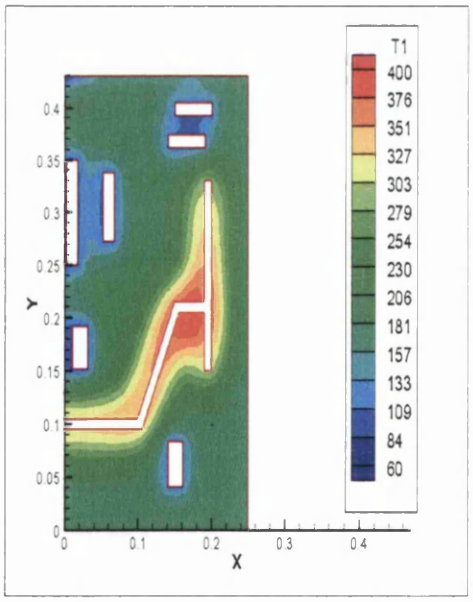

Figure 4.25

Temperature distribution in the die at t=50s for the multi-objective optimum solution for Case study 9

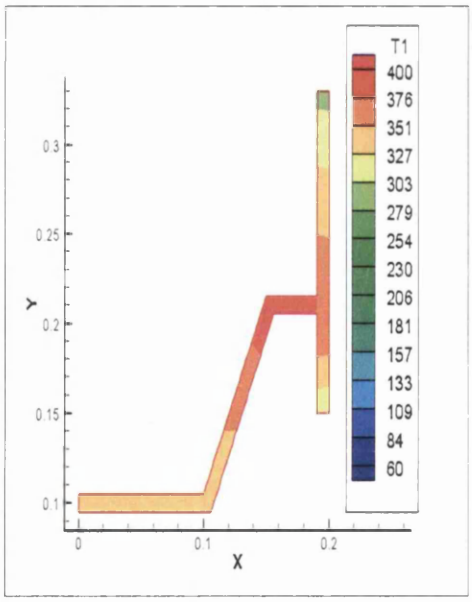

Figure 4.26

Temperature distribution in the casting at t=50s for the multi-objective optimum solution for Case study 9

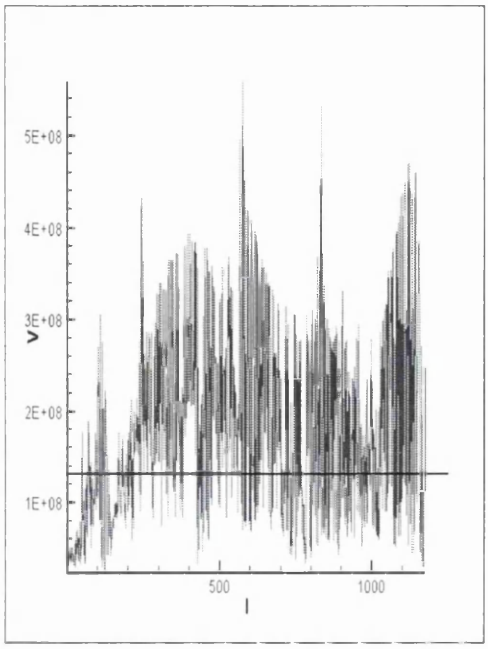

Figure 4.27

Stress distribution in the die at t=50s for the optimum solution obtained for Case study 9

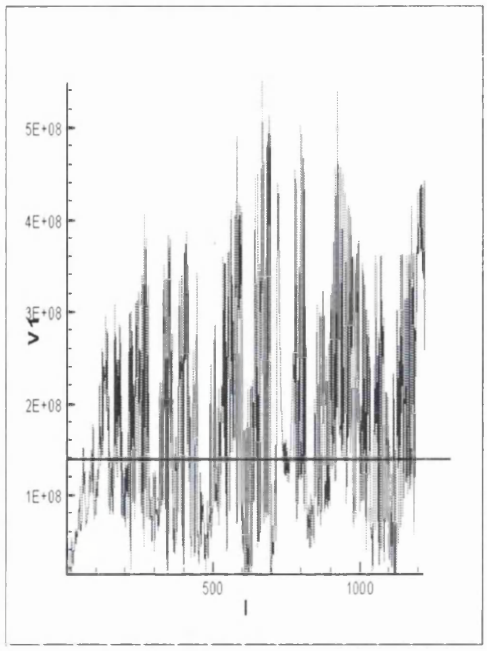

Figure 4.28

Stress distribution in the die at t=50s for the optimum solution obtained in Chapter 3 for Case study 3

For the results obtained from Case studies 8 and 9, it can be seen that higher von Mises stresses are developed near the corners of the part and coolant channels. However, the results obtained for Case study 9 was better than for Case study 8, where the temperature distribution in the cast part was more uniform than the temperature distribution in the cast part for Case study 8, therefore maintaining the near simultaneous solidification in the cast part.

4.5 Single and Multi Objective Optimisations for Cyclic Analysis

In Chapter 3, the near simultaneous solidification in the cast part with respect to the positions of the coolant channels was explored not only for the first cycle, but also for the tenth cycle. This was done to mimic the actual cycle that a die must undergo during the process warm up to achieve thermal stabilisation. Thus, the temperature distribution in the previous cycle is used for the next cycle analysis. This will also affect the von Mises stress distribution in the die as well, due to the variation in die temperature at the start of the cooling process and due to the generally higher temperature within the die.

4.5.1 Objective Functions

Again, to achieve multi-objective optimisation for cyclic analysis, the objective function may be defined as minimising the following, where $F_1(\mathbf{x})$ represents the objective function for thermal analysis and $F_2(\mathbf{x})$ represents the objective function for mechanical analysis as described in Equation 4.4 for Case study 9, which were the best objective functions from the previous calculation set.

4.5.2 Numerical Example

In this section, the comparison has been done for first and tenth cycles with the same formulation of the objective function as defined in Equation 4.4 for Case study 9.

Figure 4.29 shows the von Mises stress distribution in the die for the optimum position of coolant channels for tenth cycle at t=50s and Figure 4.30 shows the von Mises

stress distribution in the die for the optimum position of coolant channels for Case study 9 for the first cycle at t=50s. Figure 4.31 and 4.32 show the corresponding temperature distributions in the die at t=50s. Figure 4.33 and 4.34 show the corresponding temperature distributions in the cast part at t=50s. Figures 4.35 and 4.36 show the stress distributions in the die at t=50s for the multi-objective optimum solutions obtained for the tenth and first cycles respectively.

It can be seen from the results obtained for both case studies for the tenth and first cycles, the temperature distributions in the cast part were nearly uniform and also lower stress level occur through the die, where the high value was rather local. For the cyclic analysis which leads to generally high temperatures, the coolant channels were positioned to be away from the casting itself. This reflects the results discussed in Chapter 3, highlighting the need for a cyclic analysis since it has a major impact on die thermo-mechanical design.

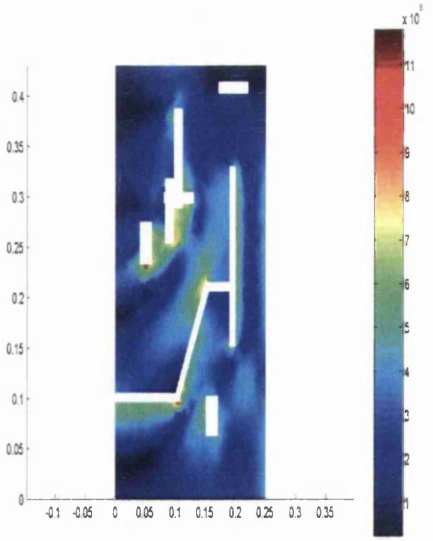

Figure 4.29

Von Mises stress in the die at t=50s for the multi objective optimum solution at the tenth cycle

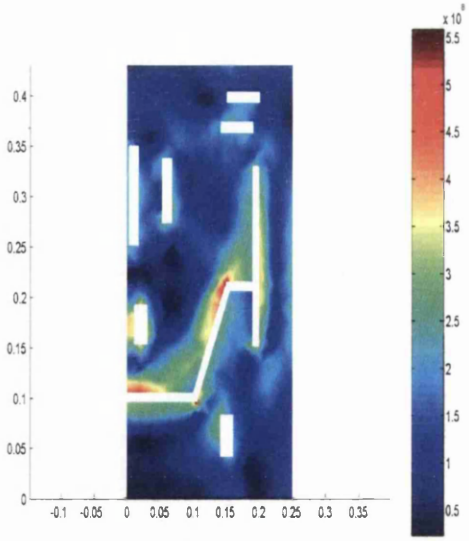

Figure 4.30

Von Mises stress in the die at t=50s for the multi-objective optimum solution at the first cycle for Case study 9

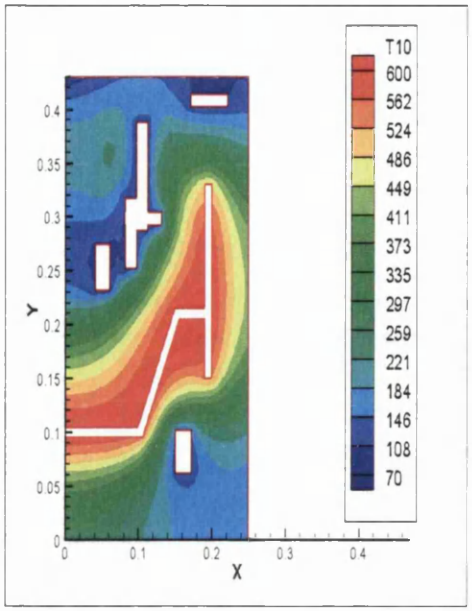

Figure 4.31

Temperature distribution in the die at t=50s for the multi-objective optimum solution at the tenth cycle

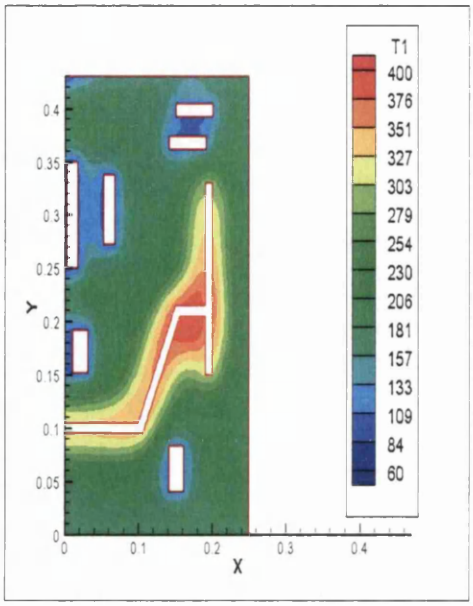

Figure 4.32

Temperature distribution in the die at t=50s for the multi-objective optimum solution at the first cycle for Case study 9

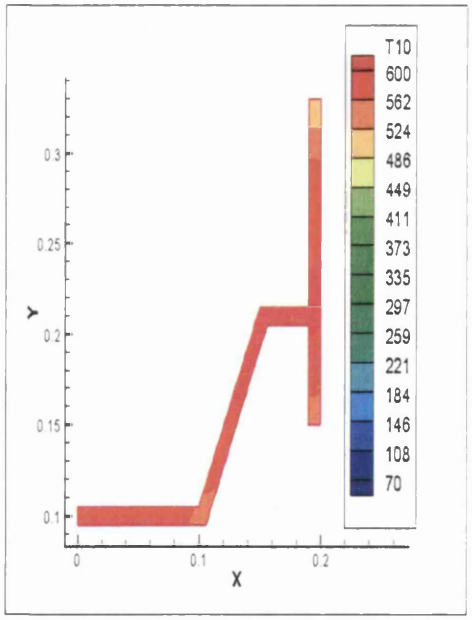

Figure 4.33

Temperature distribution in the casting at t=50s for the multi-objective optimum solution at the tenth cycle

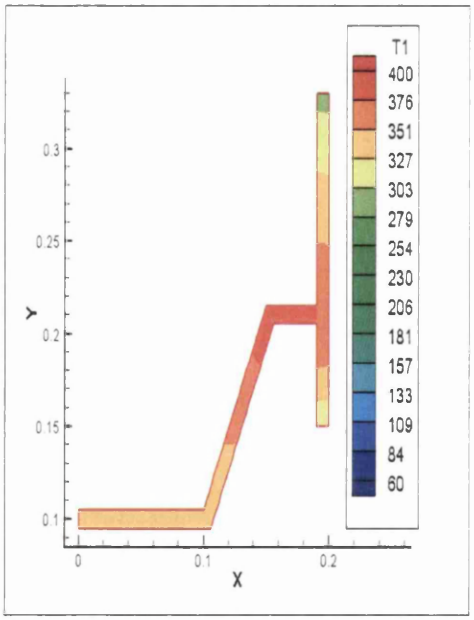

Figure 4.34

Temperature distribution in the casting at t=50s for the multi-objective optimum solution at the first cycle for Case study 9

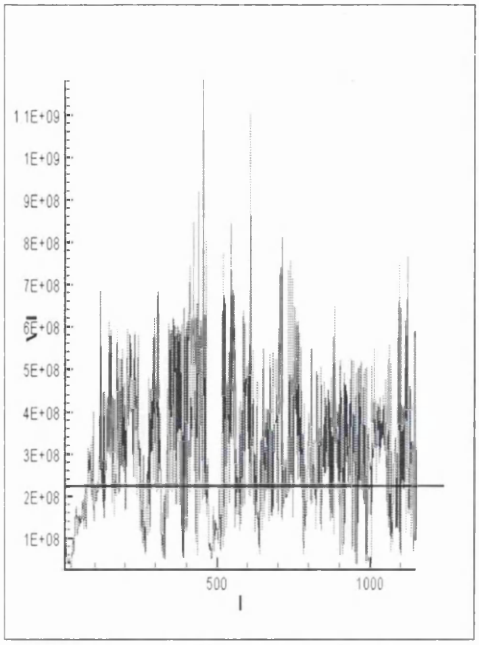

Figure 4.35

Stress distribution in the die at t=50s for the multi-objective optimum solution at the tenth cycle

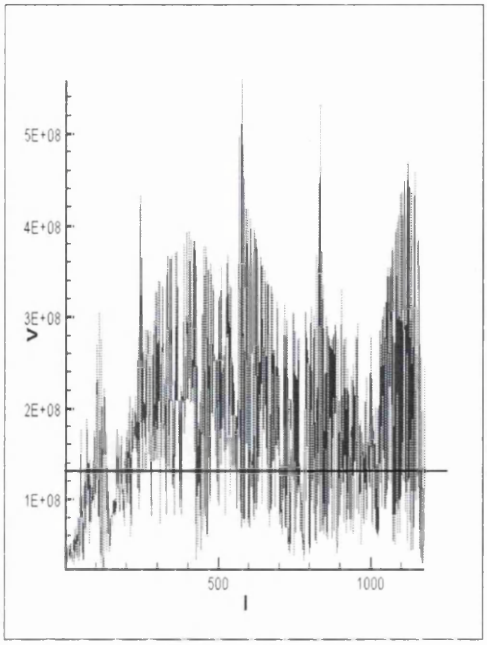

Figure 4.36

Stress distribution in the die at t=50s for the multi-objective optimum solution at the first cycle for Case study 9

However, for a more practical solution, the following design of the coolant channels system has been proposed based on a ten cycle analysis. This is proposed, by grouping together the three coolant channels which overlap. Figure 4.37 shows the von Mises stress distribution in the die for the practical solution for the tenth cycles at t=50s. Figures 4.38 and 4.39 shows the corresponding temperature distributions in the die and casting at t=50s. Figures 4.40 and 4.41 show the stress distributions in the die at t=50s for the practical solution and the multi-objective optimum solution obtained for the tenth cycle. Through this comparison it can be seen that the 'ideal' and 'practical'solutions lead to near identical results.

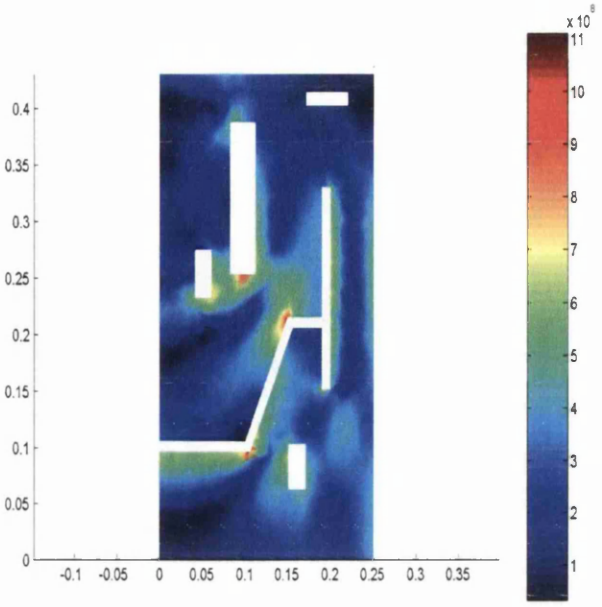

Figure 4.37

Von Mises stress in the die at t=50s for the practical solution at the tenth cycle

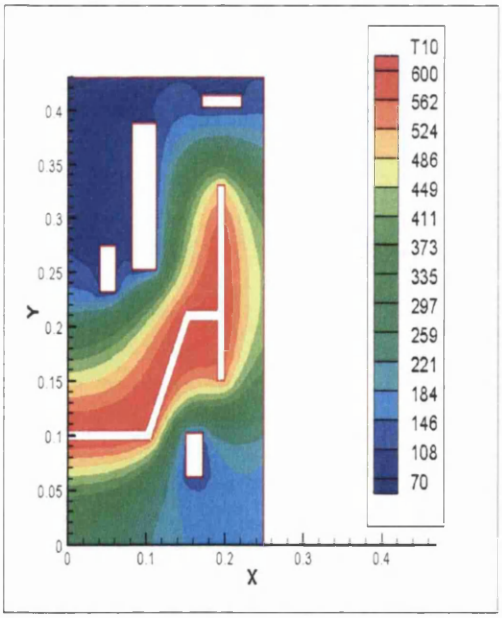

Figure 4.38

Temperature distribution in the die at t=50s for the practical solution at the tenth cycle

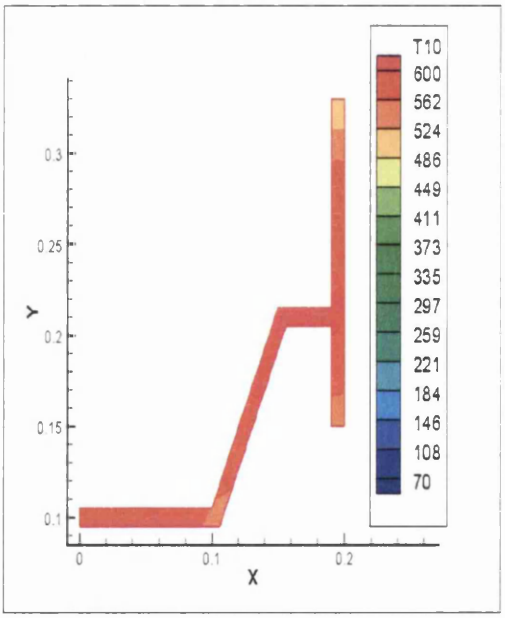

Figure 4.39

Temperature distribution in the casting at t=50s for the practical solution at the tenth cycle

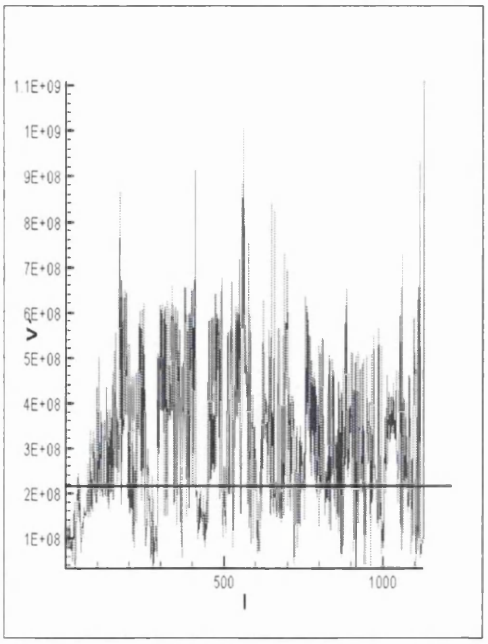

Figure 4.40

Stress distribution in the die at t=50s for the practical solution at the tenth cycle

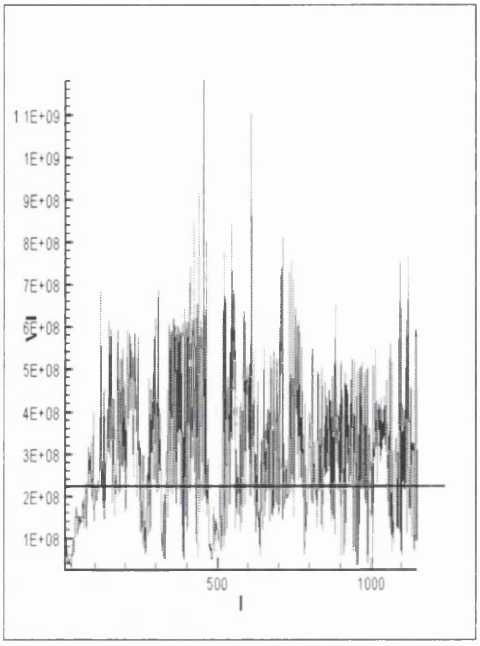

Figure 4.41

Stress distribution in the die at t=50s for the multi-objective optimum solution at the tenth cycle

4.6 Comparison of the Coolant Channel System Design

In this section, the comparison of the coolant channel system design between the result obtained from the practical solution and the coolant channel design which is implemented in the industry (GKN Squeezeform) is discussed.

The configuration of the coolant channel system implemented at GKN is designed based on intuition, where the coolant channels are positioned to be in close proximity to the cast part. Clearly, by doing so, rapid solidification can be achieved effectively, thus reducing the cooling cycle time. However, based on the simulations undertaken within this chapter, this will also lead to localised solidification within the casting and not the near simultaneous solidification that is required to ensure part integrity.

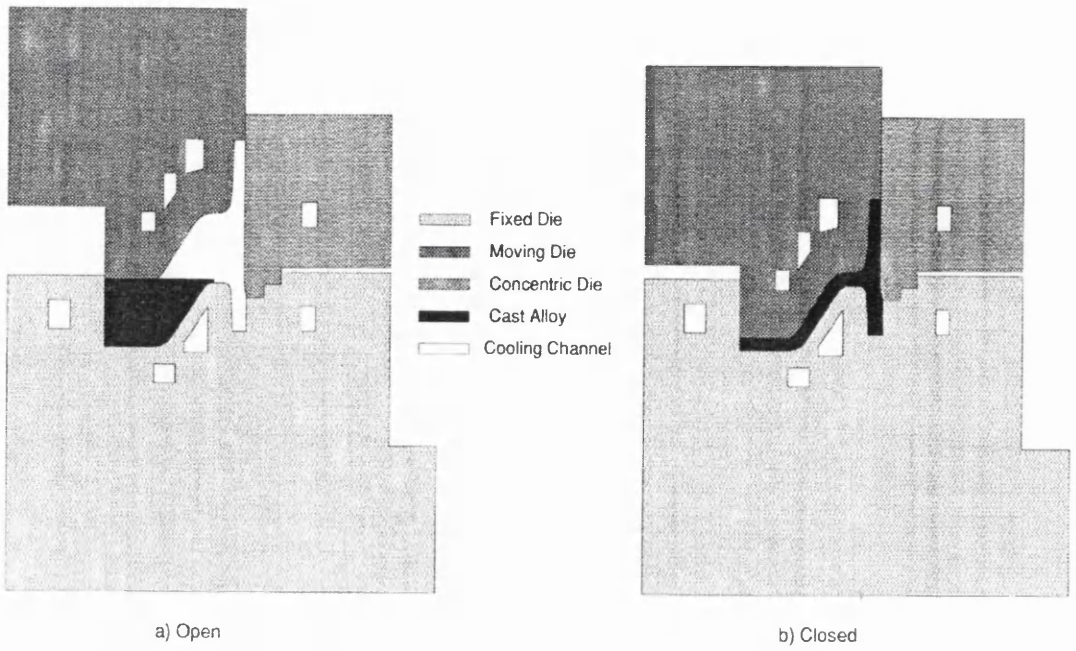

Figure 4.42

Radial cross-sectional view of the dieset arrangement at open and closed positions. (7)

4.7 Closure

The multi-objective optimisation involving thermal and mechanical aspects has successfully been implemented for the first and tenth cycles. In the multi-objective optimisation for the first and tenth cycles, the coolant channels are positioned to enclose the cast part to achieve near simultaneous solidification in the cast part and at the same time improving the von Mises stress distribution in the die. This highlights that the multi-objective optimisation approach has improved the performance from both aspects, whereas the single-objective optimisation solely concentrated on achieving better performance in thermal aspect only.

The comparison of the coolant channel system design between the results obtained from the optimisation software and the configuration which is implemented in industry has been performed. It can be seen that the intuitive design implemented in the industry is open to considerable improvements and these have been achieved, in terms of obtaining a better solidification pattern in the cast part and von Mises stress distribution in the die.

References

1. E.W. Postek, R.W. Lewis, D.T. Gethin and R.S. Ransing, 'Influence of initial stresses on the cast behaviour during squeeze forming processes', *Journal of Material Processing Technology*, **159**, 338-346 (2005).

2. Michalewicz Z. Genetic algorithms + data structures = Evolution programs. New York:Springer-Verlag,1996.

3. Bellenger E and Coorevits P. Adaptive mesh refinement for the control of cost and quality in finite element analysis. *Finite Elements in Analysis and Design*. 2005; 41:1413-1440.

4. http://www.magmasoft.com/ (2003).

5. http://www.calcom.ch/index.html/ (2003).

6. http://www.rockfield.co.uk/elfen.htm (2003).

7. www.gknplc.com/ (2003).

8. Lewis RW, Manzari MT and Gethin DT. Thermal optimisation in the sand casting process. *Engineering Computations*. 2001; **18 (3/4)**: 392-416.

9. Anderson JT. A theoretical and experimental investigation into the investment and gravity die casting processes. M.Phil Thesis, Swansea University, 1995.

10. K. Ravindran and R.W. Lewis, 'Finite element modelling of solidification effects in mould filling', *Finite Elements in Analysis and Design*, 1998;**31**, 99-116.

11.http://www.bucorp.com/Products/HotWorkSteels/DataSheets/Orvar_Superior.pdf (2003).

12. Gethin DT, Lewis RW and Tadayon MR. A finite element approach for modeling metal flow and pressurized solidification in the squeeze casting process. *Int. j. numer. Methods eng.* 1992;35:939-950.

13. M.R. Tadayon. Finite element modelling of heat transfer and solidification in the squeeze forming process. PhD thesis, Swansea University, 1992.

Chapter 5

Design Sensitivity Analysis and Design Element Concept

5.1 Introduction

As discussed in chapter two, gradient-based optimisation is one of the most popular strategies in tackling optimisation in engineering design problems. The calculation of sensitivity gradients is a core requirement for optimisation. Such calculations can be computationally demanding and any strategy that will reduce this demand is attractive. This has led to exploration of a Design Element Concept. The application of the Design Element Concept including the parameter and shape sensitivities will be discussed in the following sections.

In standard design sensitivity analysis, sensitivity gradients are calculated for each discretised element in the domain. However, the Design Element Concept allows the

design sensitivity gradients to be calculated based on zones of design elements, thus reducing the design sensitivity loop calculation that significantly decreases the demands for the optimisation process.

This chapter will focus on an exploration of techniques for computing design sensitivity on an element basis, including difference and analytical methods. This will be followed by consideration of the design element concept that will make use of the analytical techniques for design sensitivity calculation.

5.2 Analytical Methods

Where they may be applied, analytical methods have an advantage over Finite Difference Methods (FDM) due to their accuracy and efficiency in performing the gradient calculations. This is further amplified for nonlinear problems where the FE analyses are expensive. The optimisation of nonlinear problems has been explored in metal forming processes, polymer extrusion and casting processes as discussed in chapter two. There are two types of analytical methods; namely the Direct Differentiation Method (DDM) and the Adjoint Variable Method (AVM). Generally, the DDM is used if the number of Design Constraints (DC) is greater than the Number of Design Variables (NDV). In the DDM, the derivatives of the response with respect to design variables are solved as many times as there are design variables. Thus, the DDM is used if NDV < DC. In the AVM, the adjoint equation is solved as many times as there are design constraints. Therefore, it is efficient to find the design sensitivity gradients using the AVM if DC $\leq$ NDV.

In the following section, the formulations of the DDM and the AVM sensitivities will be derived.

5.2.1 Direct Differentiation Method (DDM)

The DDM can be illustrated through consideration of the general matrix equation that includes a vector containing design variables,

$$\boldsymbol{K(b)q=F} \qquad \textbf{(5.1)}$$

In equation 5.1, $\boldsymbol{b}$ is the design variable vector, $\boldsymbol{q}$ is the displacement vector, $\boldsymbol{F}$ is the global force vector and $\boldsymbol{K}$ is the global stiffness matrix. The goal is to find the sensitivity of a function ψ $(\boldsymbol{q(b)}, q_a, \boldsymbol{\sigma(b)}, \sigma_{a,}, \boldsymbol{b})$ with respect to the design variables $\boldsymbol{b}$ that typically includes shape and process parameters, such as the position of the coolant channels, interfacial heat transfer coefficient, enthalpy and material choices such as Young Modulus, Coefficient of thermal expansion, Poisson's ratio and conductivity. Thermal and Mechanical aspects are both important in the process, however, the design sensitivity analysis and Design Element Concept in this chapter will only be applied to the mechanical analysis due to the direct consequence that it has in the die, especially related to the stress in the die. Thus, the function may contain the response fields such as displacement or von Mises stress field, depending on the objective to be achieved, as well as the constraints such as displacement and von Mises stress that may be applied in order to avoid exceeding the critical limit due to certain restrictions on the structure. For instance, to avoid failure, such as plastic yielding, cracking and high cyclic stress that can also lead to fatigue failure. These are typical problems involving structural analysis. Failure initiation may be associated with high von Mises stress values.

The function has the general form

$$\psi\ (\boldsymbol{q(b)}, q_a, \boldsymbol{\sigma(b)}, \sigma_{a,}\ \boldsymbol{b}) \text{ subject to } \boldsymbol{K(b)q=F}$$

where $\nabla_b \psi$ is defined as

$$\nabla_b \psi = \left[\frac{\partial \psi}{\partial \boldsymbol{b}_1} \frac{\partial \psi}{\partial \boldsymbol{b}_2} \cdots \frac{\partial \psi}{\partial \boldsymbol{b}_n} \right] \tag{5.2}$$

In equation 5.2, q_a is the displacement constraint and σ_a is the von Mises stress constraint. Assuming that the $\boldsymbol{K}$ matrix is not singular, both sides of the equilibrium equation can be differentiated with respect to $\boldsymbol{b}$. The following expression for $\nabla_b \boldsymbol{q}$ is derived:

$$\nabla_b \boldsymbol{q} = \boldsymbol{K}^{-1} [\nabla_b \boldsymbol{F} - \nabla_b (\boldsymbol{K}\boldsymbol{q})] \tag{5.3}$$

The exact sensitivities of ψ ($\boldsymbol{q}(\boldsymbol{b})$, $q_a, \boldsymbol{\sigma}(\boldsymbol{b}), \sigma_a, \boldsymbol{b}$) can be calculated by substituting $\nabla_b \boldsymbol{q}$

$$\nabla_b \psi = \nabla_b^e \psi + \nabla_q \psi . \nabla_b \boldsymbol{q} \tag{5.4}$$

Where $\nabla_b^e \psi$ is the gradient term for explicit dependence of ψ ($\boldsymbol{q}(\boldsymbol{b})$, q_a, $\boldsymbol{\sigma}(\boldsymbol{b}), \sigma_a, \boldsymbol{b}$) on $\boldsymbol{b}$. However, in order to apply the von Mises stress constraint, instead of using Equation 5.4 which is applicable for the displacement constraint, the exact sensitivities of ψ ($\boldsymbol{q}(\boldsymbol{b})$, q_a, $\boldsymbol{\sigma}(\boldsymbol{b}), \sigma_a, \boldsymbol{b}$) can be calculated by substituting $\nabla_b \boldsymbol{q}$ in the following equation,

$$\nabla_b \psi = \nabla_b^e \psi + \nabla_\sigma \psi . \nabla_q \boldsymbol{\sigma} . \nabla_b \boldsymbol{q} \tag{5.5}$$

5.2.2 Adjoint Variable Method (AVM)

For the AVM, firstly, an augmented functional is defined,

$$L(\boldsymbol{q}, \boldsymbol{b}, \lambda) = \psi - \lambda^T (\boldsymbol{K}\boldsymbol{q} - \boldsymbol{F}) \tag{5.6}$$

where λ is a Lagrange multiplier vector and the additional condition is the equilibrium equation.

From the stationary condition,

$$\frac{\partial L}{\partial \boldsymbol{q}} = 0 \tag{5.7}$$

Differentiating the augmented functional with respect to the design variable gives

$$\frac{dL}{d\boldsymbol{b}} = \frac{d\psi}{d\boldsymbol{b}} - \lambda^T \frac{d}{d\boldsymbol{b}}(\boldsymbol{Kq} - \boldsymbol{F}) \tag{5.8}$$

Since the state equation holds,

$$\frac{dL}{d\boldsymbol{b}} = \frac{d\psi}{d\boldsymbol{b}} \tag{5.9}$$

Defining the sensitivity of the augmented functional with respect to the design variable vector leads to

$$\frac{dL}{d\boldsymbol{b}} = \frac{\partial L}{\partial \boldsymbol{b}} + \frac{\partial L}{\partial \boldsymbol{q}} \frac{d\boldsymbol{q}}{d\boldsymbol{b}} \tag{5.10}$$

By exploiting the stationary condition, the adjoint vector can be written as follows,

$$\boldsymbol{K}\lambda = \frac{\partial \psi}{\partial \boldsymbol{q}} \tag{5.11}$$

For the von Mises stress constraint, again, by exploiting the stationary condition, the adjoint vector can be written as follows,

$$\boldsymbol{K}\lambda = \frac{\partial \psi}{\partial \boldsymbol{\sigma}} . \frac{\partial \boldsymbol{\sigma}}{\partial \boldsymbol{q}} \tag{5.12}$$

So, to obtain the sensitivities it is enough to find the partial design derivatives of the augmented functional, then

$$\frac{d\psi}{db} = \frac{\partial \psi}{\partial b} + \lambda^T \left(\frac{\partial F}{\partial b} - \frac{\partial K}{\partial b} q\right) \tag{5.13}$$

5.3 Finite Difference Method (FDM)

The FDM is the simplest way to calculate sensitivity values due to the fact that, unlike the DDM and AVM, it does not require a direct access to the finite element source code. However it suffers from a few drawbacks as discussed in chapter two, notably involving the accuracy of the calculated sensitivities and also it takes longer time to calculate sensitivities due to the fact that the finite element equation has to be solved twice at each iteration of the optimisation process. However, in order to benchmark the calculated sensitivities using the analytical methods, it is necessary to derive the sensitivities using the FDM which will be discussed in the following section.

In this work, to facilitate comparison, the design sensitivities for displacements and stresses are computed using two techniques, which are forward FDM and central FDM. For the forward FDM [1], the approximation of design sensitivities for displacement is given as

$$\frac{\partial q^i}{\partial b_j} \approx \frac{q^i(b + \Delta b) - q^i(b)}{\Delta b} \tag{5.14}$$

where $q^i(b + \Delta b)$ is obtained by solving the following equation,

$$K(b + \Delta b) q(b + \Delta b) = F(b + \Delta b) \tag{5.15}$$

For stress sensitivities, the approximation is given as

$$\frac{\partial \sigma^i}{\partial b_j} \approx \frac{\sigma^i(b + \Delta b) - \sigma^i(b)}{\Delta b} \tag{5.16}$$

and $\sigma(b+\Delta b)$ is obtained from,

$$\sigma(b+\Delta b) = D(b+\Delta b)B(b+\Delta b)q(b+\Delta b) \tag{5.17}$$

For the central FDM, the design sensitivities of displacements and stresses are approximated as

$$\frac{\partial q^i}{\partial b_j} \approx \frac{q^i(b+\Delta b) - q^i(b-\Delta b)}{2\Delta b} \tag{5.18}$$

$$\frac{\partial \sigma^i}{\partial b_j} \approx \frac{\sigma^i(b+\Delta b) - \sigma^i(b-\Delta b)}{2\Delta b} \tag{5.19}$$

where $q(b-\Delta b)$ and $\sigma(b-\Delta b)$ are obtained from,

$$K(b-\Delta b)q(b-\Delta b) = F(b-\Delta b) \tag{5.20}$$

$$\sigma(b-\Delta b) = D(b-\Delta b)B(b-\Delta b)q(b-\Delta b) \tag{5.21}$$

In the following section, the parameter design sensitivity analysis will be explored for the function involving displacement and von Mises stress constraints. The calculated analytical sensitivities will be compared with the FDM method to ensure the accuracy of the calculated analytical methods. The potential list of the parameter design variables is Young Modulus, coefficient of thermal expansion and Poisson ratio, all of which reflect a material choice. The case study focuses on the thermal stresses generated in a die that is

used to form a squeeze formed part, however the work applies generally to any structural problem.

5.4 Parameter Design Sensitivity Analysis

In parameter design sensitivity analysis, there are a number of design variables that may be considered as discussed earlier in Chapter 1. In this work, Youngs Modulus was considered as the parameter design variable, chosen because it has a significant effect on the results as compared to other design variables. This is due to the direct dependency of the stress field on the associated strain and modulus values. Exploring the impact of Youngs modulus is rather hypothetical, because dies are usually fabricated from steel which dictates thermomechanical parameters within practical limits. However the choice of materials, such as alloys that have thermal properties that facilitate rapid heat removal at strategic locations within the die may be of interest (implying strong modulus gradients). Youngs Modulus will be used in this work as a means of investigating the simulation approach. This is also quite relevant in the design sensitivity analysis using the Design Element Concept, since a die is typically fabricated based on a number of blocks (with the potential for using different materials) and it is particularly useful in a way that the defined zones using the Design Element Concept can be considered as a direct mapping to a number of blocks that make up the die.

5.4.1 The Stiffness Matrix Derivative for Parameter Sensitivity

The key factor in the calculation of sensitivities using the analytical methods is to formulate the derivative of the stiffness matrix with respect to the design variable. For example, considering the Young Modulus, E, the stiffness matrix derivative is given by

$$\frac{\partial \mathbf{K}}{\partial \mathrm{E}} = \mathbf{B}^{T} \frac{\partial \mathrm{D}}{\partial \mathrm{E}} \mathbf{B} \mathbf{J}_{\mathrm{D}} \pi r_{\mathrm{bar}} \tag{5.22}$$

From the equation above, it can be seen that only the D matrix is differentiated with respect to the Young Modulus because it only appears in this matrix.

5.4.2 The Derivative of von Mises Stress with respect to Displacement Vector

It can be seen from the derivations of the DDM and the AVM that the derivative of von Mises stress with respect to displacement vector is present in both methods. Thus, this section focuses on this derivation. For an axi-symmetric problem, the von Mises stress is given by [2,3]:

$$\sigma_{e} = \sqrt{\sigma_{r}^{2} + \sigma_{\theta}^{2} + \sigma_{z}^{2} + 3\tau_{rz}^{2} - \sigma_{r}\sigma_{\theta} - \sigma_{r}\sigma_{z} - \sigma_{\theta}\sigma_{z}} \tag{5.23}$$

By using the chain rule of differentiation, the derivative of the von Mises stress with respect to the displacement vector is given as:

$$\frac{\partial \sigma_{e}}{\partial \mathbf{q}} = \frac{\partial \sigma_{e}}{\partial \sigma_{r}} \frac{\partial \sigma_{r}}{\partial \mathbf{q}} + \frac{\partial \sigma_{e}}{\partial \sigma_{\theta}} \frac{\partial \sigma_{\theta}}{\partial \mathbf{q}} + \frac{\partial \sigma_{e}}{\partial \sigma_{z}} \frac{\partial \sigma_{z}}{\partial \mathbf{q}} + \frac{\partial \sigma_{e}}{\partial \tau_{rz}} \frac{\partial \tau_{rz}}{\partial \mathbf{q}} \tag{5.24}$$

where

$$\frac{\partial \sigma_e}{\partial \sigma_r} = \frac{2\sigma_r - \sigma_\theta - \sigma_z}{2\sqrt{\sigma_e}} \tag{5.25}$$

$$\frac{\partial \sigma_e}{\partial \sigma_\theta} = \frac{2\sigma_\theta - \sigma_r - \sigma_z}{2\sqrt{\sigma_e}} \tag{5.26}$$

$$\frac{\partial \sigma_e}{\partial \sigma_z} = \frac{2\sigma_z - \sigma_r - \sigma_\theta}{2\sqrt{\sigma_e}} \tag{5.27}$$

$$\frac{\partial \sigma_e}{\partial \tau_{rz}} = \frac{6\tau_{rz}}{2\sqrt{\sigma_e}} \tag{5.28}$$

5.5 Parameter Design Sensitivity Analysis Example

The design sensitivity analysis example of the axi-symmetric squeeze formed wheel is presented. The thermal stress analysis requires a temperature prescription within the die as an input and this was derived from a thermal analysis using the procedure that has been described fully in Chapter 3. In this instance, the initial temperature of the cast metal was 700°C. The cast material is Aluminium LM25 whereas for the die, the material is steel H13. The die features two coolant channels that are fixed in position and it has an initial temperature of 200°C [4]. The heat transfer conditions in the coolant system corresponds to a heat transfer coefficient and reference temperature of 1000W/m^{2}K (Appendix II) and 100 °C respectively and heat is removed from the external surfaces in accordance with a heat transfer coefficient to 25 W/m^{2}K [5,6] and an ambient temperature of 25 °C. Very good contact is assumed at the die and casting interface, hence an interfacial coefficient of 5000 W/m^{2}K [6,7] was applied.

5.5.1 Transient Thermo-Mechanical Problem

Figure 5.1 shows the temperature field in the die at t=50s after the cast part has completely solidified. At t=50s, the temperature field in the die was directly used for the calculation of thermal stresses for the structural evaluation. Figure 5.2, 5.3 and 5.4 show the x-displacement, y-displacement and von Mises stress in the die at t=50s. The range of x and y displacements is 10^{-4}m and 10^{8} Pa for von Mises stress. The temperature distribution in the die leads to a complex stress pattern where high von Mises stresses are developed near the coolant channels and also in the corner regions within the die.

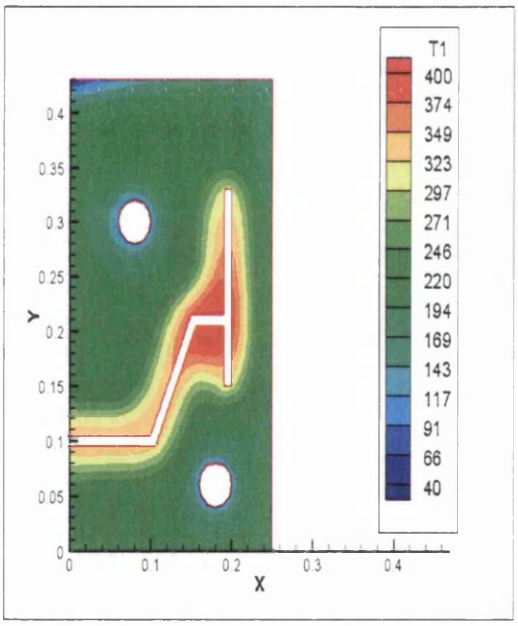

Figure 5.1

Temperature field in the die at t=50s

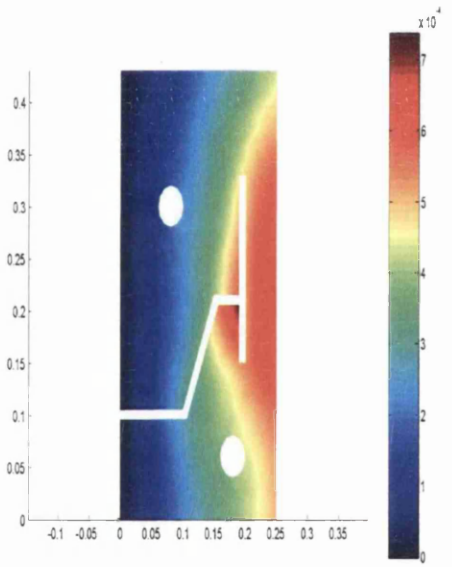

Figure 5.2

X-displacement in the die at t=50s

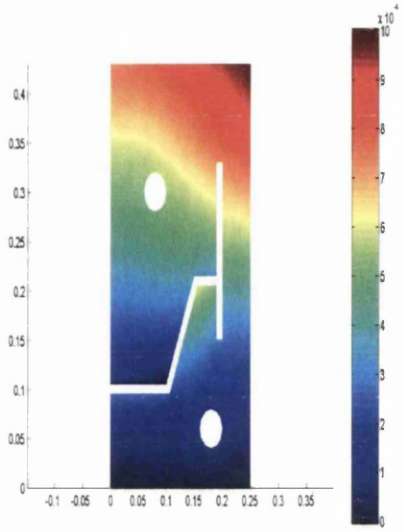

Figure 5.3

Y-displacement in the die at t=50s

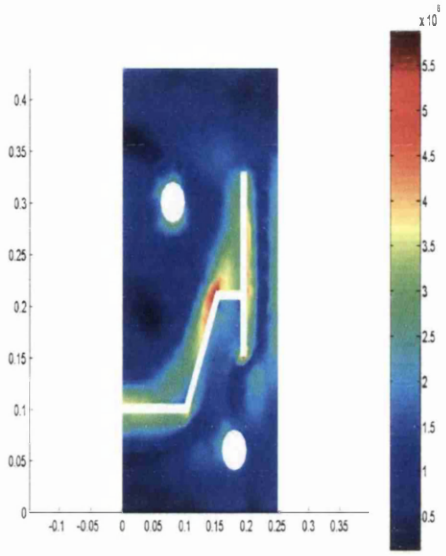

Figure 5.4

Von Mises stress distribution in the die at t=50s

5.5.2 Displacement Sensitivities

Displacement and von Mises stress constraints can be applied anywhere in the die. In this work, two displacement constraints have been selected and these have been applied near the casting where the y and x-displacements have been set not to exceed $1x10^{-4}$ m applied at points F and G respectively. These have been chosen to avoid high displacements at the casting, which are typically the crucial areas in which the high von Mises stress are developed and as a consequence, failure initiation might occur. Figure 5.5 shows the application points for the two displacement constraints in the die. Figure 5.6 shows the design sensitivity of displacement with respect to the Young Modulus for the application of displacement constraint at point F. From this figure, it can be seen that the region near the upper section of casting has a higher effect on the displacement constraint at point F

due to small changes of the Youngs Modulus. From a practical point of view, material consistency in this part of the die is required due to the sensitivity of this region to the displacement constraint at point F. Also, from Figure 5.6, elements near the upper part of casting in the die have higher values of sensitivities as compared to the other elements.

Figure 5.7 shows the design sensitivity of displacement with respect to the Young Modulus for the application of displacement constraint at point G. From this figure, it can be seen that the region near right middle section of the die has a higher effect on the displacement constraint at point G due to small changes of the Youngs Modulus. Again this points to the requirement for consistent material properties in this region due to the high sensitivity values with respect to the constraint at point G. From Figure 5.7, elements near the right middle section of the die have higher values of sensitivities as compared to the other elements.

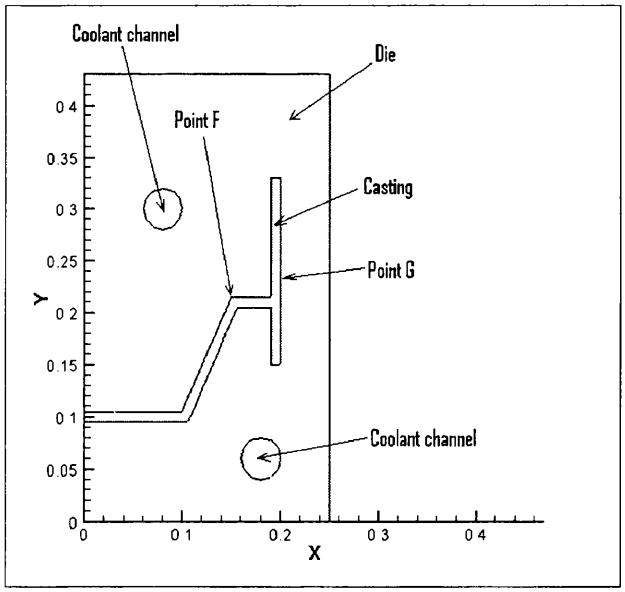

Figure 5.5

Application of displacement and von Mises stress constraints

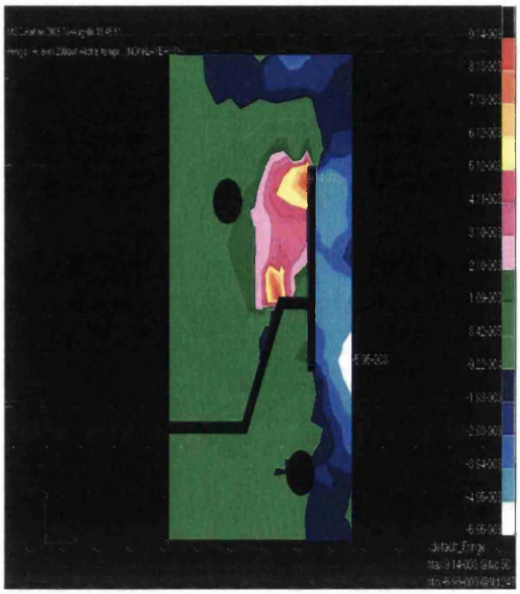

Figure 5.6

Design sensitivity of displacement field with respect to Young Modulus in the die for the application of displacement constraint at point F

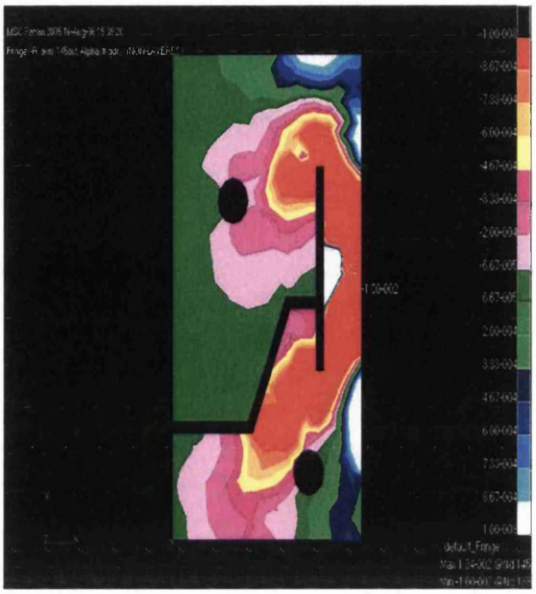

Figure 5.7

Design sensitivity of displacement field with respect to Young Modulus in the die for the application of displacement constraint at point G

5.5.3 Von Mises Stress Sensitivities

The same constraints as defined in the section 5.5.2 have been applied where the von Mises stress has been set not to exceed $1x10^8$ Pa. This has been chosen due to the high von Mises stress values in these areas.

Figure 5.8 shows the design sensitivity of von Mises stress with respect to the Young Modulus for the application of von Mises stress constraint at point F. It can be seen that the regions near the upper coolant channel and the upper part the die have a higher effect on von Mises stress constraint at point F due to small changes in Youngs Modulus and therefore material consistency in this part of the die is required due to the sensitivity of these regions to the von Mises stress constraint at point F. From Figure 5.8, the

sensitivities were higher in the upper part of the die and the upper coolant channel. Figure 5.9 shows the design sensitivity of von Mises stress with respect to the Young Modulus for the application of von Mises stress constraint at point G. It can be seen that the region near the right middle section of the die has higher effect on von Mises stress constraint at point G due to small changes in Youngs Modulus. Again this points to the requirement for consistent material properties in these regions due to the high sensitivity values with respect to the constraint at point G. From Figure 5.9, the higher sensitivity values were distributed in the right middle section of the die.

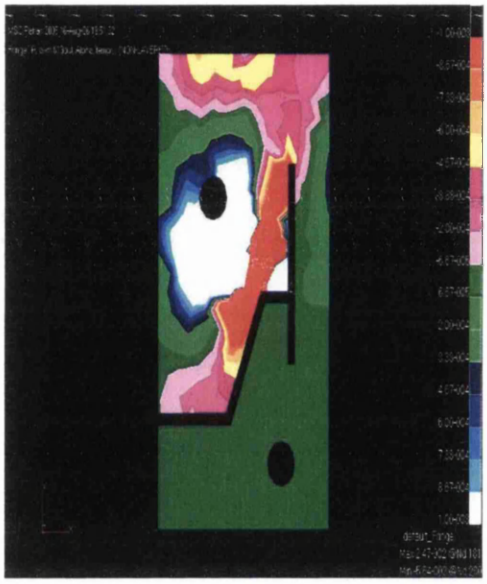

Figure 5.8

Design sensitivity of von Mises stress with respect to Young Modulus in the die for the application of von Mises stress constraint at point F

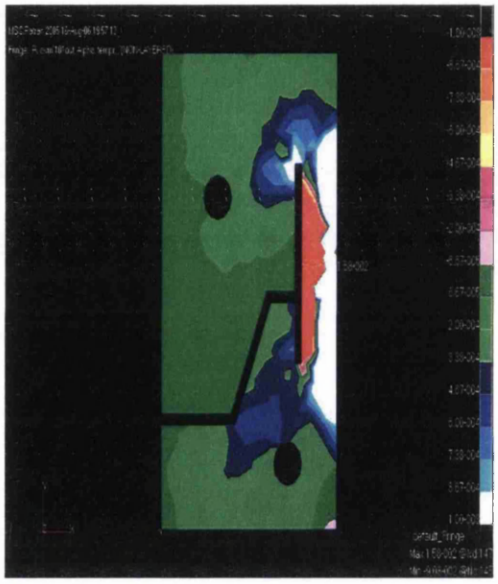

Figure 5.9

Design sensitivity of von Mises stress with respect to Young Modulus in the die for the application of von Mises stress constraint at point G

5.6 Analytical Methods vs Finite Difference Method

Traditionally sensitivity is computed through a difference formula [1] and therefore it is appropriate to compare the results from the analytical with difference counterparts. Thus in this section, the calculated analytical design sensitivity gradients for a few elements are tabulated and then compared with the results from a simple difference based calculation. The calculated design sensitivity gradients can be described as accurate sensitivity gradients if the percentage errors are very small. Figure 5.10 shows the points where the analytical and Finite Difference design sensitivity gradients have been compared.

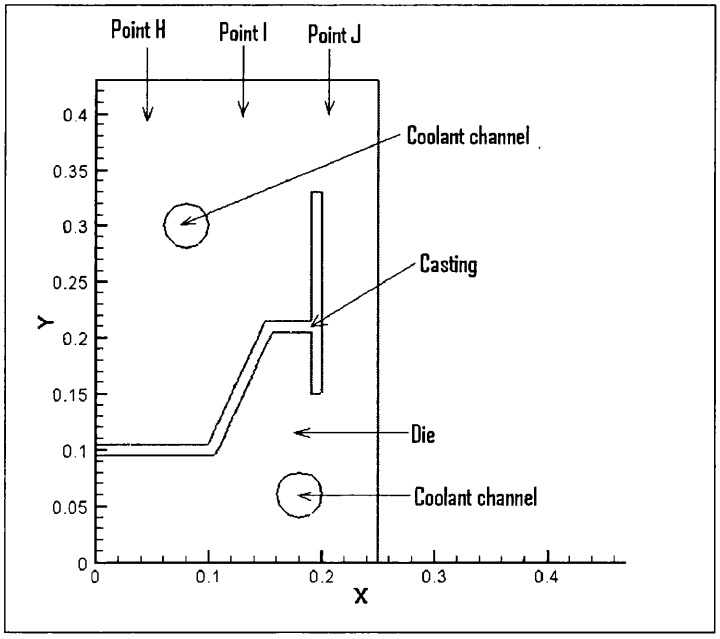

Figure 5.10

The points where the comparison of analytical and Finite Difference design sensitivity gradients have been compared

5.6.1 Design Sensitivities of Displacement

Tables 5.1, 5.2 and 5.3 itemise the design sensitivities of displacement with respect to the Young modulus at points H, I and J respectively for the application of a displacement constraint at point F. Tables 5.4, 5.5 and 5.6 show the design sensitivities of displacement with respect to the Young modulus at points H, I and J respectively for the application of displacement constraint at point G. Clearly the differences in percentage errors were small and this was also found to apply to all other elements in the calculation domain as well.

	Dq/de ($1x10^{-13}$)
AVM & DDM	-1.108

	% perturb	dq/de ($1x10^{-13}$)	% error
FDM (F)	0.2	-1.105	0.27
FDM (F)	2	-1.119	0.99
FDM (C)	0.2	-1.109	0.09
FDM (C)	2	-1.115	0.45

Table 5.1

Comparison of the analytical methods and FDM design derivatives at point H for the application of displacement constraint at point F

	dq/de ($1x10^{-14}$)
AVM & DDM	-6.277

	% perturb	dq/de ($1x10^{-14}$)	% error
FDM (F)	0.2	-6.260	0.27
FDM (F)	2	-6.241	0.57
FDM (C)	0.2	-6.279	0.03
FDM (C)	2	-6.293	0.25

Table 5.2

Comparison of the analytical methods and FDM design derivatives at point I for the application of displacement constraint at point F

	dq/de ($1x10^{-13}$)
AVM & DDM	-2.129

	% perturb	dq/de ($1x10^{-13}$)	% error
FDM (F)	0.2	-2.122	0.32
FDM (F)	2	-2.112	0.79
FDM (C)	0.2	-2.130	0.05
FDM (C)	2	-2.141	0.56

Table 5.3

Comparison of the analytical methods and FDM design derivatives at point J for the application of displacement constraint at point F

	dq/de ($1x10^{-15}$)
AVM & DDM	3.503

	% perturb	dq/de ($1x10^{-15}$)	% error
FDM (F)	0.2	3.486	0.49
FDM (F)	2	3.469	0.97
FDM (C)	0.2	3.505	0.06
FDM (C)	2	3.493	0.29

Table 5.4

Comparison of the analytical methods and FDM design derivatives at point H for the application of displacement constraint at point G

	dq/de ($1x10^{-15}$)
AVM & DDM	9.484

	% perturb	dq/de ($1x10^{-15}$)	% error
FDM (F)	0.2	9.448	0.38
FDM (F)	2	9.419	0.69
FDM (C)	0.2	9.490	0.06
FDM (C)	2	9.456	0.29

Table 5.5

Comparison of the analytical methods and FDM design derivatives at point I for the application of displacement constraint at point G

	dq/de ($1x10^{-14}$)
AVM & DDM	3.842

	% perturb	dSe/de ($1x10^{-14}$)	% error
FDM (F)	0.2	3.835	0.18
FDM (F)	2	3.869	0.7
FDM (C)	0.2	3.844	0.05
FDM (C)	2	3.851	0.23

Table 5.6

Comparison of the analytical methods and FDM design derivatives at point J for the application of displacement constraint at point G

5.6.2 Design Sensitivities of von Mises Stress

Tables 5.7, 5.8 and 5.9 show the design sensitivities of von Mises stress with respect to the Young modulus at points H, I and J respectively for the application of von Mises stress constraint at point F. Tables 5.10, 5.11 and 5.12 show the design sensitivities of von Mises stress with respect to the Young modulus at points H, I and J respectively for the application of von Mises stress constraint at point G. Again, the differences in percentage errors were small and this applies to all other elements as well.

	dSe/de ($1x10^{-14}$)
AVM & DDM	-5.272

	% perturb	dSe/de ($1x10^{-14}$)	% error
FDM (F)	0.2	-5.259	0.25
FDM (F)	2	-5.305	0.63
FDM (C)	0.2	-5.273	0.02
FDM (C)	2	-5.292	0.38

Table 5.7

Comparison of the analytical methods and FDM design derivatives at point H for the application of von Mises stress constraint at point F

	dSe/de ($1x10^{-14}$)
AVM & DDM	-2.093

	% perturb	dSe/de ($1x10^{-14}$)	% error
FDM (F)	0.2	-2.081	0.57
FDM (F)	2	-2.111	0.86
FDM (C)	0.2	-2.095	0.14
FDM (C)	2	-2.103	0.48

Table 5.8

Comparison of the analytical methods and FDM design derivatives at point I for the application of von Mises stress constraint at point F

	dSe/de ($1x10^{-14}$)
AVM & DDM	-3.479

	% perturb	dSe/de ($1x10^{-14}$)	% error
FDM (F)	0.2	-3.470	0.25
FDM (F)	2	-3.447	0.92
FDM (C)	0.2	-3.480	0.03
FDM (C)	2	-3.497	0.52

Table 5.9

Comparison of the analytical methods and FDM design derivatives at point J for the application of von Mises stress constraint at point F

	dSe/de ($1x10^{-14}$)
AVM & DDM	1.570

	% perturb	dSe/de ($1x10^{-14}$)	% error
FDM (F)	0.2	1.558	0.76
FDM (F)	2	1.555	0.95
FDM (C)	0.2	1.568	0.13
FDM (C)	2	1.561	0.57

Table 5.10

Comparison of the analytical methods and FDM design derivatives at point H for the application of von Mises stress constraint at point G

	dSe/de ($1x10^{-14}$)
AVM & DDM	1.352

	% perturb	dSe/de ($1x10^{-14}$)	% error
FDM (F)	0.2	1.363	0.81
FDM (F)	2	1.365	0.96
FDM (C)	0.2	1.354	0.15
FDM (C)	2	1.361	0.66

Table 5.11

Comparison of the analytical methods and FDM design derivatives at point I for the application of von Mises stress constraint at point G

	dSe/de ($1x10^{-14}$)
AVM & DDM	1.999

	% perturb	dSe/de ($1x10^{-14}$)	% error
FDM (F)	0.2	2.010	0.55
FDM (F)	2	2.016	0.85
FDM (C)	0.2	1.998	0.05
FDM (C)	2	2.005	0.3

Table 5.12

Comparison of the analytical methods and FDM design derivatives at point J for the application of von Mises stress constraint at point G

As an additional point, it can be seen from the tabulated results, the calculated sensitivities for both displacement and von Mises stress using the Central (C) FDM were much better than the Forward (F) scheme, where in these examples, the percentage errors for the Central FDM were very small. This is an expected result due to the improved performance of central FDM in capturing gradient values. However, due to a few drawbacks using the FDM as discussed previously, they are merely used for benchmarking the calculated sensitivities using the analytical methods. The results confirm the accuracy of the analytical approach that also has a significantly smaller computational requirement.

5.7 The Design Element Strategy

Instead of considering sensitivity calculation for each discretised element, it is useful if the design variables in the optimisation process are quantified in a way that they will be dealt with in a number of groups bounded by zones defined by a designer. For instance, a die is constructed from a number of steel blocks, thus, allowing some pre-selection of zone material properties involving composite dies. Also, the design element strategy can be applied to design problems involving shape optimisation where instead of considering changes to only one particular nodal coordinate, a number of nodes can be grouped together (for example a cooling channel) to facilitate design element sensitivity gradient calculation.

5.8 Design Element Concept

In the previous section, sensitivity was calculated based on the full element subdivision. This will have a significant effect in terms of the efficiency of the optimisation process, since there is generally a requirement for thousands of elements in a domain to obtain a good numerical solution. Thus, by applying the Design Element Concept, the sensitivity calculation can be reduced by application to the design elements only. In design sensitivity analysis using the Design Element Concept, the finite elements that are used to solve the governing equations are grouped together into zones to form fewer large elements, i.e design elements. Figure 5.11 illustrates the application of the Design Element Concept in a die. The figure, for instance, shows four design elements based on the designer's preference. However, the choice of design element can present difficulties since it is potentially aribitrary, but each should lead to the same optimised solution for the approach to be effective. This will be explored through the case studies which will be discussed in the following sections.

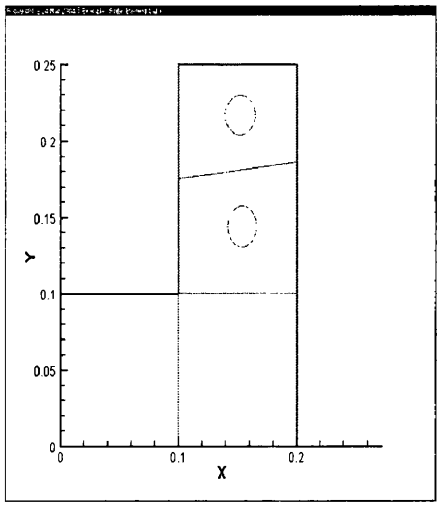

Figure 5.11

Example Design Element division into four zones

5.9 Derivations of Design Element Concept using the DDM and the AVM

In this section, the sensitivity calculations with respect to the Design Element Concept will be discussed mathematically for both analytical methods; the DDM and the AVM. As discussed previously, both methods have their own advantages for certain applications of design optimisation depending on the number of design variables and applied constraints. Thus, the derivations for both methods in association with the design element scheme are set out below. The derivation is similar to that described above in Sections 5.2.1 and 5.2.2, however, in order to illustrate how the Design Element Concept is implemented, a complete derivation is required. .

5.9.1 Direct Differentiation Method (DDM)

Again, consider the equilibrium equation,

$$\boldsymbol{K(b)q=F} \tag{5.29}$$

Where $\boldsymbol{b}$ is the design variable vector, $\boldsymbol{q}$ is the displacement vector, $\boldsymbol{F}$ is the global force vector and $\boldsymbol{K}$ is the global stiffness matrix. The goal is to find the sensitivity of a function ψ $(\boldsymbol{q(b)}, q_a, \boldsymbol{\sigma(b)}, \sigma_{a,,} \boldsymbol{b})$ with respect to the design variables $\boldsymbol{b}$,

$$\nabla_b \psi \text{ subject to } \boldsymbol{K(b)q=F} \tag{5.30}$$

where $\nabla_b \psi$ is defined as

$$\nabla_b \psi = \left[\frac{\partial \psi}{\partial \boldsymbol{b}_1} \frac{\partial \psi}{\partial \boldsymbol{b}_2} \cdots \frac{\partial \psi}{\partial \boldsymbol{b}_n} \right] \tag{5.31}$$

q_a is the displacement constraint and σ_a is the von Mises stress constraint. Assuming that the $\boldsymbol{K}$ matrix is not singular, both sides of the equilibrium equation are differentiated with respect to $\boldsymbol{b}$. The following expression for $\nabla_b \boldsymbol{q}$ can be derived:

$$\nabla_b \boldsymbol{q} = \boldsymbol{K}^{-1}[\nabla_b \boldsymbol{F} - \nabla_b(\sum \boldsymbol{K}_{de} \boldsymbol{q})] \tag{5.32}$$

where $\boldsymbol{K}_{de}$ represents the discretised elements in the defined design elements. In the following examples, the die has been divided into zones of 3, 7, 10, 14 and 28 Design Elements. This has been chosen to see the difference in the calculated sensitivities for different sub-divisions of design elements in the die. Figures 5.12, 5.13, 5.14, 5.15 and 5.16 show the divisions of the zones in the die for 3, 7, 10, 14 and 28 Design Elements.

Thus, the design element sensitivity gradient for each design element is merely the summation of the derivatives of the stiffness matrices $\sum \boldsymbol{K}_{de}$ for the discretised elements inside the particular design element. This follows the finite element method procedure

where the total stiffness matrix of the structure is the summation of the individual finite element stiffness matrix in the domain.

The exact sensitivities of ψ ($\boldsymbol{q(b)}$, q_a, $\boldsymbol{\sigma(b)}$,$\sigma_{a,}$ $\boldsymbol{b}$) can be calculated by substituting $\nabla_b \boldsymbol{q}$

$$\nabla_b \psi = \nabla_b^e \psi + \nabla_q \psi . \nabla_b \boldsymbol{q} \tag{5.33}$$

Where $\nabla_b^e \psi$ is the gradient term for the explicit dependence of ψ ($\boldsymbol{q(b)}$, q_a, $\boldsymbol{\sigma(b)}$,$\sigma_{a,}$ $\boldsymbol{b}$) on $\boldsymbol{b}$.

For a von Mises stress constraint, the exact sensitivities of ψ ($\boldsymbol{q(b)}$, q_a, $\boldsymbol{\sigma(b)}$,$\sigma_{a,}$ $\boldsymbol{b}$) can be calculated by substituting $\nabla_b \boldsymbol{q}$

$$\nabla_b \psi = \nabla_b^e \psi + \nabla_\sigma \psi . \nabla_q \boldsymbol{\sigma} . \nabla_b \boldsymbol{q} \tag{5.34}$$

5.9.2 Adjoint Variable Method (AVM)

The derivation of sensitivities using the AVM is the same as derived previously. The only difference is that the sensitivity for each design element is merely the summation of the individual discretised element sensitivity inside that particular design element. Again, this reflects the assembly of the global stiffness matrix as used in the finite element method.

5.10 Parameter Design Element Concept example

The design sensitivity example of the axi-symmetric squeeze casting die is presented. In this example, to facilitate comparison, the same initial and boundary conditions were applied as described in the previous section.

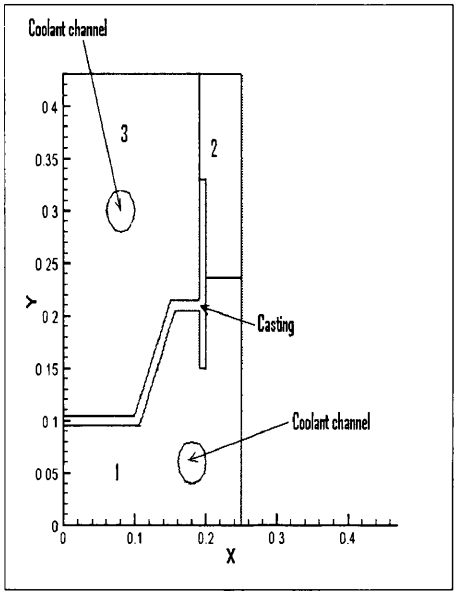

Figure 5.12

The division of zones in the die for 3 Design Elements

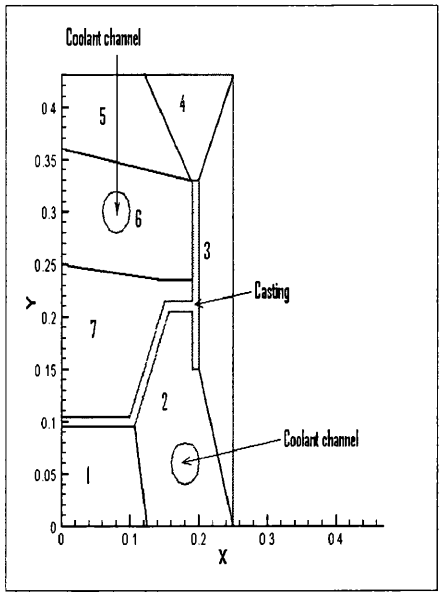

Figure 5.13

The division of zones in the die for 7 Design Elements

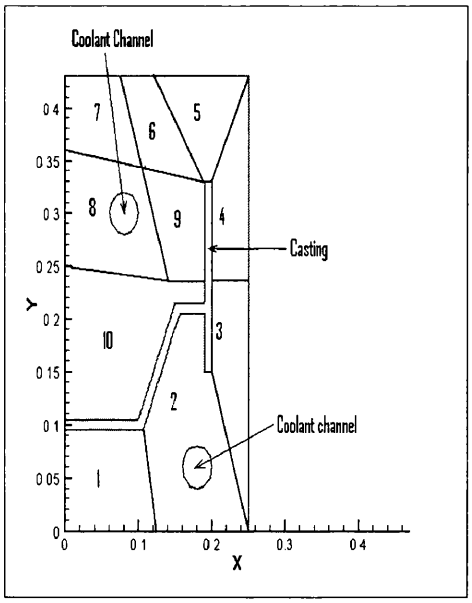

Figure 5.14

The division of zones in the die for 10 Design Elements

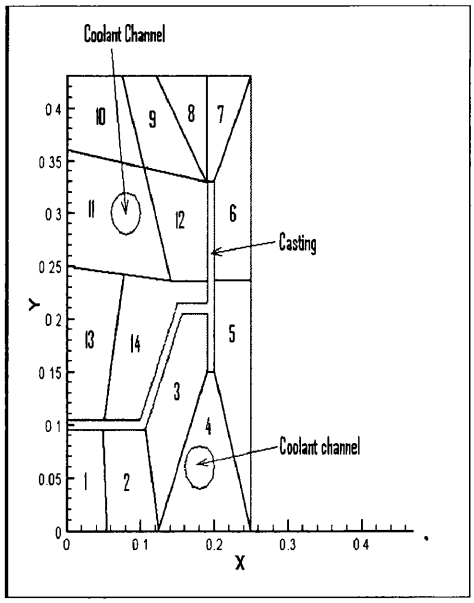

Figure 5.15

The division of zones in the die for 14 Design Elements

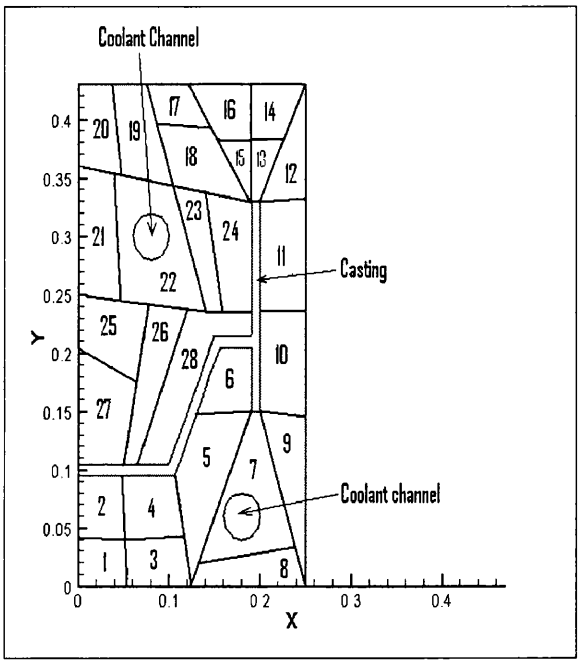

Figure 5.16

The division of zones in the die for 28
Design Elements

5.10.1 Displacement Design Element Sensitivities

The same points for the application of design constraints as in the previous section have been applied. In implementation, there are a number of design element subdivisions that may be used, for example, each block in the die may be a design element. This will lead to just a few design elements and these may be insufficient to capture stress or thermal gradients within the die with sufficient accuracy. Thus a number of design element subdivisions will be explored and the options are presented in Figures 5.12 to 5.16.

Figures 5.17, 5.18, 5.19, 5.20 and 5.21 show the design element sensitivity of displacement with respect to Young Modulus for the application of the displacement constraint at locations F for 3, 7, 10, 14 and 28 Design Elements respectively. Figures 5.22, 5.23, 5.24, 5.25 and 5.26 show the design element sensitivity of displacement with

respect to Young Modulus for the application of the displacement constraint at locations G for 3, 7, 10, 14 and 28 Design Elements respectively. It can be seen that for the results obtained for both displacement constraints, the division of design elements affected the sensitivity distribution in the die and convergence can be observed as more design elements are employed.

As discussed in Chapter two, at the Finite Element level, all the calculated sensitivities using the analytical methods may be compared with the FDM method to ensure the accuracy of the calculated sensitivities. In terms of validation of the approach in this work involving the sensitivities for the Design Element Concept, the same procedure has been implemented where all the calculated design element sensitivities using analytical methods will be compared with the FDM method. This is now practical since the Design Element Concept is a macro scale sensitivity of the FE sensitivities as discussed in the previous sections. The comparison of the results between the two methods was carried out and it is effectively a validation loop, where the results showed closed agreement. The comparison was done for the patterns obtained from both, the AVM and the DDM solutions, where they were compared with the pattern obtained from the FDM solutions. This comparison will be presented in section 5.11.

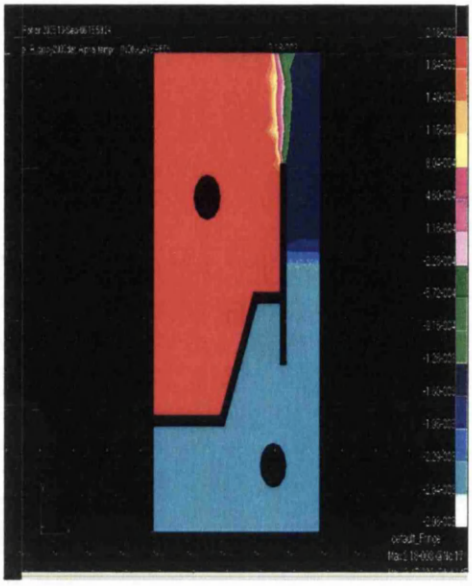

Figure 5.17

Design element sensitivity of displacement with respect to Young Modulus for the application of displacement constraint at point F for 3 design elements

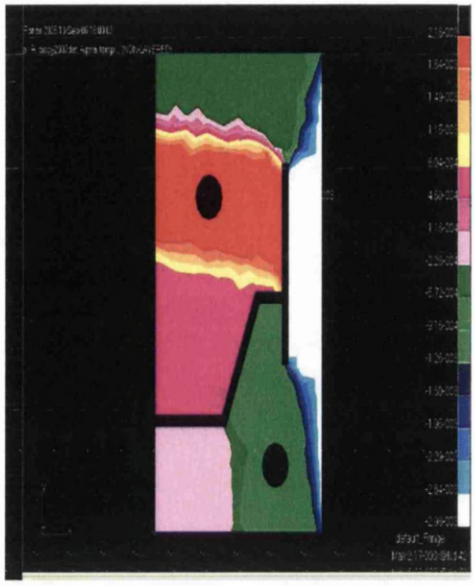

Figure 5.18

Design element sensitivity of displacement with respect to Young Modulus for the application of displacement constraint at point F for 7 design elements

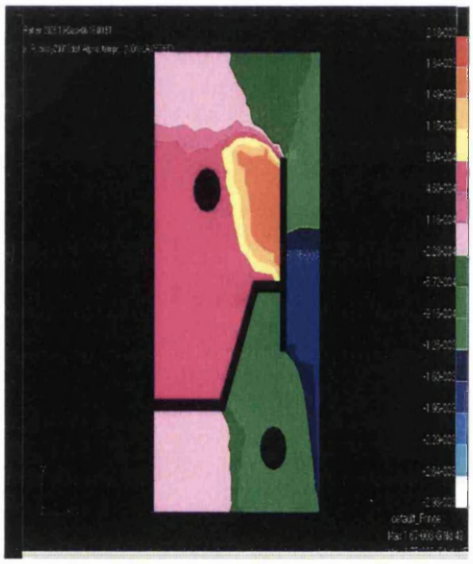

Figure 5.19

Design element sensitivity of displacement with respect to Young Modulus for the application of displacement constraint at point F for 10 design elements

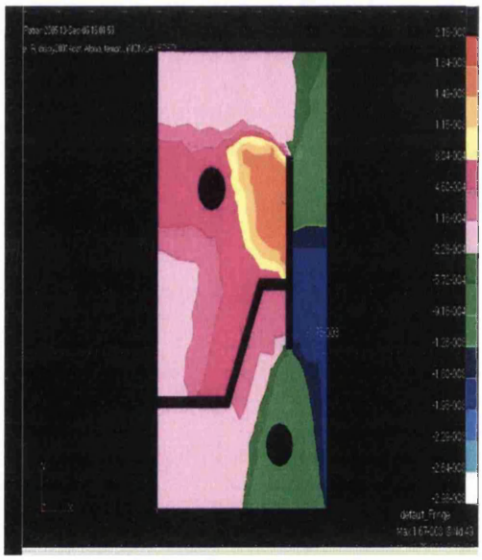

Figure 5.20

Design element sensitivity of displacement with respect to Young Modulus for the application of displacement constraint at point F for 14 design elements

Figure 5.21

Design element sensitivity of displacement with respect to Young Modulus for the application of displacement constraint at point F for 28 design elements

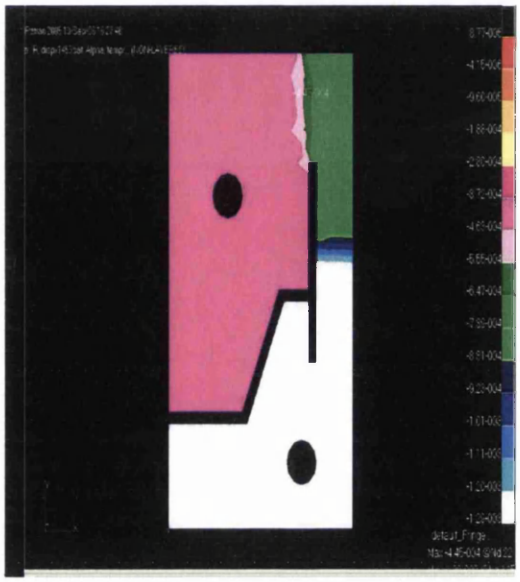

Figure 5.22

Design element sensitivity of displacement with respect to Young Modulus for the application of displacement constraint at point G for 3 design elements

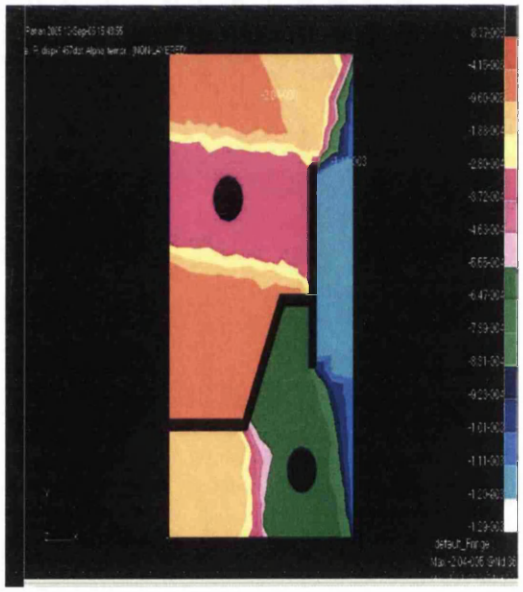

Figure 5.23

Design element sensitivity of displacement with respect to Young Modulus for the application of displacement constraint at point G for 7 design elements

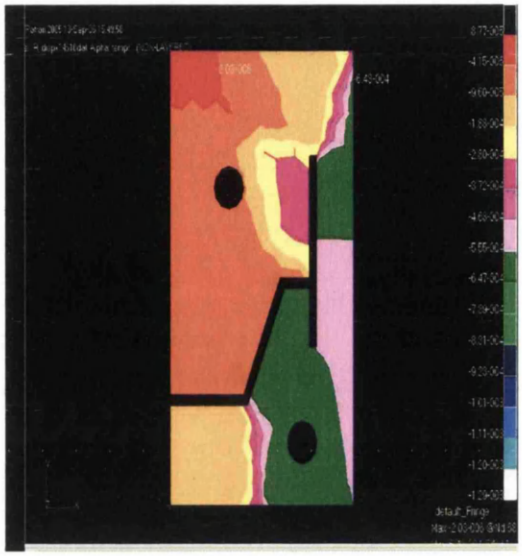

Figure 5.24

Design element sensitivity of displacement with respect to Young Modulus for the application of displacement constraint at point G for 10 design elements

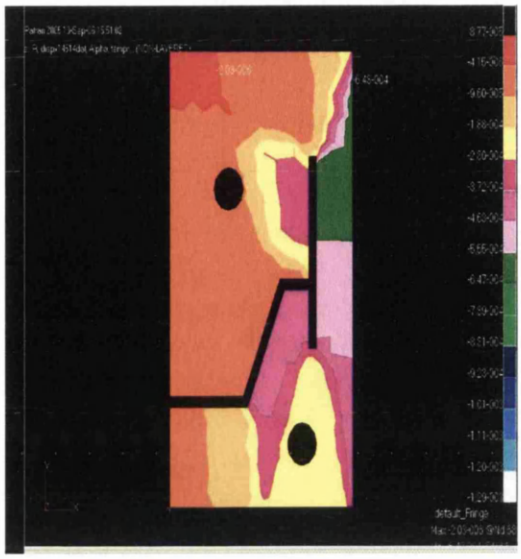

Figure 5.25

Design element sensitivity of displacement with respect to Young Modulus for the application of displacement constraint at point G for 14 design elements

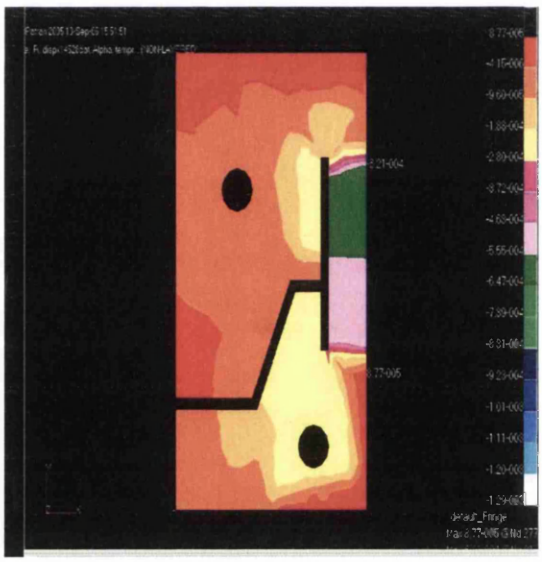

Figure 5.26

Design element sensitivity of displacement with respect to Young Modulus for the application of displacement constraint at point G for 28 design elements

5.10.2 Von Mises stress design element sensitivities

The same points for the application of von Mises stress constraints as defined in the previous section have been applied. Figures 5.27, 5.28, 5.29, 5.30 and 5.31 show the design element sensitivity of von Mises stress with respect to Young Modulus for the application of von Mises stress constraint at points F for 3, 7, 10, 14 and 28 design elements respectively. Figures 5.32, 5.33, 5.34, 5.35 and 5.36 show the design element sensitivity of von Mises stress with respect to Young Modulus for the application of von Mises stress constraint at points G for 3, 7, 10, 14 and 28 design elements respectively. Again, for von Mises stress constraints, it can be seen that as more design elements are explored, convergence is obtained as shown by Figures 5.27 to 5.31 and Figures 5.32 to 5.36.

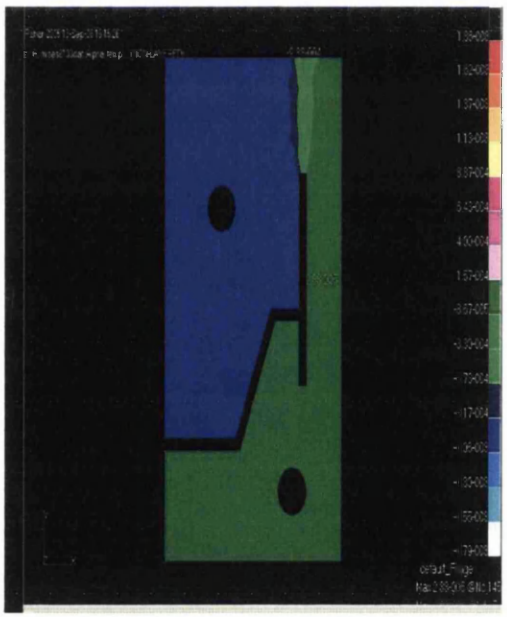

Figure 5.27

Design element sensitivity of von Mises stress with respect to Young Modulus for the application of von Mises stress constraint at point F for 3 design elements

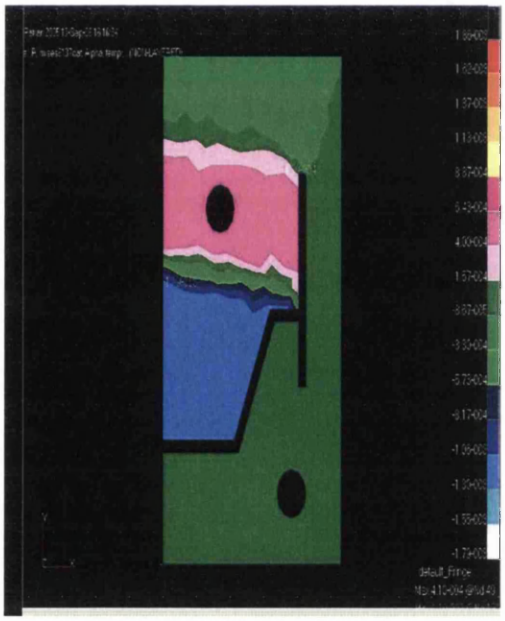

Figure 5.28

Design element sensitivity of von Mises stress with respect to Young Modulus for the application of von Mises stress constraint at point F for 7 design elements

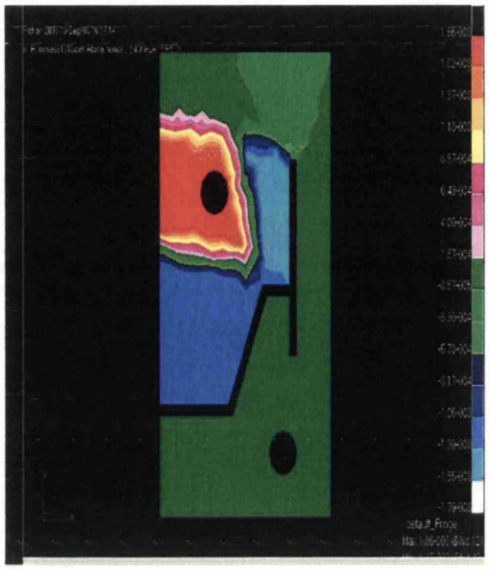

Figure 5.29

Design element sensitivity of von Mises stress with respect to Young Modulus for the application of von Mises stress constraint at point F for 10 design elements

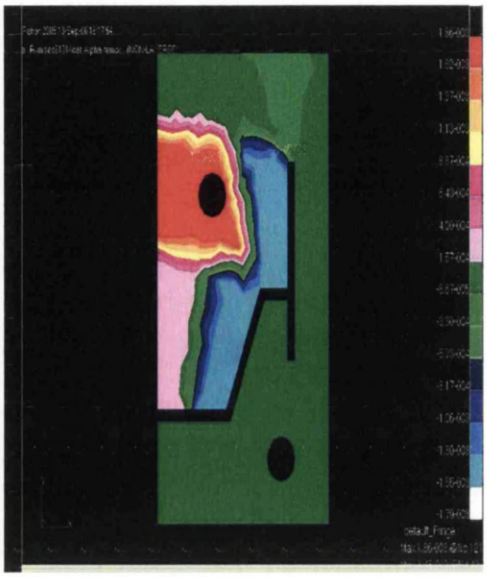

Figure 5.30

Design element sensitivity of von Mises stress with respect to Young Modulus for the application of von Mises stress constraint at point F for 14 design elements

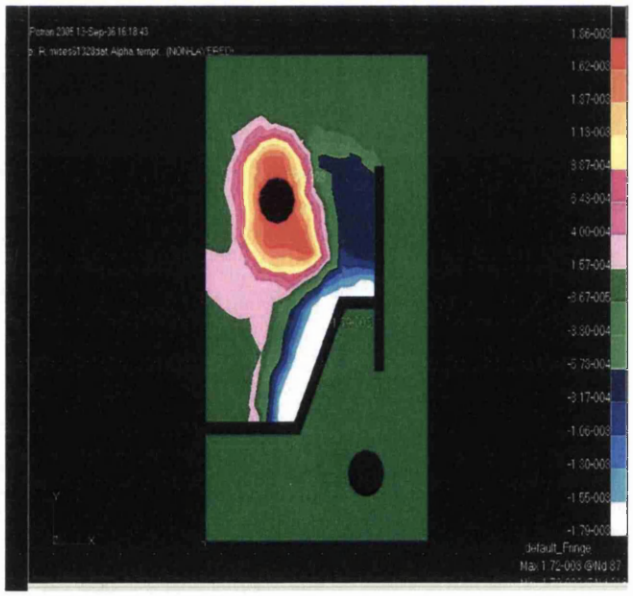

Figure 5.31

Design element sensitivity of von Mises stress with respect to Young Modulus for the application of von Mises stress constraint at point F for 28 design elements

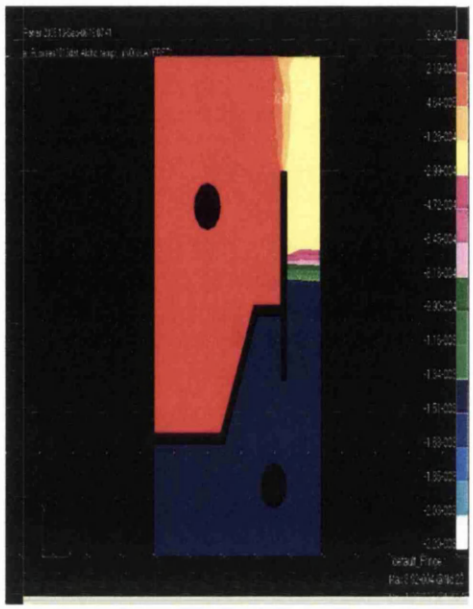

Figure 5.32

Design element sensitivity of von Mises stress with respect to Young Modulus for the application of von Mises stress constraint at point G for 3 design elements

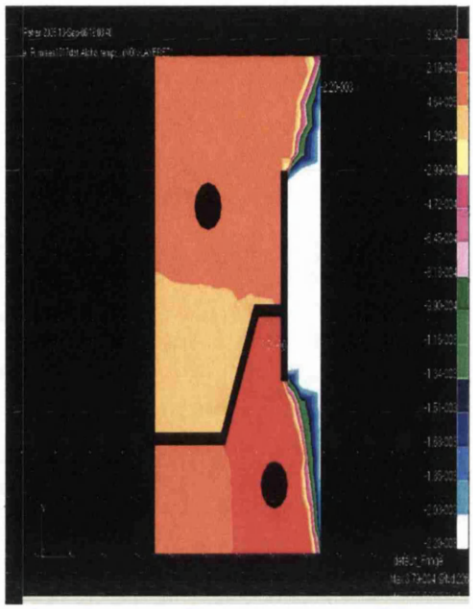

Figure 5.33

Design element sensitivity of von Mises stress with respect to Young Modulus for the application of von Mises stress constraint at point G for 7 design elements

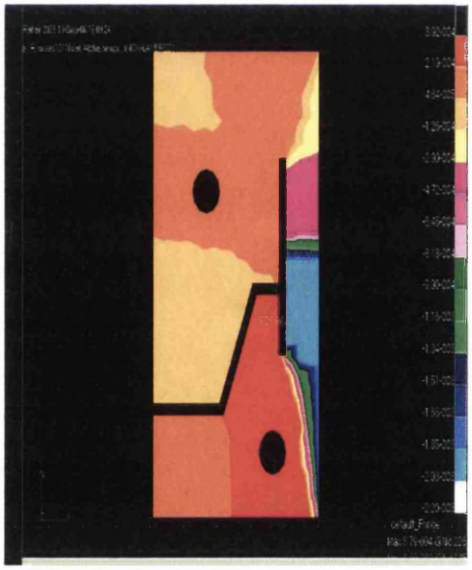

Figure 5.34

Design element sensitivity of von Mises stress with respect to Young Modulus for the application of von Mises stress constraint at point G for 10 design elements

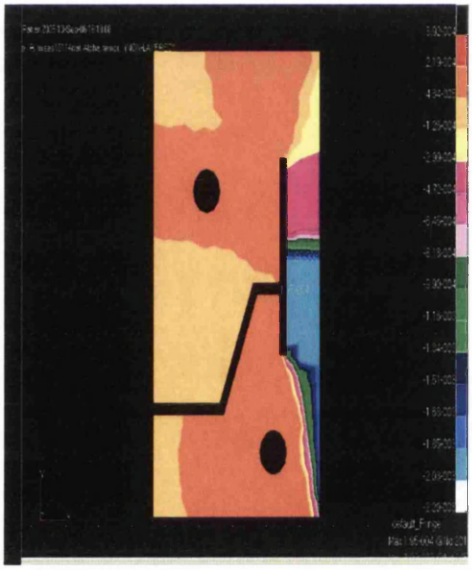

Figure 5.35

Design element sensitivity of von Mises stress with respect to Young Modulus for the application of von Mises stress constraint at point G for 14 design elements

Figure 5.36

Design element sensitivity of von Mises stress with respect to Young Modulus for the application of von Mises stress constraint at point G for 28 design elements

Clearly the Design Element for both displacement and von Mises stress have tremendously reduced the number of design variables. However, the computational time to calculate the gradients is almost the same with the full field solution. The reduction of the design variables from hundreds to only a few design elements has reduced the calculation time in the optimisation process by a factor of more than ten times since the updating of new solution using the gradient-based optimisation is done accordingly for each design variable. This is due to the fact that the gradient-based optimisation updates the new solution based on the Taylor series formulation, where the sensitivity with respect to each design variable is needed in deriving to the optimal solution.

5.11 Analytical Methods vs Finite Difference Method

In this section, the calculated analytical design element sensitivity gradients are tabulated and then compared with the results from a simple difference based calculation. In this section only a limited comparison is presented, because following from the comparison presented in section 5.6 (other tabulations) good agreement was shown for all cases.

5.11.1 Design Element Sensitivities of Displacement

Table 5.13 and 5.14 show the design element sensitivities of displacement with respect to the Young modulus for the application of displacement constraints at point F and G respectively for 14 design elements. The results are tabulated up to three decimal places due to the fairly close values that were obtained from the FDM and the analytical methods.

Design Element	FDM (F) 0.2%	% Error	FDM (F) 2.0%	% Error	FDM (C) 0.2%	% Error	FDM (C) 2.0%	% Error	AVM & DDM
1	2.371×10^{-15}	0.78	2.439×10^{-15}	2.05	2.389×10^{-15}	0.04	2.369×10^{-15}	0.88	2.390×10^{-15}
2	1.689×10^{-14}	0.23	1.710×10^{-14}	1.42	1.687×10^{-14}	0.08	1.698×10^{-14}	0.71	1.686×10^{-14}
3	4.949×10^{-14}	0.67	5.029×10^{-14}	0.94	4.982×10^{-14}	2.01 $\times 10^{-3}$	4.951×10^{-14}	0.62	4.982×10^{-14}
4	2.177×10^{-14}	0.17	2.201×10^{-14}	1.29	2.173×10^{-14}	0.02	2.173×10^{-14}	0.92	2.173×10^{-14}
5	1.416×10^{-13}	0.28	1.433×10^{-13}	0.92	1.419×10^{-13}	0.12	1.411×10^{-13}	0.59	1.421×10^{-13}
6	1.867×10^{-13}	0.79	1.909×10^{-13}	1.47	1.882×10^{-13}	0.03	1.886×10^{-13}	0.21	1.882×10^{-13}
7	-8.833×10^{-13}	0.56	-8.868×10^{-13}	0.17	-8.882×10^{-13}	2.25 $\times 10^{-3}$	-8.889×10^{-13}	0.07	-8.883×10^{-13}
8	-9.559×10^{-13}	0.09	-9.560×10^{-13}	0.08	-9.568×10^{-13}	5.22 $\times 10^{-3}$	-9.576×10^{-13}	0.07	-9.569×10^{-13}
9	-5.200×10^{-13}	0.5	-5.171×10^{-13}	0.05	-5.172×10^{-13}	0.04	-5.171×10^{-13}	0.05	-5.174×10^{-13}
10	-5.051×10^{-13}	0.98	-5.097×10^{-13}	0.11	-5.101×10^{-13}	0.01	-5.103×10^{-13}	0.02	-5.102×10^{-13}
11	1.854×10^{-11}	0.31	1.856×10^{-11}	0.19	1.858×10^{-11}	0.07	1.858×10^{-11}	0.05	1.859×10^{-11}
12	-1.436×10^{-11}	0.97	-1.442×10^{-11}	0.55	-1.452×10^{-11}	0.14	-1.451×10^{-11}	0.07	-1.450×10^{-11}
13	1.925×10^{-12}	0.47	1.935×10^{-12}	0.05	1.934×10^{-12}	5.16 $\times 10^{-3}$	1.934×10^{-12}	5.16 $\times 10^{-3}$	1.934×10^{-12}
14	-1.375×10^{-11}	0.93	-1.379×10^{-11}	0.63	-1.390×10^{-11}	0.14	-1.388×10^{-11}	0.07	-1.388×10^{-11}

Table 5.13

Comparison of the analytical methods and FDM design derivatives for the application of displacement constraint at point F for 14 Design Elements

Design Element	FDM (F) 0.2%	% Error	FDM (F) 2.0%	% Error	FDM (C) 0.2%	% Error	FDM (C) 2.0%	% Error	AVM & DDM
1	2.246×10^{-13}	0.94	2.238×10^{-13}	0.56	2.225×10^{-13}	0.03	2.240×10^{-13}	0.67	2.225×10^{-13}
2	1.112×10^{-12}	0.63	1.090×10^{-12}	1.32	1.101×10^{-12}	0.36	1.112×10^{-12}	0.63	1.105×10^{-12}
3	1.934×10^{-12}	0.56	1.942×10^{-12}	1.03	1.945×10^{-12}	1.03x 10-3	1.932×10^{-12}	0.67	1.945×10^{-12}
4	1.871×10^{-12}	1.29	1.835×10^{-12}	0.65	1.843×10^{-12}	0.16	1.842×10^{-12}	0.26	1.847×10^{-12}
5	-1.887×10^{-11}	0.4	-1.868×10^{-11}	1.14	-1.896×10^{-11}	0.08	-1.896×10^{-11}	0.08	-1.895×10^{-11}
6	-2.993×10^{-12}	0.43	-2.981×10^{-12}	0.83	-3.005×10^{-12}	0.02	-2.997×10^{-12}	0.07	-3.006×10^{-12}
7	1.245×10^{-12}	1.38	1.216×10^{-12}	0.98	1.230×10^{-12}	0.14	1.216×10^{-12}	0.96	1.228×10^{-12}
8	7.941×10^{-13}	0.15	7.862×10^{-13}	1.14	7.943×10^{-13}	0.12	7.902×10^{-13}	0.64	7.953×10^{-13}
9	6.114×10^{-13}	0.82	6.069×10^{-13}	0.41	6.102×10^{-13}	0.13	6.130×10^{-13}	0.58	6.094×10^{-13}
10	3.471×10^{-13}	0.84	3.435×10^{-13}	0.2	3.445×10^{-13}	0.08	3.474×10^{-13}	0.93	3.442×10^{-13}
11	6.436×10^{-13}	0.68	6.358×10^{-13}	0.55	6.404×10^{-13}	0.17	6.426×10^{-13}	0.52	6.393×10^{-13}
12	1.506×10^{-12}	1.27	1.475×10^{-12}	0.79	1.488×10^{-12}	0.1	1.502×10^{-12}	0.98	1.487×10^{-12}
13	4.635×10^{-14}	0.07	4.607×10^{-14}	0.68	4.617×10^{-14}	0.46	4.638×10^{-14}	2.15×10^{-3}	4.638×10^{-14}
14	-2.613×10^{-15}	0.53	-2.601×10^{-15}	0.99	-2.629×10^{-15}	0.05	-2.624×10^{-15}	0.12	-2.627×10^{-15}

Table 5.14

Comparison of the analytical methods and FDM design derivatives for the application of displacement constraint at point G for 14 Design Elements

5.11.2 Design Element Sensitivities von Mises stress

Table 5.15 and 5.16 show the design element sensitivities of von Mises stress with respect to the Young modulus for the application of von Mises stress constraints at point F and G respectively for 14 design elements.

Design Element	FDM (F) 0.2%	% Error	FDM (F) 2.0%	% Error	FDM (C) 0.2%	% Error	FDM (C) 2.0%	% Error	AVM & DDM
1	3.292×10^{-14}	0.51	3.280×10^{-14}	0.88	3.306×10^{-14}	0.09	3.296×10^{-14}	0.39	3.309×10^{-14}
2	-1.965×10^{-13}	0.67	-1.972×10^{-13}	1.02	-1.956×10^{-13}	0.20	-1.961×10^{-13}	0.46	-1.952×10^{-13}
3	1.834×10^{-12}	0.65	1.845×10^{-12}	1.26	1.819×10^{-12}	0.16	1.812×10^{-12}	0.55	1.822×10^{-12}
4	-8.846×10^{-12}	0.48	-8.818×10^{-12}	0.79	-8.909×10^{-12}	0.22	-8.852×10^{-12}	0.41	-8.889×10^{-12}
5	-1.734×10^{-11}	0.63	-1.731×10^{-11}	0.80	-1.750×10^{-11}	0.29	-1.754×10^{-11}	0.52	-1.745×10^{-11}
6	-1.225×10^{-11}	0.56	-1.219×10^{-11}	1.05	-1.232×10^{-11}	0.07	-1.226×10^{-11}	0.48	-1.232×10^{-11}
7	-2.326×10^{-12}	0.68	-2.320×10^{-12}	0.94	-2.338×10^{-12}	0.17	-2.356×10^{-12}	0.59	-2.342×10^{-12}
8	-1.916×10^{-12}	0.57	-1.909×10^{-12}	0.93	-1.929×10^{-12}	0.10	-1.936×10^{-12}	0.47	-1.927×10^{-12}
9	-1.577×10^{-12}	0.57	-1.569×10^{-12}	1.07	-1.583×10^{-12}	0.19	-1.578×10^{-12}	0.50	-1.586×10^{-12}
10	-1.605×10^{-12}	0.86	-1.610×10^{-12}	0.55	-1.612×10^{-12}	0.43	-1.620×10^{-12}	0.06	-1.619×10^{-12}
11	5.023×10^{-12}	0.63	5.032×10^{-12}	0.82	5.001×10^{-12}	0.22	5.015×10^{-12}	0.48	4.991×10^{-12}
12	1.662×10^{-11}	0.54	1.683×10^{-11}	0.72	1.675×10^{-11}	0.28	1.679×10^{-11}	0.47	1.671×10^{-11}
13	4.466×10^{-13}	0.58	4.490×10^{-13}	0.04	4.484×10^{-13}	0.2	4.494×10^{-13}	0.02	4.493×10^{-13}
14	4.780×10^{-12}	0.27	4.758×10^{-12}	0.19	4.769×10^{-12}	0.04	4.768×10^{-12}	0.02	4.767×10^{-12}

Table 5.15

Comparison of the analytical methods and FDM design derivatives for the application of von Mises stress constraint at point F for 14 Design Elements

Design Element	FDM (F) 0.2%	% Error	FDM (F) 2.0%	% Error	FDM (C) 0.2%	% Error	FDM (C) 2.0%	% Error	AVM & DDM
1	-2.459 x10^{-13}	0.32	-2.480 x10^{-13}	0.53	-2.469 x10^{-13}	0.08	-2.463 x10^{-13}	0.16	-2.467 x10^{-13}
2	-1.573 x10^{-12}	0.19	-1.565 x10^{-12}	0.69	-1.575 x10^{-12}	0.06	-1.570 x10^{-12}	0.38	-1.576 x10^{-12}
3	-4.156 x10^{-12}	0.72	-4.211 x10^{-12}	0.60	-4.187 x10^{-12}	0.02	-4.181 x10^{-12}	0.12	-4.186 x10^{-12}
4	-2.197 x10^{-12}	0.32	-2.218 x10^{-12}	0.59	-2.207 x10^{-12}	0.09	-2.213 x10^{-12}	0.36	-2.205 x10^{-12}
5	-4.633 x10^{-12}	0.30	-4.670 x10^{-12}	0.49	-4.642 x10^{-12}	0.11	-4.636 x10^{-12}	0.24	-4.647 x10^{-12}
6	-6.396 x10^{-12}	0.48	-6.462 x10^{-12}	0.54	-6.431 x10^{-12}	0.06	-6.457 x10^{-12}	0.47	-6.427 x10^{-12}
7	-1.251 x10^{-12}	0.40	-1.255 x10^{-12}	0.72	-1.248 x10^{-12}	0.16	-1.242 x10^{-12}	0.32	-1.246 x10^{-12}
8	-3.465 x10^{-13}	0.23	-3.471 x10^{-13}	0.40	-3.456 x10^{-13}	0.03	-3.451 x10^{-13}	0.17	-3.457 x10^{-13}
9	-1.851 x10^{-13}	0.48	-1.856 x10^{-13}	0.76	-1.840 x10^{-13}	0.11	-1.849 x10^{-13}	0.38	-1.842 x10^{-13}
10	-2.032 x10^{-14}	0.30	-2.038 x10^{-14}	0.59	-2.029 x10^{-14}	0.15	-2.021 x10^{-14}	0.25	-2.026 x10^{-14}
11	-8.080 x10^{-13}	0.26	-8.096 X10^{-13}	0.46	-8.055 x10^{-13}	0.05	-8.036 x10^{-13}	0.29	-8.059 x10^{-13}
12	-2.810 x10^{-12}	0.71	-2.853 x10^{-12}	0.81	-2.838 x10^{-12}	0.28	-2.843 x10^{-12}	0.50	-2.830 x10^{-12}
13	-9.200 x10^{-14}	0.96	-9.283 x10^{-14}	0.06	-9.350 x10^{-14}	0.65	-9.288 x10^{-14}	0.01	-9.289 x10^{-14}
14	-1.649 x10^{-13}	1.02	-1.664 x10^{-13}	0.12	-1.667 x10^{-13}	0.06	-1.667 x10^{-13}	0.06	-1.666 x10^{-13}

Table 5.16

Comparison of the analytical methods and FDM design derivatives for the application of von Mises stress constraint at point G for 14 Design Elements

From this tabulation, it can be seen that the results showed closed agreement. It reflects the results obtained for the comparison done for the full field solution from the AVM and the DDM, where again, the percentage errors obtained were also small.

5.12 Shape Design Element

The Design Element Concept is not only applicable to parameter sensitivity, it can also be applied to shape sensitivity. In this section, a new and novel application of shape design element of coolant channels is demonstrated. Shape sensitivity can to some extent be applied to part shape design, but often this is driven by end application considerations. In this work it may be applied to process design through for example positioning of the cooling system within the die. This will be explored within the case studies that will be considered in this project. However, in the following case studies, the coolant channel was not moved around, it was just the case of showing how the sensitivity of the chosen position will respond with respect to the application of the von Mises stress constraint.

5.12.1 Shape Parameterisation of Coolant Channel

One of the important aspects in performing shape sensitivities for coolant channel geometry is the parameterisation of the coolant channel. To illustrate this, Figure 5.37 shows the X and Y coordinates of the coolant channel centre. The shape sensitivities with respect to the X and Y coordinates are calculated after parameterisation and the von Mises stress constraints have been applied at points F and G as shown in Figure 5.5. These have been chosen due to the high von Mises stress values in these areas. The parameterisation of the coolant channels is as follows,

$x = X - r \cos \alpha$

$y = Y - r \sin \alpha$

where, r is the radius of the coolant channel and α is the angle as shown in Figure 5.37.

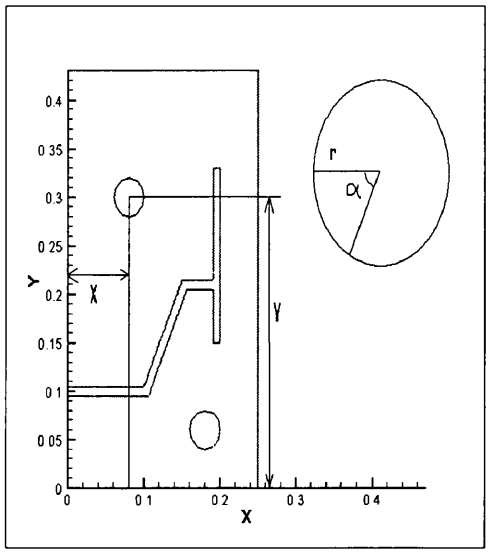

Figure 5.37

The definition of X and Y coordinates of the centre of the coolant channels

5.12.2 The Stiffness Matrix Derivative for Shape Sensitivities

Again, in performing analytical design element shape sensitivity analysis, the success of the computation is largely dependent on the calculated stiffness matrix derivative. Thus, for an axi-symmetric problem, the derivative of the stiffness matrix with respect to the design variable, associated with the Y-coordinate of the centre of the coolant channel, is given as:

$$\frac{\partial \mathbf{K}}{\partial \mathbf{Y}} = \left(\frac{\partial \mathbf{B}^T}{\partial \mathbf{Y}} \mathrm{D}\mathbf{B}\mathbf{J}_\mathrm{D} + \mathbf{B}^T \mathrm{D} \frac{\partial \mathbf{B}}{\partial \mathbf{Y}} \mathbf{J}_\mathrm{D} + \mathbf{B}^T \mathrm{D}\mathbf{B} \frac{\partial \mathbf{J}_\mathrm{D}}{\partial \mathbf{Y}}\right) \pi \mathbf{r}_{\mathbf{bar}} \qquad (5.35)$$

The derivative of the stiffness matrix with respect to the X-coordinate of the centre of the coolant channel is of the form,

$$\frac{\partial \mathbf{K}}{\partial \mathbf{X}} = (\frac{\partial \mathbf{B}^T}{\partial \mathbf{X}} \mathrm{DBJ_D r_{bar}} + \mathbf{B}^T \mathrm{D} \frac{\partial \mathbf{B}}{\partial \mathbf{X}} \mathbf{J_D r_{bar}} + \mathbf{B}^T \mathrm{DB} \frac{\partial \mathbf{J_D}}{\partial \mathbf{X}} \mathbf{r_{bar}} + \mathbf{B}^T \mathrm{DBJ_D} \frac{\partial \mathbf{r_{bar}}}{\partial \mathbf{X}}) \pi \quad (5.36)$$

5.12.3 Shape Design Element Concept Example

This section will highlight the influence of the tendency of the movement of the coolant channel having a radius of 0.02m in certain directions, for instance X and Y axis, with respect to the von Mises stress constraint at a particular point in the die. The same initial and boundary conditions were applied as described previously. Tables 5.17 and 5.18 show the design element sensitivities of von Mises stress with respect to Y and X coordinates for the lower coolant channel for the application of the von Mises stress constraint at point F. It can be seen that the tendency to move the lower coolant channel in the X-direction has a higher influence than the Y-direction with respect to the von Mises stress constraint at point F. Tables 5.19 and 5.20 show the design element sensitivities of von Mises stress with respect to Y and X coordinates of the lower coolant channel for the application of von Mises stress constraint at point G. However, from these results, the tendency to move the lower coolant channel in the Y-direction has a higher influence than the X-direction with respect to the von Mises stress constraint at point G.

Tables 5.21 and 5.22 show the design element sensitivities of von Mises stress with respect to Y and X coordinates of the upper coolant channel for the application of von Mises stress constraint at point F. Tables 5.23 and 5.24 show the design element sensitivities of von Mises stress with respect to Y and X coordinates of the upper coolant

channel for the application of von Mises stress constraint at point G. It can be seen that the tendency to move the upper coolant channel in the Y-direction has a higher influence than in X-direction with respect to both von Mises stress constraints at points F and G. Also, the percentage errors were small thus proving the accuracy of the analytical method. In this example, only the DDM was used. This is because from the parameter sensitivity examples, it can be seen that clearly both methods yield the same results. In this section, the full picture of the shape sensitivity cannot be shown because of the calculated sensitivities were only evaluated on a certain number of elements in the die.

Thus, based on the cooling system design sensitivity, the degree to which the tendency to move the coolant channel either in X or Y-direction can be drawn with respect to the particular von Mises stress constraint in the die. Also, based on the above examples, from the practical point of view, it can be seen that generally if the coolant channel is moved in direction y, it will have a more significant impact on von Mises stress when compared with a move in direction x.

	dSe/de ($1x10^{-4}$)
DDM	8.759

	% perturb	dSe/de ($1x10^{-4}$)	% error
FDM (C)	0.2	8.759	8.52 $x10^{-4}$
FDM (C)	2	8.765	0.07

Table 5.17

The design element sensitivities of von Mises stress with respect to Y coordinate of the lower coolant channel for the application of von Mises stress constraint at point F

	dSe/de ($1x10^{-3}$)
DDM	-1.332

	% perturb	dSe/de ($1x10^{-3}$)	% error
FDM (C)	0.2	-1.331	0.02
FDM (C)	2	-1.302	2.27

Table 5.18

The design element sensitivities of von Mises stress with respect to X coordinate of the lower coolant channel for the application of von Mises stress constraint at point F

	dSe/de ($1x10^{-1}$)
DDM	-2.670

	% perturb	dSe/de ($1x10^{-1}$)	% error
FDM (C)	0.2	-2.670	3.12 $x10^{-4}$
FDM (C)	2	-2.669	0.02

Table 5.19

The design element sensitivities of von Mises stress with respect to Y coordinate of the lower coolant channel for the application of von Mises stress constraint at point G

	dSe/de ($1x10^{-2}$)
DDM	-6.368

	% perturb	dSe/de ($1x10^{-2}$)	% error
FDM (C)	0.2	-6.368	2.97 $x10^{-3}$
FDM (C)	2	-6.385	0.27

Table 5.20

The design element sensitivities of von Mises stress with respect to X coordinate of the lower coolant channel for the application of von Mises stress constraint at point G

	dSe/de ($1x10^{-1}$)
DDM	-5.799

	% perturb	dSe/de ($1x10^{-1}$)	% error
FDM (C)	0.2	-5.799	1.84 $x10^{-3}$
FDM (C)	2	-5.809	0.17

Table 5.21

The design element sensitivities of von Mises stress with respect to Y coordinate of the upper coolant channel for the application of von Mises stress constraint at point F

	dSe/de ($1x10^{-2}$)
DDM	-1.792

	% perturb	dSe/de ($1x10^{-2}$)	% error
FDM (C)	0.2	-1.792	5.3 $x10^{-4}$
FDM (C)	2	-1.791	0.05

Table 5.22

The design element sensitivities of von Mises stress with respect to X coordinate of the upper coolant channel for the application of von Mises stress constraint at point F

	dSe/de ($1x10^{-1}$)
DDM	1.020

	% perturb	dSe/de ($1x10^{-1}$)	% error
FDM (C)	0.2	1.020	4.76 $x10^{-3}$
FDM (C)	2	1.016	0.37

Table 5.23

The design element sensitivities of von Mises stress with respect to Y coordinate of the upper coolant channel for the application of von Mises stress constraint at point G

	DSe/de ($1x10^{-2}$)
DDM	-2.859

	% perturb	dSe/de ($1x10^{-2}$)	% error
FDM (C)	0.2	-2.859	2.12 10^{-3}
FDM (C)	2	-2.858	0.03

Table 5.24

The design element sensitivities of von Mises stress with respect to X coordinate of the upper coolant channel for the application of von Mises stress constraint at point G

5.13 Closure

The design element concept with the aim of reducing effort in sensitivity calculation in the optimisation process has been proposed. In this work, the die has been divided into 5 divisions of design elements, where the zones of defined design elements may correspondingly represent the number of blocks that make up the die. From the examples provided, it can be seen that as a number of divisions of design elements are increased, convergence of sensitivity is obtained for both displacement and von Mises stress constraints. Also, the shape sensitivities procedure of the coolant channels has been described, thus, enabling the coolant channels to be moved as an entity for each coolant channel for the shape optimisation problem. For the shape sensitivity, based on the calculated sensitivity, the extent to which the tendency to move the coolant channel either

in X or Y-direction can be determined with respect to the particular von Mises stress constraint in the die.

References

1. E.J. Haug, K.K. Choi and V. Komkov, ' Design sensitivity analysis of structural systems', London, UK: Academic Press;1986.

2. M.A. Crisfield, ' Finite elements and solution procedures for structural analysis, Vol.1, Linear analysis' Swansea, UK: Pineridge Press, 1986.

3. W.F. Chen and D.J. Han, ' Plasticity for structural Engineers', New York: Springer Verlag, 1988.

4. www.gknplc.com/ (2003).

5. Lewis RW, Manzari MT and Gethin DT. Thermal optimisation in the sand casting process. *Engineering Computations*. 2001; **18 (3/4)**: 392-416.

6. Anderson JT. A theoretical and experimental investigation into the investment and gravity die casting processes. M.Phil Thesis, Swansea University, 1995.

7. K. Ravindran and R.W. Lewis, 'Finite element modelling of solidification effects in mould filling', *Finite Elements in Analysis and Design*, 1998;**31**, 99-116.

Chapter 6

Conclusions and Proposals for further work

6.1 Conclusions

The application of the automatic optimisation in the squeeze forming process with respect to the positions of the coolant channels using genetic algorithms has successfully been implemented. The accomplishment of this work, has been dependent on the successful integration of the finite element method, mesh generator and the genetic algorithm software. The validation aspects were implemented in the 2D planar and axi-symmetric casting processes and the results showed good agreement with the published works, thus highlighting the effectiveness of this method. The thermal optimisation of the squeeze forming for the non-cyclic and cyclic processes has been explored. The exploration

started from the simple analysis for two defined points in the casting and also considering the whole domain. Furthermore, optimisation of the process under the influence of the contact pressure by changing the interfacial heat transfer coefficient value has been dealt with. The application to include multi-objective optimisation involving the thermal aspect in the casting and mechanical aspect in the die has been explored. Also, the application of design sensitivity analysis and Design Element Concept has been applied successfully to the process involving parameter and shape sensitivities. From this work, the following conclusions may be drawn:

1) This work suggests that for both thermodynamic and thermomechanical optimisations, there is a need to derive an objective function that reflects the whole domain, rather than selective points within the domain. This is due to the fact that by considering only two points in the casting, although the solution achieved a near the global optimal, some of the results obtained were far away from achieving the desired practical objective, which was to obtain near simultaneous solidification in the casting. Under this circumstance, the coolant channels are positioned to surround the casting.

2) The optimal results obtained for the cyclic analysis were different from the non-cyclic simulations. This suggests that for the actual design practice in the industry, it is required that the design process takes into account this aspect, since it gives a large difference in the obtained results. This is due to the increase in temperature and its change in distribution through the die. In this work, it has been found that cyclic stabilisation is approached after the tenth cycle.

3) Optimisation of the positions of the coolant channels has also been explored under the influence of the pressure relaxation by changing the interfacial heat transfer coefficient at the die-casting interface. This has been done for the first cycle up to the fifth cycle. This exploration significantly highlights the need to consider such a factor due to the direct dependency of temperature distribution in the casting and die on the interfacial heat transfer coefficient. The results obtained showed the lack of agreement with die design based on intuition. In the current optimised design, the coolant channels were positioned further away generally to satisfy the requirement of the objective function, which was to achieve near simultaneous solidification in the casting.

4) The work has also demonstrated the application of the multi-objective optimisation to the squeeze forming process. The results obtained for first and tenth cycles showed similarity in form, where the coolant channels are positioned to surround the casting with high temperature surrounding the casting. At the same time, from the graphs of stress distribution, the fluctuation of stress distribution in the die and average von Mises stress value for the optimal solution were reduced in comparison with the results obtained considering the thermal optimisation only.

5) The design sensitivity analysis and Design Element Concept have been implemented in the squeeze forming process simulation. In this work, all the design sensitivity gradients for full field solution and also the calculated sensitivity gradients based on Design Elements using analytical methods have been compared with the FDM method, effectively completing the validation loop for this part of the optimisation process. For parameter design sensitivity analysis, the region where it is more sensitive to the change

in design variable, for instance Youngs Modulus (that is relevant to composite dies), has been identified based on the sensitivity distribution.

6) For the application of Design Element Concept to the process, 5 types of discretisation of zones of Design Element have been proposed, with 3, 7, 10, 14 and 28 Design Element subdivisions in the die. From the examples provided, it can be seen that the general pattern of sensitivity distribution tends to reach a converged state as the number of design elements is increased. Even the 28 Design Element sensitivity gradients still have significant computational saving when compared with sensitivity gradients calculated based on the discretised finite element mesh.

7) Shape Design Element sensitivity involving the coolant channel has been performed. Before calculating the shape sensitivity, parameterisation of the edge of the coolant channel with respect to X or Y axis is required in order to consider the coolant channel as an entity. Based on the calculated shape sensitivities, the influence of the tendency to move the coolant channel in either X or Y direction with respect to the von Mises stress constraint at a particular point in the die can be identified. In this work, for the geometric configuration analysed, it has been found that if the coolant channel is moved in direction y, it will have a more significant impact on von Mises stress when compared with a move in the direction x.

6.2 Proposals for Further Work

The recommendations for further work are suggested as follows:

1) There is a need to include a thermomechanical model of the casting as well, even though for now the model is complex and computationally very demanding.

2) In the modeling of the squeeze forming process, it is appropriate to consider a die as a number of steel blocks, rather than only as one piece. This is due to the standard practice that generally applies in the casting and squeeze forming processes. This is also likely to affect the stress distribution in the die, since the steel blocks can move relative to each other.

3) It is also attractive to explore for the future work in optimisation of the squeeze forming process to consider the timing of the pressure control cycle as a design parameter to be optimised. This is because of the significant effects that this has on the process, due to the direct dependency of the interfacial heat transfer coefficient with respect to the pressure application.

4) For optimisation using genetic algorithm program, there is the need to implement parallel processing due to the computational demanding, when considering nonlinearities that are present, for instance in the casting, even for a non-cyclic simulation.

5) The application of Design Element Concept to the squeeze forming process considering all the non-linearity aspects that are present will be desirable for the future research due to the new application of such technique to the process. Then, the calculated

Design Element sensitivity gradients using analytical methods can be supplied to the gradient-based optimisation software to search for the optimal solution. It is also required that the design elements needs more exploration and coupling with optimisation to see if the same layout is achieved as a final validation step.

6) There is also a need to apply some practical validations of the coolant channels design, since the design that has been proposed is significantly different from an intuitive scheme.

Appendix I

Genetic Algorithms Operators

The purpose of this Appendix is to explain the basic issues concerned with genetic algorithms and how they are applied in the context of the current casting process optimisation.

I.1 Uniform Mutation

The uniform mutation operator substitutes the actual value of a given gene with a random number belonging to the admissible range of variation of the gene. A gene is a design variable and in this work, for instance, it represents the position of the coolant channel. This operation is illustrated in detail in Figure AI.1, where the values in the blue box, for instance, represent the positions of the coolant channels. The mutation effectively introduces a new set of coolant channel coordinates.

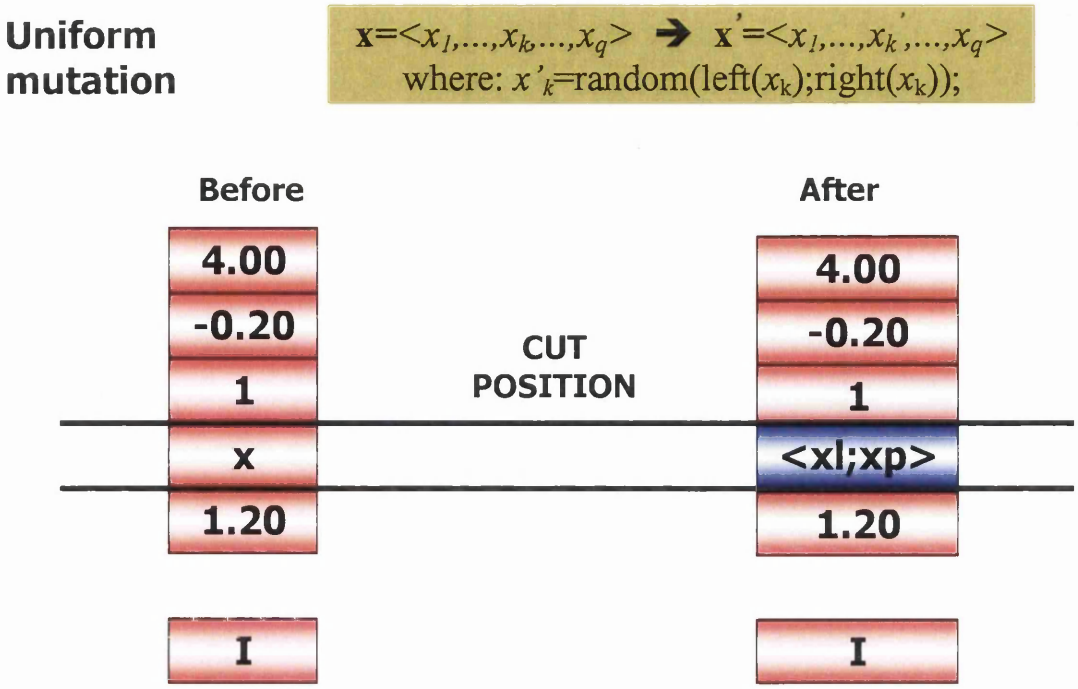

Figure AI.1

Uniform mutation operator

I.2 Non-Uniform Mutation

The non-uniform mutation operator is the operator responsible for the fine tuning capabilities of the system as shown in Figure AI.2. The function $\Delta(t,y)$ returns a value in the range [0,y] such that the probability of $\Delta(t,y)$ being close to 0 increases as t (number of generation) increases. This property causes this operator to search the space uniformly initially (when t is small), and very locally at later stages. The letter r represents a random binary number.

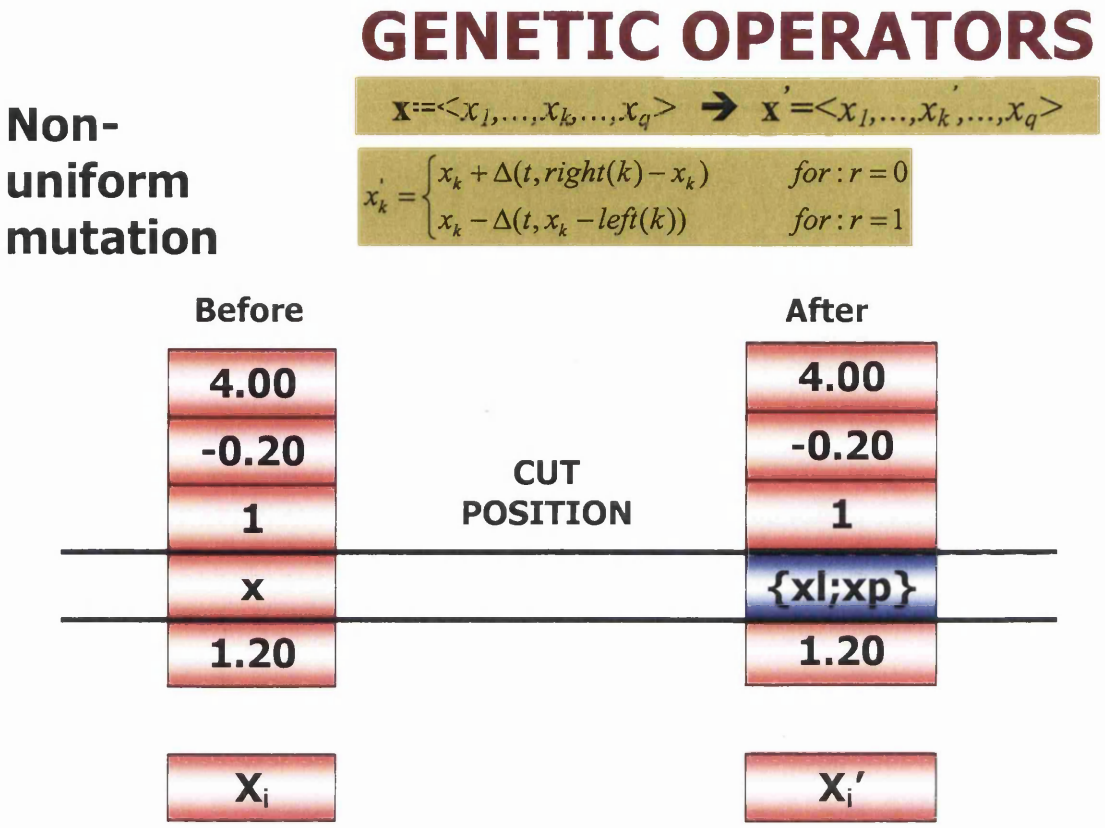

Figure AI.2

Non-uniform mutation operator

Effectively this refines the coolant channel position as the optimisation solution proceeds.

I.3 Boundary Mutation

In boundary mutation, which is a variation of the uniform mutation, the gene (design variable) receives one of limiting values (either left or right) with the same probability as shown in Figure AI.3. Thus, the mutation effectively introduces a new set of coolant channel coordinates.

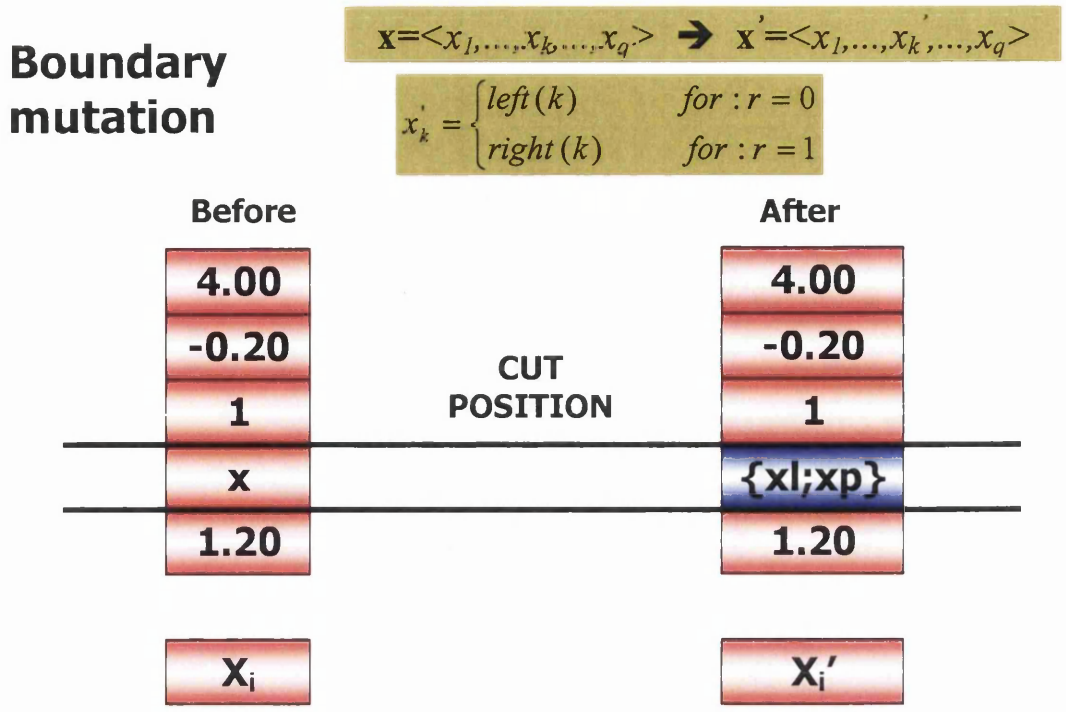

Figure AI.3

Boundary mutation operator

In effect, this produces diversity in the coolant channel position and prevents the algorithm to get locked in a local extreme by making it explore other regions.

I.4 Simple Crossover

In simple crossover, a pair of offspring chromosomes is created from two parent chromosomes. A chromosome is a series of design variables and in this work, for instance, a chromosome is a series of positions of the coolant channels in X and Y directions. The new offspring chromosomes inherit genes from both parents. This concept is shown in Figure AI.4.

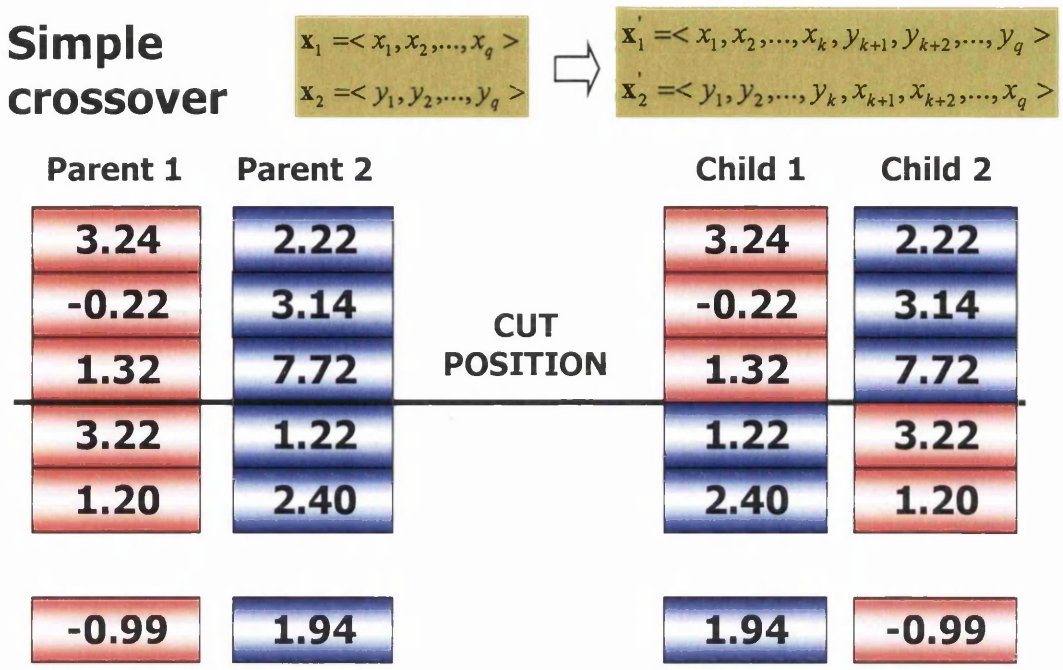

Figure AI.4

Simple crossover operator

Efficiently this produces a new pair of two sets of coolant channel position which have some parts from the previous two sets of coolant channel position.

I.5 Arithmetic Crossover

Arithmetic crossover creates a new offspring chromosome inheriting a linear combination from both parent chromosomes as illustrated in Figure AI.5.

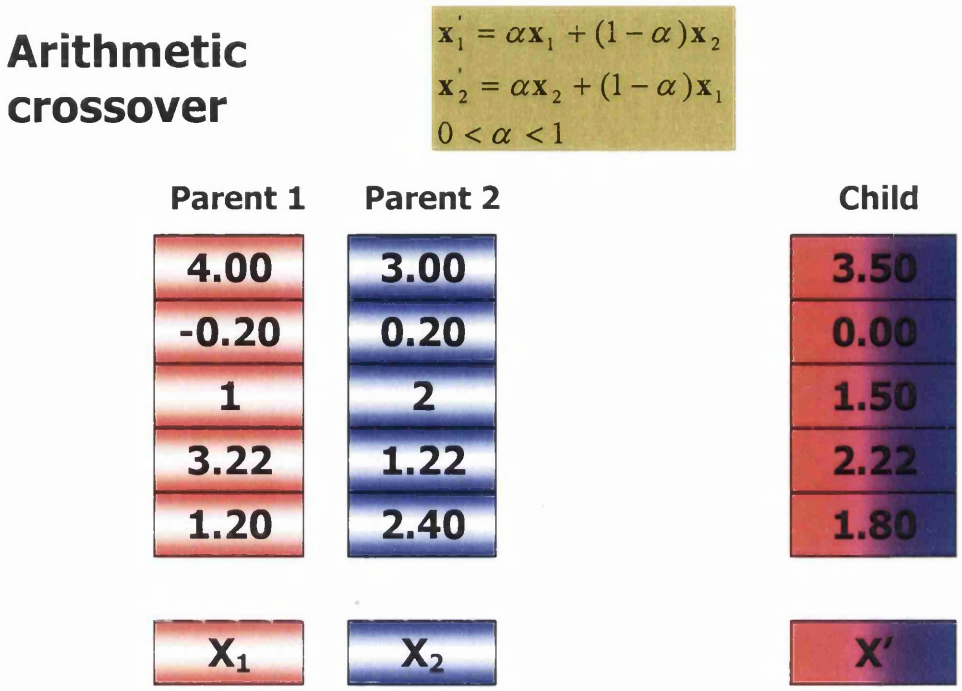

Figure AI.5

Arithmetic crossover operator

In effect, this produces a new set of coolant channel position based on the two previous sets of coolant channel position

I.6 Cloning

The cloning operator increases the probability of surviving for the best chromosome by duplicating it in the subsequent generation. Figure AI.6 demonstrates the working principle of cloning operator.

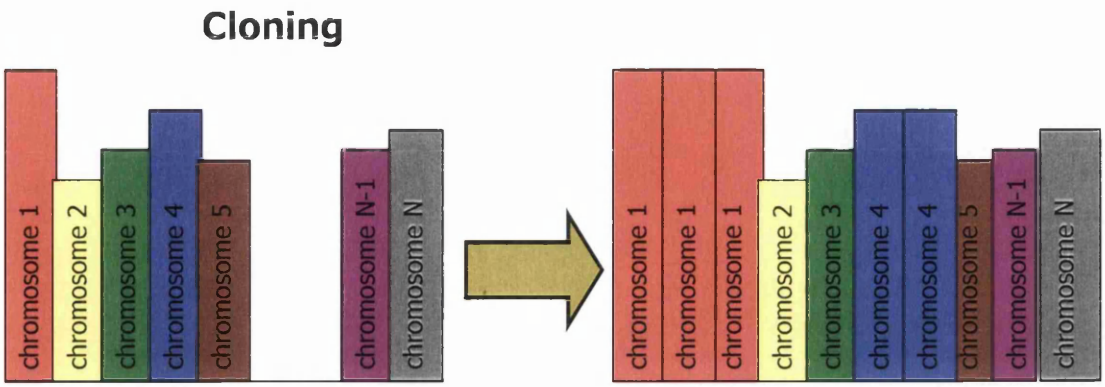

Figure AI.6

Cloning operator

This retains the best set of coolant channel position and therefore increases the survival of the set of coolant channel position as the optimisation solution proceeds.

I.7 Selection

The ranking selection increases the probability of surviving of the chromosomes which have greater fitness function as illustrated in Figure AI.7.

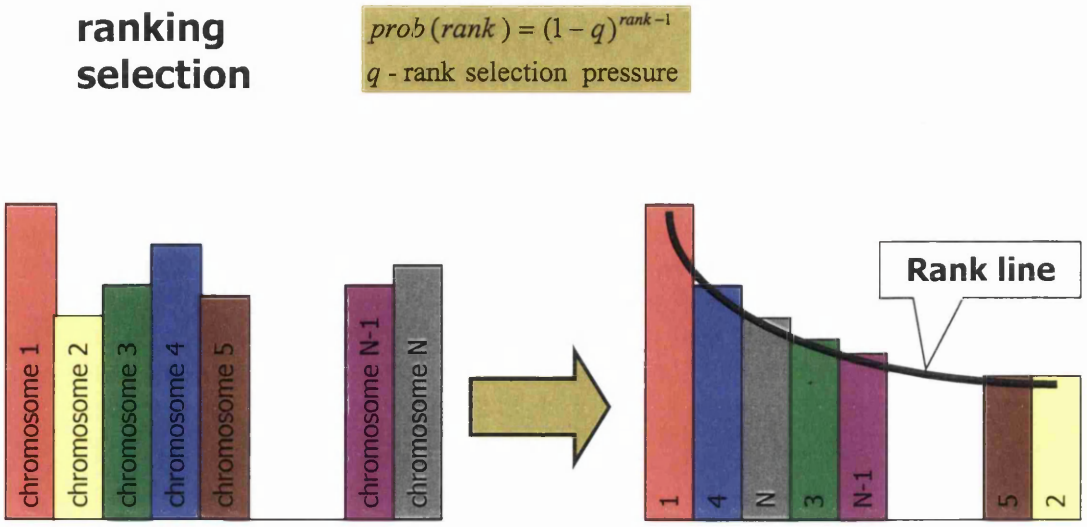

Figure AI.7

Ranking selection operator

Effectively, this preserves the survival of sets of coolant channel position with greater fitness function as optimisation solution proceeds.

Appendix II

Heat Transfer Coefficient

II.1 Forced Convection

Convection is classified as natural (or free) or forced convection, depending on how the fluid motion is initiated. In forced convection, the fluid is forced to flow over a surface or in a pipe by external means such as a pump or a fan. The following is set out as a summary, details are explained in A1 and A2.

II.2 Nusselt Number

Nusselt number is defined as;

$$Nu = \frac{hL_c}{k}$$

Where Nu is the Nusselt number, h is the heat transfer coefficient, L_c is the characteristic length and k is the thermal conductivity of the fluid. The Nusselt number is defined to nondimensionalise the heat transfer coefficient. However, for noncircular tubes, the characteristic length, L_c is the hydraulic diameter, D_h which is defined as follows;

$$D_h = \frac{4A_c}{p}$$

where A_c is the area of the duct and p is the perimeter of the duct.

II.3 Turbulent Flow in Tubes

For fully developed turbulent flow in smooth tubes, a simple relation for the Nusselt number is defined as follows:

$Nu = 0.023Re^{0.8}Pr^{0.3}$

II.4 Reynolds Number

The Reynolds number, Re is given by the following equation:

$$\mathrm{Re} = \frac{\rho v_f D_h}{\mu} = \frac{v_f D_h}{\nu}$$

Where ρ is the density of the fluid, D_h is the hydraulic diameter, v_f is the density of the fluid, μ is the dynamic viscosity and υ is the kinematic viscosity. These equations have been used to guide the choice of heat transfer coefficient and example values are derived below.

II.5 Heat Transfer Coefficient Calculations

II.5.1 Water as Coolant Liquid

At T_f=20°C for water as coolant liquid, the following properties were used;

ρ = 998 kg/m^3 Pr = 7.01 (Prandtl Number)

k = 0.598W/mK $\upsilon = \mu/\rho = 1.002\text{x}10^{-3}/998 = 1.0\text{x}10\text{-}6\text{m}^2/\text{s}$

In general, for all coolant channels, the hydraulic diameter, D_h = 0.02m :

Assuming the velocity of the water, v_f = 0.22m/s ;

$\text{Re} = 0.22\text{x}(0.02)/1.0\text{x}10^{-6}$

Re = 4400 > 4000 (Turbulent)

Thus,

$\text{Nu} = 0.023\text{Re}^{0.8}\text{Pr}^{0.3}$

$\text{Nu} = 0.023(4400)^{0.8}(7.01)^{0.3}$

Nu = 33.9

Given that Nusselt number is,

$$Nu = \frac{hD_h}{k}$$

Heat transfer coefficient at the coolant channels can be calculated as :

$h = 33.9\text{x}(0.598)/0.02$

$h = 1000\text{W/m}^2\text{K}$

II.5.2 Oil as Coolant Liquid

At T_f=100°C for oil as coolant liquid, the following properties were used;

$\rho = 840\text{kg/m}^3$ Pr = 279.1 (Prandtl Number)

k = 0.1367W/mK $\upsilon = \mu/\rho = 2.046\text{x}10^{-5}\text{m}^2/\text{s}$

In general, for all coolant channels, the hydraulic diameter, D_h = 0.02m :

Assuming the velocity of the oil, v_f = 7m/s ;

Re = $7x(0.02)/2.046x10^{-5}$

Re = 6842.6 > 4000 (Turbulent)

Thus,

Nu = $0.023Re^{0.8}Pr^{0.3}$

Nu = $0.023(6842.6)^{0.8}(279.1)^{0.3}$

Nu = 145.3

Given that Nusselt number is,

$$Nu = \frac{hD_h}{k}$$

Heat transfer coefficient at the coolant channels can be calculated as :

h = 145.3x(0.1367)/0.02

h = $1000W/m^2K$

References

A1. Y.A. Cengel and R.H. Turner, 'Fundamentals of thermal-fluid sciences' Singapore: McGraw Hill, International Edition 2005.

A2. Y.A. Cengel, 'Introduction to Thermodynamics and heat transfer', USA: McGraw Hill, International Edition 1997.

Appendix III

Comparison of Thermal and Pressure Induced Stresses

III.1 Pressure Induced Stress

Figure AIII.1 shows the pressure induced stress distribution by applying the pressure at 60 MPa in normal direction from internal side of the casting for the initial geometry from GKN.

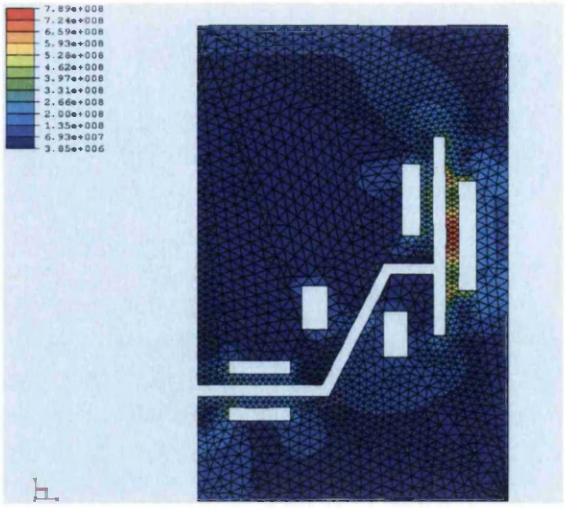

Figure AIII.1

Pressure induced stress distribution by applying pressure at 60 MPa (in normal direction) from internal side of the casting for the initial geometry from GKN

III.2 Thermal Induced Stress

Figure AIII.2 shows the thermal induced stress distribution for the initial geometry from GKN and Figure AIII.3 shows the corresponding thermal distribution in the die.

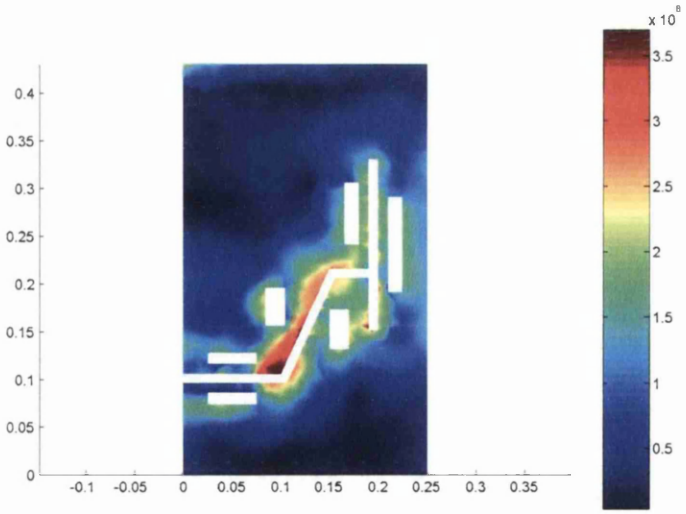

Figure AIII.2

Thermal induced stress distribution in the die t=50s for the initial geometry from GKN

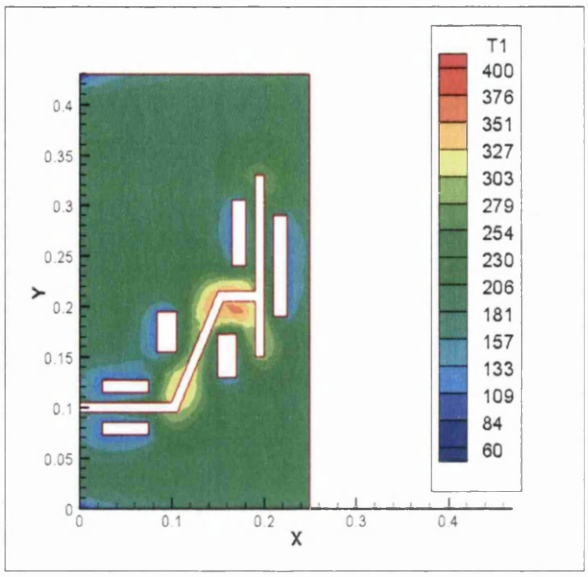

Figure AIII.3

Temperature distribution in the die at t=50s for the initial geometry from GKN